ARISTOTLE UNIVERSITY OF THESSALONIKI
Interinstitutional Program of Postgraduate Studies in
PALAEONTOLOGY – GEOBIOLOGY

ANASTASIA KATSAGONI
Geologist

CONTRIBUTION TO THE TAPHONOMIC STUDY OF THE LOWER PLEISTOCENE SITE TSIOTRA VRYSSI (MYGDONIA BASIN, GREECE): CARNIVORE TOOTH MARKS ON UNGULATE BONES

MASTER THESIS

DIRECTION: Macropalaeontology
Directed by: Aristotle University of Thessaloniki

THESSALONIKI
2021

Interinstitutional Program of Postgraduate Studies in PALAEONTOLOGY – GEOBIOLOGY

supported by:

Τμήμα Γεωλογίας ΑΠΘ
School of Geology AUTh

Τμήμα Βιολογίας ΑΠΘ
School of Biology AUTh

Τμήμα Γεωλογίας & Γεωπεριβάλλοντος
ΕΚΠΑ

Faculty of Geology & Geoenvironment
NKUA

Τμήμα Γεωλογίας Παν/μίου Πατρών
Department of Geology, Patras Univ.

Τμήμα Γεωγραφίας Παν/μίου Αιγαίου
Department of Geography, Aegean Univ.

ANASTASIA KATSAGONI
ΑΝΑΣΤΑΣΙΑ ΚΑΤΣΑΓΩΝΗ
Πτυχιούχος Γεωλόγος

CONTRIBUTION TO THE TAPHONOMIC STUDY OF THE LOWER PLEISTOCENE SITE TSIOTRA VRYSSI (MYGDONIA BASIN, GREECE): CARNIVORE TOOTH MARKS ON UNGULATE BONES

ΣΥΜΒΟΛΗ ΣΤΗΝ ΤΑΦΟΝΟΜΙΚΗ ΜΕΛΕΤΗ ΤΗΣ ΚΑΤΩ-ΠΛΕΙΣΤΟΚΑΙΝΙΚΗΣ ΑΠΟΛΙΘΩΜΑΤΟΦΟΡΟΥ ΘΕΣΗΣ ΤΣΙΟΤΡΑ ΒΡΥΣΗ (ΛΕΚΑΝΗ ΜΥΓΔΟΝΙΑΣ, ΕΛΛΑΔΑ): ΔΗΚΤΙΚΑ ΊΧΝΗ ΣΑΡΚΟΦΑΓΩΝ ΣΕ ΟΣΤΑ ΟΠΛΗΦΟΡΩΝ

Υποβλήθηκε στο ΔΠΜΣ Παλαιοντολογία-Γεωβιολογία

Ημερομηνία Προφορικής Εξέτασης: 15/10/2021
Oral Examination Date: 15/10/2021

Three-member Examining Board

Professor Aikaterini Harvati-Papatheodorou, Supervisor
Professor Dimitrios S. Kostopoulos, Member
Professor Evangelia Tsoukala, Member

Τριμελής Εξεταστική Επιτροπή

Καθηγήτρια Αικατερίνη Χαρβάτη-Παπαθεοδώρου, Επιβλέπουσα
Καθηγητής Δημήτριος Κωστόπουλος, Μέλος Τριμελούς Εξεταστικής Επιτροπής
Καθηγήτρια Ευαγγελία Τσουκαλά, Μέλος Τριμελούς Εξεταστικής Επιτροπής

External Assistant/Εξωτερικός Συνεργάτης (σύμφωνα με ΕΔΕ5/ 8-9-2020)
Dr. George E. Konidaris/Δρ. Γεώργιος Ε. Κονιδάρης

CONTRIBUTION TO THE TAPHONOMIC STUDY OF THE LOWER PLEISTOCENE SITE TSIOTRA VRYSSI (MYGDONIA BASIN, GREECE): CARNIVORE TOOTH MARKS ON UNGULATE BONES
– *Master Thesis*

ΣΥΜΒΟΛΗ ΣΤΗΝ ΤΑΦΟΝΟΜΙΚΗ ΜΕΛΕΤΗ ΤΗΣ ΚΑΤΩ-ΠΛΕΙΣΤΟΚΑΙΝΙΚΗΣ ΑΠΟΛΙΘΩΜΑΤΟΦΟΡΟΥ ΘΕΣΗΣ ΤΣΙΟΤΡΑ ΒΡΥΣΗ (ΛΕΚΑΝΗ ΜΥΓΔΟΝΙΑΣ, ΕΛΛΑΔΑ): ΔΗΚΤΙΚΑ ΊΧΝΗ ΣΑΡΚΟΦΑΓΩΝ ΣΕ ΟΣΤΑ ΟΠΛΗΦΟΡΩΝ
– *Μεταπτυχιακή Διπλωματική Εργασία*

Citation:
Katsagoni A., 2021. – Contribution to the taphonomic study of the Lower Pleistocene site Tsiotra Vryssi (Mygdonia basin, Greece): carnivore tooth marks on ungulate bones. Master Thesis, Interinstitutional Program of Postgraduate Studies in Palaeontology-Geobiology. School of Geology, Aristotle University of Thessaloniki, 117 pp.

Cover Figure: Pales and Garcia (1981)

Content

Acknowledgments

I would first like to thank my supervisor, Professor Aikaterini Harvati-Papatheodorou for giving me the opportunity to conduct an important part of my research at the Palaeoanthropology Section (Institute for Archaeological Sciences) of the Eberhard-Karls University of Tübingen in Germany as well as for her comments on the manuscript. I also want to thank the members of the examining board, Professor Dimitrios S. Kostopoulos for his scientific support through all phases of the master thesis, along with his comments on the manuscript, and Professor Evangelia Tsoukala for her comments and suggestions that significantly improved the final text. To Dr. George Konidaris, I am grateful for his active involvement in all steps of this research. His guidance through the researching phase and his repeated feedback on the manuscript were instrumental to the completion of this work. I thank Dr. Sireen El Zaatari for providing me access to the confocal profilometer (University of Tübingen) and MSc Annabelle-Louise Lockey for her instructions on its use, Dr. Domenico Giusti for his help with the QGIS analysis, and MSc Anastasia Gkeme for sharing her data regarding the classification of the *Equus* specimens into the medium- and large-sized species. Moreover, I want to thank all field team members who participated in the excavations and unearthed the material concerning this study, and especially Emer. Prof. George D. Koufos, Prof. Dimitris Kostopoulos, Prof. Katerina Harvati, Dr. George Konidaris, Dr. Vangelis Tourloukis, Dr. Domenico Giusti and Msc Nicholas Thompson. The excavations were supported by the European Research Council STG no. 283503 (PaGE) and the European Research Council CoG 724703 (CROSSROADS), both awarded to Professor Aikaterini Harvati-Papatheodorou. My research at the University of Tübingen was supported by the Erasmus+ student exchange program.

I am grateful to my family for supporting me throughout my studies and helping me getting a step closer to achieving my goals. I also want to thank my friends Aggelos, Anastasia, Anna, and Olga for helping me get through what proved to be

a challenging period. Finally, I thank my fellow graduate students Anastasia, Georgia, Krystalia, and Stelios for their company during the many hours in the lab.

Abstract

In recent years the need for a multivariate approach in the identification of taphonomic agents in Pleistocene localities has been highlighted. The aim of the present study is to identify the main biotic agent responsible for the modifications of large ungulate bones from the late Villafranchian fauna of the Lower Pleistocene locality Tsiotra Vryssi (Mygdonia basin, Greece). For this purpose, the study employs the analysis of skeletal part representation and gross bone damage patterns, as well as tooth mark frequency, spatial distribution, and morphometry. Skeletal part representation and gross bone damage patterns reveal intense ravaging, with a preferential deletion of nutrient dense elements and bone portions (stylopodial epiphyses and tibiae proximal halves). Carnivore tooth marks appear on all limb long bones, with varied spatial distribution and in different frequencies. The frequency of tooth-marking decreases from stylopodials, to zygopodials, and finally metapodials, which are only moderately tooth-marked. Tooth marks dimensions suggest that they were inflicted by a large carnivore. The intensity of bone modification and the bone consumption sequence indicates that the hyaenid *Pachycrocuta brevirostris* is the most fitting candidate for being the main agent of bone alterations at TSR. This hypothesis is reinforced by the similarities with the late Villafranchian fauna of Venta Micena in Spain, an assemblage interpreted as a bone accumulation and denning site of *Pachycrocuta brevirostris*. Finally, in order to acquire detailed quantitative data, a high-resolution 3D micromorphological analysis was conducted on selected tooth marks with the use of a confocal profilometer. This is the first time that such an analysis is employed for a Lower Pleistocene assemblage modified by carnivores from Europe and the first one, where *Pachycrocuta* constitutes the main biotic agent of bone modifications. This database will be a useful tool for future comparative analyses and will contribute to the taphonomic interpretation of other fossiliferous sites.

Περίληψη

Τα τελευταία χρόνια έχει επισημανθεί η αναγκαιότητα μιας πολυμεταβλητής προσέγγισης όσον αφορά τον προσδιορισμό των παραμέτρων που συνέβαλαν στην ταφονομική ιστορία πλειστοκαινικών θέσεων. Η παρούσα μελέτη έχει ως στόχο τον προσδιορισμό του κύριου βιοτικού φορέα που ευθύνεται για τις τροποποιήσεις οστών μεγάλων οπληφόρων ζώων της πανίδας του άνω Βιλλαφραγκίου από την θέση Τσιότρα Βρύση του Κάτω Πλειστόκαινου, (λεκάνη Μυγδονίας, Ελλάδα). Για το σκοπό αυτό χρησιμοποιούνται η ανάλυση της αντιπροσώπευσης των σκελετικών στοιχείων, τα πρότυπα καταστροφής των οστών, καθώς και η συχνότητα, η χωρική κατανομή και η μορφομετρία των δηγμάτων σαρκοφάγων. Η αντιπροσώπευση των σκελετικών τμημάτων και τα πρότυπα καταστροφής των οστών αποκαλύπτουν έντονη δράση σαρκοφάγων, με κατά προτίμηση κατανάλωση των πιο θρεπτικών σκελετικών στοιχείων και τμημάτων (επιφύσεις στυλοποδίων και εγγύς μισό κνήμης). Τα ίχνη από δαγκώματα σαρκοφάγων εμφανίζονται σε όλα τα επιμήκη οστά των άκρων, με ποικίλη χωρική κατανομή και σε διαφορετικές συχνότητες. Η συχνότητα των δηκτικών ιχνών μειώνεται από τα στυλοπόδια, στα ζευγοπόδια, και τέλος στα μεταπόδια, τα οποία εμφανίζουν ίχνη σε μέτρια συχνότητα. Οι διαστάσεις των ιχνών υποδηλώνουν ότι προκλήθηκαν από κάποιο σαρκοφάγο μεγάλου μεγέθους. Η σφοδρότητα της τροποποίησης των οστών και η αλληλουχία κατανάλωσή τους υποδεικνύει ότι η ύαινα *Pachycrocuta brevirostris* αποτελεί τον πιθανότερο κύριο φορέα αλλοιώσεων των οστών στη θέση. Αυτή η υπόθεση ενισχύεται από τις ομοιότητες με την απολιθωμένη πανίδα θηλαστικών του άνω Βιλλαφραγκίου Venta Micena στην Ισπανία, η οποία έχει ερμηνευθεί ως θέση συγκέντρωσης οστών και λημέρι της *Pachycrocuta brevirostris*. Τέλος, για την απόκτηση λεπτομερών ποσοτικών δεδομένων, πραγματοποιήθηκε τρισδιάστατη μικρομορφολογική μελέτη υψηλής ανάλυσης σε επιλεγμένα δηκτικά ίχνη με τη χρήση ομοεστιακού μικροσκοπίου. Αυτή είναι η πρώτη φορά που μια τέτοια ανάλυση εφαρμόζεται για μια απολιθωματοφόρα θέση του Κάτω Πλειστόκαινου της Ευρώπης, τα οστά της οποίας έχουν τροποποιηθεί από σαρκοφάγα, και η πρώτη, όπου η *Pachycrocuta*

αποτελεί τον κύριο βιοτικό παράγοντα τροποποίησης των οστών. Η παραχθείσα βάση δεδομένων θα αποτελέσει ένα χρήσιμο εργαλείο για μελλοντικές συγκριτικές αναλύσεις και θα συμβάλει στην ταφονομική ερμηνεία άλλων απολιθωματοφόρων θέσεων.

1. Introduction

1.1. Taphonomy

Taphonomy is the detailed study of the transition of organic remains from the biosphere to the lithosphere (Efremov, 1940). It includes the analysis of information loss and gain during death and burial, including alterations caused by predation and scavenging (Wilson, 1988). The taphonomic history of animal remains refers to the timeline of the taphonomic agents and processes that affected them (Lyman, 1994). A taphonomic agent is defined as the source of modification of animal carcasses, and can be either biotic (e.g., carnivores, humans) or abiotic (e.g., water, weathering) (Gifford-Gonzalez, 1991), while a taphonomic process is the action of a taphonomic agent on animal carcasses (Lyman, 1994). Although taphonomic processes such as transport, disarticulation, and breakage result in loss of information about the initial thanatocoenoses, they leave taphonomic signatures that can provide valuable insight into the paleobiology of fossil assemblages (Wilson, 1988; Fernández-López, 1991; De Renzi, 1997; Palmqvist and Arribas, 2001). Geological context and spatial distribution of fossils can indicate the paleoenvironment and the events that led to the formation of an assemblage, while the analysis of the fossils themselves can give further insight into their taphonomic history (Shipman, 1981). The study of bone modifications is an important part of any complete taphonomic analysis because it can provide information about the processes that lead to the formation of a bone assemblage, by identifying the actors that contributed to its creation (Fisher, 1995).

Carnivores are an important agent of bone modification that occurs during the consumption of blood, soft tissue, marrow and even the bones themselves (Gifford-Gonzalez, 2018). They modify bones mostly through the contact of their teeth with bone tissue (Binford, 1981). Apart from teeth to bone contact, licking can also significantly alter the morphology of bones, typically on their fractured edges

(Haynes, 1983). Carnivores perform a rather standardized sequence in the way they consume large carcasses, leaving parallel alterations across different taxa, although predator anatomy and contextual factors can influence the severity and placement of marks (Gifford-Gonzalez, 2018). Since modern carnivores can inflict recognizable gnaw damage, the same can be hypothesized about extinct species (Haynes, 1983).

In recent years, the need for standardization in methodology, as well as for a multivariate approach in taphonomic analysis has been highlighted. In this framework, standardized methods have been proposed for the quantification of both gross bone damage and bone surface modifications (e.g., Parkinson et al., 2014; Domínguez-Rodrigo et al., 2015; Pante et al., 2017).

1.2. Geological setting and fossiliferous Locality

The Mygdonia basin (Fig. 1.1) is a tectonic depression with east-west expansion, that started forming during the early–middle Miocene. Its geological history can be divided into two main periods. The first occurred during the Neogene–Early Pleistocene, when the basin was filled with fluvial/fluvio-torrential and lacustrine sediments. Subsequently, a new tectonic event that occurred in the early Middle Pleistocene segmented the basin into multiple smaller basins that were filled with sediments of primarily lacustrine nature (Psilovikos, 1977). The deposits of the Mygdonia Basin are divided into two main lithostratigraphic units, the Pre-Mygdonian Group that spans from the Neogene to the Early Pleistocene, and the Mygdonian Group from the Middle Pleistocene to the Holocene (Koufos et al., 1995). The Pre-Mygdonian group is subdivided into the Chryssavgi, the Gerakarou and, the Platanochori Formations (Koufos et al., 1995). Six late Villafranchian fossiliferous localities have been discovered in the upper part of the Gerakarou Formation: Gerakarou-1 (GER), Vassiloudi (VSL), Krimni-1 and -2 (KRI and KRM), Kalamoto-2 (KLT), and Tsiotra Vryssi (TSR) (Fig 1.2) (Koufos et al., 1995; Tsoukala and Chatzopoulou, 2005; Konidaris et al., 2015).

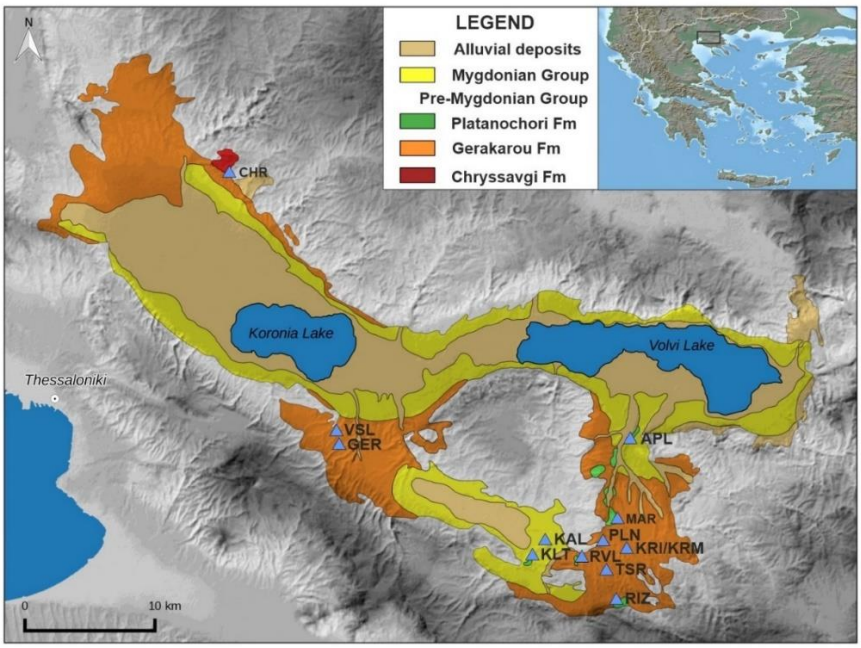

Figure 1.1: Geological map with the Neogene and Quaternary lithostratigraphic units, and the fossiliferous localities of the Mygdonia Basin (taken from Konidaris et al., 2021; modified from Konidaris et al., 2015; data from Koufos et al., 1995).

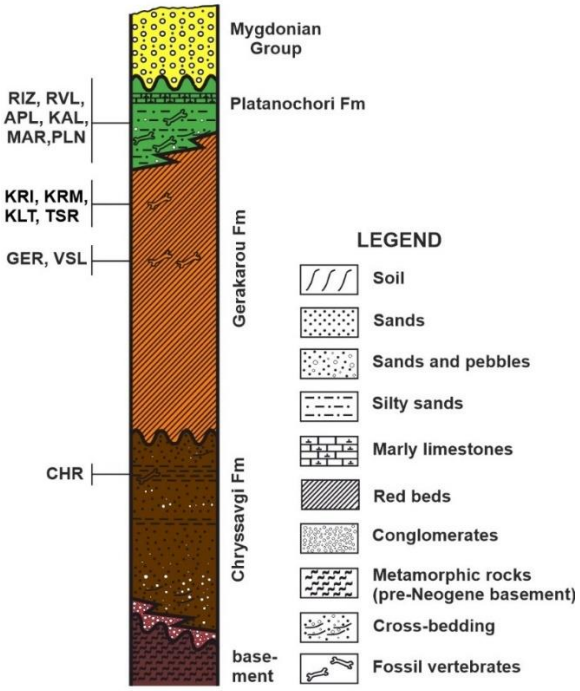

Figure 1.2: Simplified composite stratigraphic column of the Mygdonia basin (taken from Konidaris et al., 2021; data from Koufos et al., 1995).

The fossiliferous locality Tsiotra Vryssi (TSR) is located southeast of Thessaloniki (Central Macedonia, Greece) (Fig. 1.1). It was discovered in 2014 during a targeted survey by a joint team from the Aristotle University of Thessaloniki and the Eberhard Karls University of Tübingen (Konidaris et al., 2015), and has since yielded a wealth of large mammal fossils (Fig. 1.3), as well as some micromammals, reptiles, and birds. Two main depositional units have been identified in TSR, Geo 1 and the fossiliferous Geo 2 (Giusti et al., 2019). The spatial distribution of the fossil remains suggests that the deposition is a result of multiple dispersion events and anisotropic rearrangement of a lag, autochthonous assemblage. The accumulation of fossils occurred on the banks of a migrating northwest-southeast oriented fluvial system (Giusti et al., 2019). Cosmogenic radionuclide, magnetostratigraphy and biochronological data reveal a dating of 1.78–1.5 Ma for the locality (Konidaris et al., 2021). The preliminary faunal list of the large mammals is given in Table 1.1.

Order	**Family**	**Genus**	**Species**
Proboscidea	Elephantidae	*Mammuthus*	*meridionalis*
Carnivora	Canidae	*Canis*	sp.
	Ursidae	*Ursus*	*etruscus*
	Hyaenidae	*Pachycrocuta*	*brevirostris*
	Felidae	*Megantereon*	sp.
Perissodactyla	Equidae	*Equus*	sp. (medium-sized)
		Equus	sp. (large-sized)
	Rhinocerotidae	*Stephanorhinus*	sp.
Artiodactyla	Giraffidae	*Palaeotragus*	sp.
	Cervidae	*Cervus*	sp.
		Praemegaceros	sp.
	Bovidae	*Pontoceros*	sp.
		Leptobos	sp.
		Bison	cf. *degiulli*

Table 1.1: Preliminary faunal list of the large mammals from Tsiotra Vryssi (Konidaris et al., 2021).

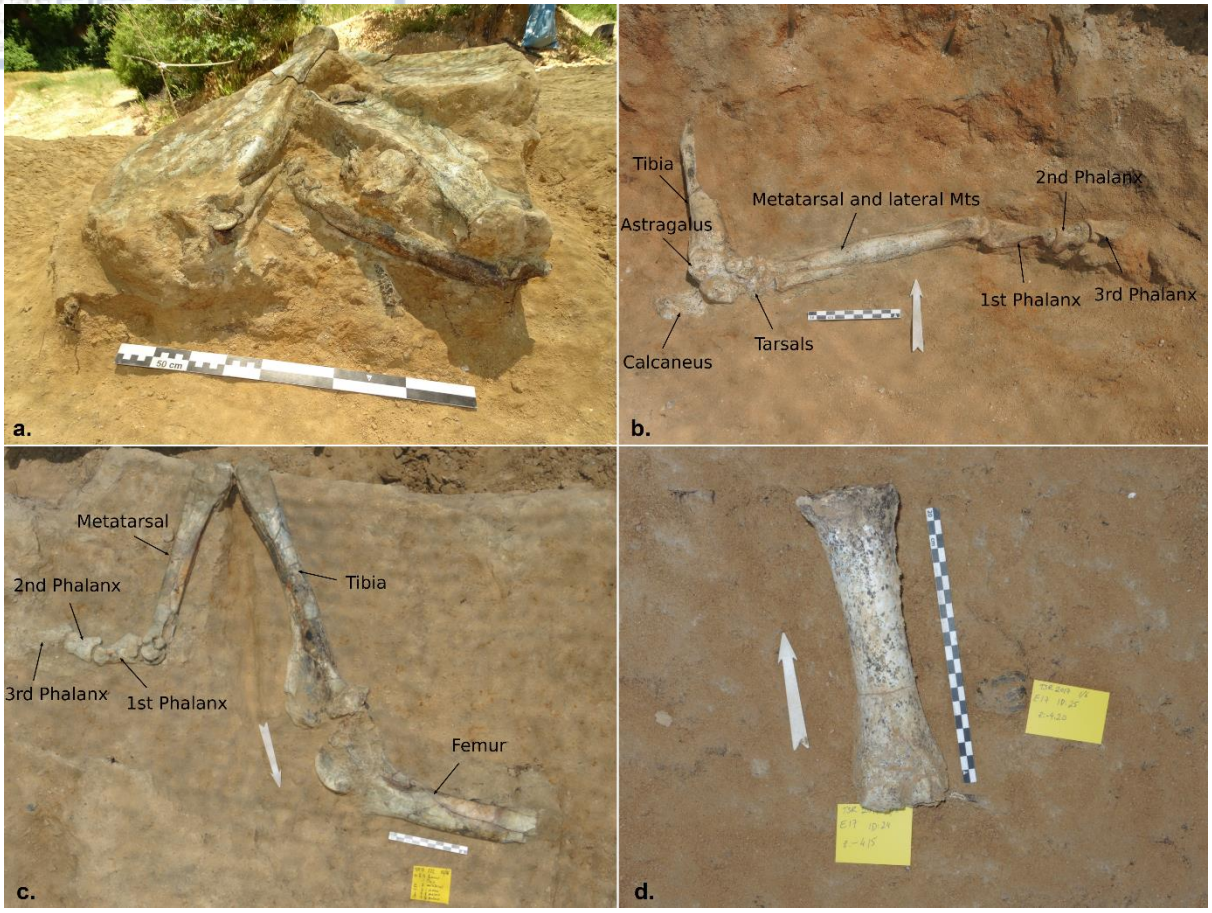

Figure 1.3: Excavation photos from Tsiotra Vryssi. (a) Concentration of various skeletal elements, (b) articulated partial hind limb of *Equus* sp., (c) articulated partial hind limb of a Bovini individual, (d) metacarpal of *Bison* cf. *degiulli*. (Photographs courtesy of and copyright PaGE and CROSSROADS projects).

2. Materials and methods

2.1. Studied Material

The studied material originates from the locality Tsiotra Vryssi and consists of ungulate bones, which belong to the size groups 4 and 5 of Palombo (2010), i.e., 150–1000 kg (Table 2.1). Size group 4 includes both the medium- and the large-sized *Equus* species, and size group 5 the Bovini *Bison* cf. *degiulli* and *Leptobos* sp., the giraffid *Palaeotragus* sp. and the deer *Praemegaceros* sp. (see Sections 2.2.1 and 3.1). Additionally, all collected bones that could not be taxonomically identified, but belong to either size group 4 or 5, were included in the analyses. The material includes specimens collected during the excavation seasons of 2014–2019. The material is stored at the Museum of Geology, Palaeontology and Palaeoanthropology of the Aristotle University of Thessaloniki (LGPUT).

2.2. Methodology

2.2.1. Body mass estimations

The different prey taxa were classified by size following the size categories of Palombo (2010) (Table 2.1). This classification takes into account, among other parameters, the prey-predator relationships including the hunting behaviour of Early and Middle Pleistocene predators and the size of their most common prey.

Size groups	Kg
Group 1	≤10
Group 2	10–49
Group 3	50–149
Group 4	150–349
Group 5	350–1000
Group 6	≥ 1000

Table 2.1: Size groups proposed by Palombo (2010) and their respective body mass ranges in kg.

The body weight of the *Equus* individuals was calculated according to the method of Eisenmann and Sondaar (1998) for estimating weight using metapodial variables. Only metapodials that belong to complete/partially complete front and hind limbs of subadult juvenile – adult individuals were taken into consideration. These individuals were identified following the epiphyseal bone fusing sequence in horses (Budras et al., 2011). More specifically, for the front limb, the criterion used was the fusion of the distal radial epiphysis, that occurs between 20–24 months of age. For the hind limb, the criterion used was the fusion of the tibial distal epiphysis, that occurs between 17–24 months of age. The equations for weight estimation proposed by Eisenmann and Sondaar (1998) are the following:

For metacarpals: Ln of the weight = -4.525 + 1.434 (Ln of the product of MC10 by MC13). R = 0.94

For metatarsals: Ln of the weight = -4.585 + 1.443 (Ln of the product of MT10 by MT13). R = 0.94

where MC10 and MT10 refer to the distal supra-articular width of the third metacarpal and metatarsal, respectively, while MC13 and MT13 refer to the distal minimal depth of the medial condyle of the third metacarpal and metatarsal, respectively (Eisenmann et al., 1988).

The body mass of *Palaeotragus* sp. and *Praemegaceros* sp. was calculated according to the prediction equations of Damuth and MacFadden (1990). The equations used regard both dental and postcranial measurements. More specifically, for *Palaeotragus* dental elements, the equations used were those applying to all selenodonts, based on the length of M_1, M_2 and M_3. For postcranial elements, the equations regarding artiodactyls were applied, based on metatarsal measurements (M1, M2, M3, M4, M6 and M7). For *Praemegaceros* dental

elements, the equations for all selenodonts were applied for M^1 and M^2 lengths. For postcranial elements the equations used regard cervids only, for measurements of the distal tibia (T4, T5). For each genus, the mean value was calculated for the mass values resulting from dental and postcranial measurements separately, and then a total mean from those two results was computed. This last mean is the value used as the estimated body mass.

The body mass of *Bison* cf. *degiulli* was taken from Kostopoulos et al. (2018), where a mass of 600 kg is estimated for the early bison of Mygdonia. For *Leptobos* sp., the body mass of *L. etruscus* (426 kg) was used, which was taken from Maniakas (2019).

2.2.2. Skeletal part representation

NISP - MNE - MNI - MAU - articulated/isolated elements

The representation of skeletal parts is provided in terms of number of identified specimens (NISP), minimum number of elements (MNE), minimum number of individuals (MNI) and minimum animal units (MAU). The MNE was calculated taking into account anatomical overlap between fragments by determining their location on the complete bone, as well as the size of individuals and their ontogenetic age based on the fusion of epiphyses. MNE is calculated separately for long limb bones of *Equus*, Bovini, *Palaeotragus* and *Praemegaceros*. MAU was calculated according to Binford (1984), where the MNE of each element is divided by the number of times it appears in one complete skeleton. MAU values are given separately for each taxon, as well as for the indeterminate specimens, and the total sample. MNI was calculated based on the MNE values, and following Howard (1930), where it is defined as the number of the left or right skeletal element occurring in greatest abundance. Additionally, the percentage of articulated and isolated elements was calculated for all long limb bones. As articulated we regard two or more adjoining elements that appear connected (Fourvel and Mwebi, 2011).

Bone damage patterns

The representation of surviving bone portions was studied for each element as described by Marean and Spencer (1991). These authors separate each element to a proximal and distal end, a proximal and distal shaft, and a middle shaft (Fig. 2.1). The surviving portions were recorded for each long limb bone element.

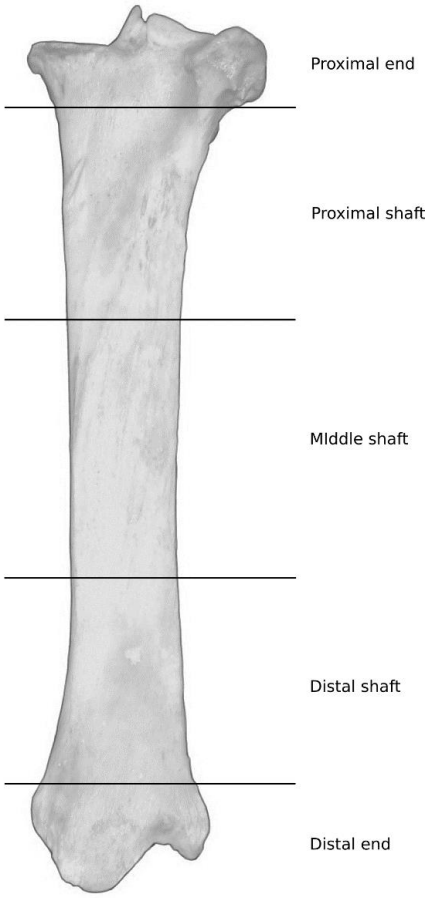

Figure 2.1: Bone portions of a tibia as described by Marean and Spencer (1991).

Domínguez-Rodrigo et al. (2015) introduced a new methodology for quantifying damage in long limb bones (humerus, femur, radius-ulna, tibia), based on taphotypes. The word taphotype refers to the variability caused by taphonomic agents (Wauthoz et al., 2003). In their study, Domínguez-Rodrigo et al. (2015)

present two approaches: the paleontological and neotaphonomic (Classification system I) (CSI) and the archaeological approach (Classification system II) (CSII). The first approach was applied in the present study. This system is used for long limb bones and bone fragments of which the complete diaphyseal circumference is preserved, classifying them in 16 taphotypes (Fig. 2.2). Each taphotype corresponds to the deletion of specific bone portions as described below.

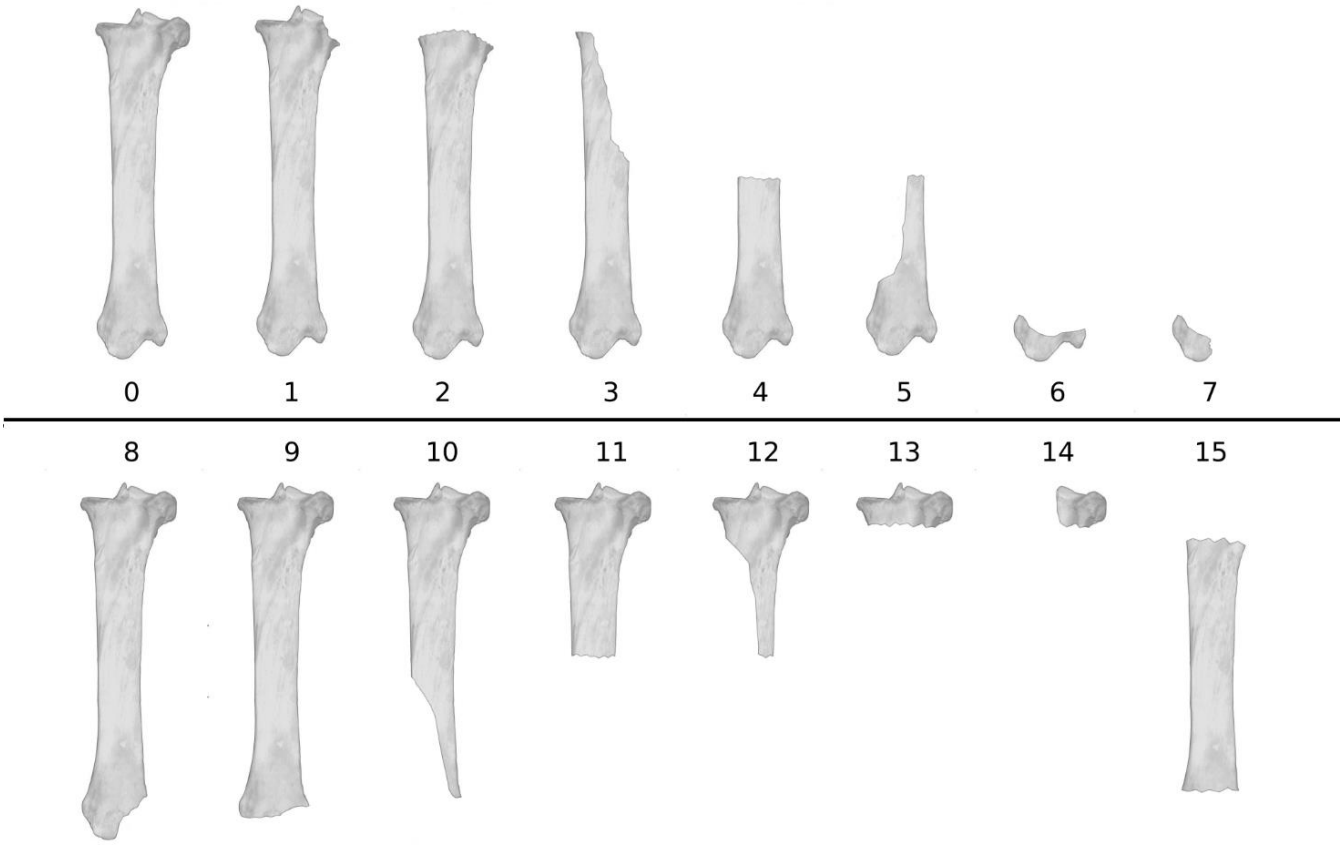

Figure 2.2: The taphotypes proposed by Domínguez-Rodrigo et al. (2015). Schematic representation in a tibia of a horse.

0. Complete bone
1. Almost complete bone where part of the proximal epiphysis is modified.
2. Deletion of the proximal epiphysis. (In taphotypes 3 through 7 the proximal end is considered deleted).
3. Deletion of a minimum of one fourth of the proximal half of the shaft. The destruction can extend to the distal half of the shaft, provided that a substantial part of the proximal shaft is still present.
4. Deletion of the proximal half of the shaft (approximately).
5. Deletion of the proximal half of the shaft, in addition to a minimum of one fourth of the distal half of the shaft.
6. Deletion of the whole shaft, with survival of the distal end and, if present, the immediate near-epiphysis.
7. Similar to taphotype 6, with the additional modification or deletion of the of the distal epiphysis.
8. Almost complete bone where part of the distal epiphysis is modified.
9. Deletion of the distal epiphysis. (In taphotypes 10 through 14 the proximal end is considered deleted).
10. Deletion of a minimum of one fourth of the distal half of the shaft. The destruction can extend to the proximal half of the shaft, provided that a substantial part of the distal shaft is still present.
11. Deletion of the distal half of the shaft.
12. Deletion of the distal half of the shaft, in addition to a minimum of one fourth of the proximal half of the shaft.
13. Deletion of the whole shaft with survival of the proximal end.
14. Survival of the proximal epiphysis, with possible modification or partial deletion.
15. Cylindrical shaft fragment with both ends deleted.

The possible correlation of mineral density, marrow cavity volume, fat weight and abundance of epiphyses was examined through regression analysis following

the methodology of Palmqvist and Arribas (2001). The bone mineral density values are expressed in grams per cubic centimetre (g/cm^3) and the marrow content in grams (g). Data for mineral density is taken from Lam et al. (1999), and for marrow content from Outram and Rowley-Conwy (1998).

2.2.3. Carnivore tooth mark analysis

Tooth mark identification

All specimens were examined for the presence of bone surface modifications under strong light and magnification lenses. Tooth marks were identified according to the criteria of Binford (1981), Eickhoff and Herrmann (1985) and Pobiner (2008) and classified into four basic types: pits, punctures, scores, and furrows. More specifically:

i. Tooth pits and punctures have a circular, oval, or polygonal shape and a bowl-shaped cross section. Their long axis is at most three times the length of their short axis. They are formed as pressure is directly applied from teeth on the surface of bones. Pits are relatively shallow deformations of histological structure that do not penetrate the whole thickness of compact cortical bone. Punctures are larger than pits and are formed when the bone collapses under the tooth. They may penetrate all the layers of compact cortical bone (Fig. 2.3).

ii. Tooth scores and furrows are linear with U-shaped cross sections that usually have a smooth base. Their length can vary as well as their orientation, which is usually more or less perpendicular or transverse in relation to the long axis of long bones. Scores and furrows are formed when teeth are dragged across the bone surface. Tooth scores are shallower and smaller than furrows and, unlike the latter, do not penetrate the cortical surface of compact bone (Fig. 2.4). Furrowing is the deletion caused by gnawing of cancellous bone (Haynes, 1980; Domínguez-Rodrigo et al., 2012).

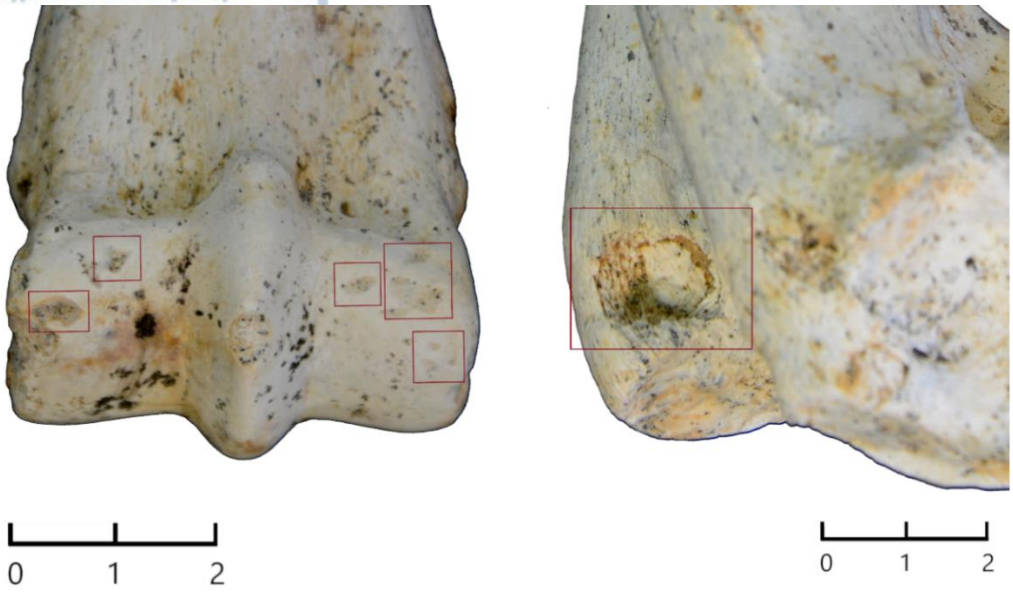

Figure 2.3: Pits on the distal part of an equid metatarsal (specimen F18-41; left) and puncture on the distal part of an equid humerus (specimen G20-6; right). Scale in cm.

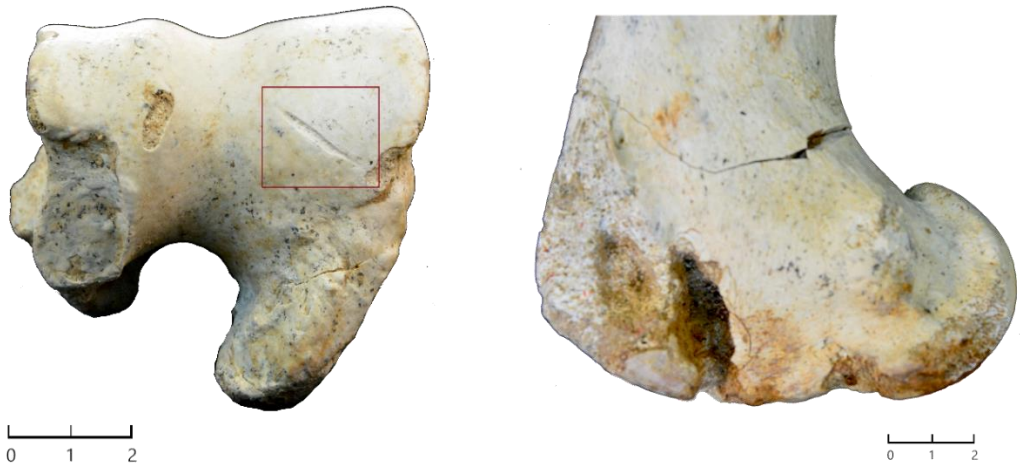

Figure 2.4: Score on the distal part of an equid humerus (specimen G20-6); left) and furrowing on the distal part of an equid femur (specimen H21-11); right). Scale in cm.

Frequencies and anatomical distribution

The percentage of tooth-marked elements was calculated separately in *Equus* and Bovini for cervical vertebrae, scapulae, pelves, humeri, radio-ulnae, metacarpals, femora, tibiae, metatarsals and phalanges. Additionally, for all long bones, the presence of different types of tooth modification was noted for each bone portion (proximal epiphysis, proximal shaft, middle shaft, distal shaft, distal epiphysis), following the bone portion classification of Marean and Spencer (1991).

Additionally, GIS image analysis proposed by Parkinson et al. (2014) was performed, using QGIS (https://www.qgis.org/en/site/). The exact location of each tooth mark was plotted for the anterior, posterior, lateral, medial, proximal, and distal view of each bone. All marks were plotted on elements of the right side. A different layer was created for each tooth mark category (pits, scores, punctures), where information about the dimensions (length and width), bone section and specimen ID were also noted. Pits and punctures were plotted in point feature layer files, while scores were plotted in linear feature layer files. Furthermore, an additional point feature layer file was created where all types of tooth marks were plotted. The scores were represented by points in the middle of each linear feature that corresponded to the initial score. This layer file was used to conduct a spatial analysis for all tooth marks. For each element, a heatmap of tooth mark density (Kernel Density Estimation) was created, for all views of the bone that exhibited tooth marks. The GIS method was applied to equid and bovid specimens separately, for each different type of long bone. Cervid, giraffid and unidentifiable bones were excluded, as their number was very small (in many cases only one specimen for each element was available) for this kind of analysis.

Macroscopic and microscopic metrical analysis

Tooth marks were measured with the use of a digital calliper at 0.01 mm precision directly on the bones, under strong light and magnification. Length and breadth measurements were taken for each pit, score, and puncture. The measured length refers to the maximum dimension of the mark, while breadth

refers to the maximum dimension transversal to length (Andrés et al., 2012). The bone portion of each tooth mark was also recorded. Tooth marks with unclear borders due to extensive pitting or scoring were not measured.

The mean length and width values of the tooth marks were plotted along with data from actualistic studies conducted by Domínguez-Rodrigo and Piqueras (2003), Delaney-Rivera et al. (2009), Sala et al. (2012, 2014), Andrés et al. (2012), and Yravedra et al. (2014). Statistical analysis was conducted for tooth marks that were abundant both in the *Equus* and Bovini sample. Those included scores on middle shafts and pits on epiphyses and middle shafts. The Shapiro-Wilk test was employed, to investigate the possibility of normal distribution in each sample and the Mann-Whitney test, to compare statistical differences in length and width between the *Equus* and Bovini samples. Statistical analyses were performed with PAST v. 4.03 (Hammer et al., 2001; https://www.nhm.uio.no/english/research/infrastructure/past/).

Sampling: A sample of tooth marks was also studied digitally following the methodology of Pante et al. (2017). These authors propose a standardized and replicable method for quantifying microscopic characteristics of bone surface modification. The selection was random and was not influenced by the size and placement of the tooth marks. The study of the TSR tooth marks was performed using replicas of the original marks. It has been proven that replicas can provide highly accurate data, often even better than the original specimens (Bello et al., 2011). All selected marks were cleaned with cotton swabs and water, or acetone, when necessary. High resolution silicone, President MicroSystemTM (Coltène) regular body dental impression, was used to create imprints (moulds) of the selected tooth marks. Then, replicas of the tooth marks were made by filling the moulds with a mixture of Epo-Tek 301 epoxy resin and hardener.

Scanning and processing of 3D reconstructions: The scanning procedure was performed in the laboratory of the Palaeoanthropology Section of the Eberhard Karls University of Tübingen. 3D reconstructions of the tooth marks were produced using a Sensofar Plμ Neox Confocal Imaging Profiler with 10×

objective lens with a vertical resolution of <50 nm, a lateral sampling interval of 1.66 mm, and an aperture of 0.30. Each tooth mark was represented by multiple neighbouring scans that were then patched together. The 3D reconstructions acquired were then processed using SensoMAP 7.4 software following the methodology of Pante et al. (2017).

The first step was to combine the different scans of each sample into one singe studiable using the “Patch” operator. Following this, the non-measured points were filled using the “Fill non measured points” operator, and more specifically the algorithm that creates a smooth shape by filing the missing points based on calculations from neighbouring points (Fig. 2.5). Next, in order to produce a more defined image of the tooth mark, the form of the bone is removed, using the “Remove form” operator, so that the area outside the mark appears as level as possible (Figs. 2.6, 2.13). The marks themselves are excluded from the form correction, so their shape is not affected. The polynomial algorithm method was applied, with usually a degree of 3 or 4, while some specimens with particularly uneven surfaces required a higher polynomial degree. The last step before the measuring of the parameters was the extraction of each mark separately, in the cases where more than one mark was present.

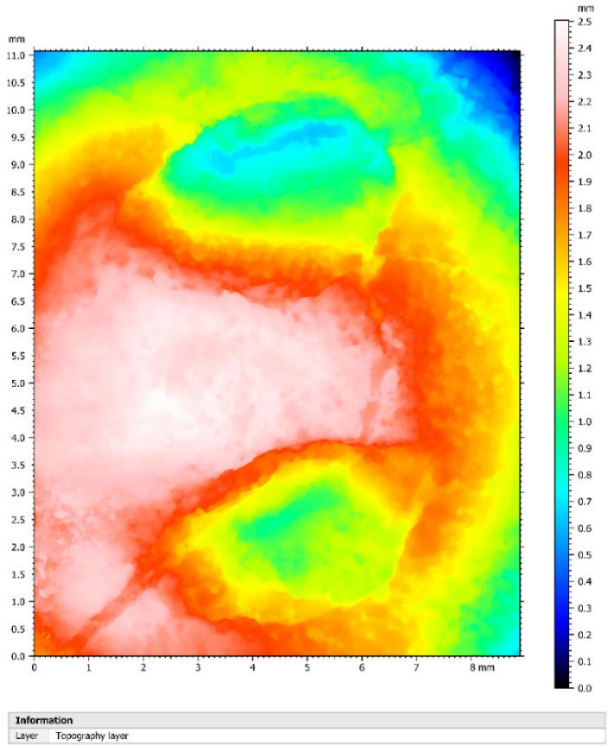

Figure 2.5: Studiable with non – measured points filled in.

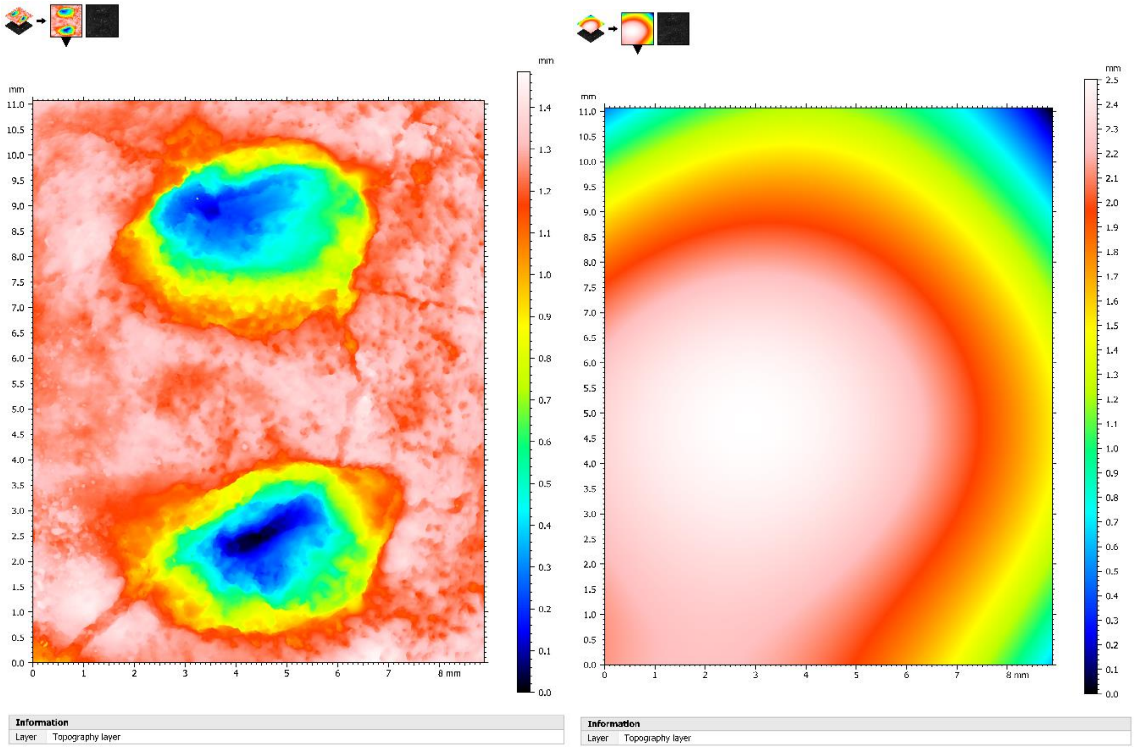

Figure 2.6: Studiable after the removal of the bone form (left) and the removed form (right).

Measuring of 3D reconstructions: The measurements taken for each mark are the following: length, width, projected area, volume, maximum depth, mean depth.

The length and width of the mark were measured using the “Distance” tool. As mentioned previously, the length and width correspond to the definition of Andrés et al. (2012), where length is the maximum dimension of the mark and breadth the maximum dimension transversal to length (Fig. 2.7.).

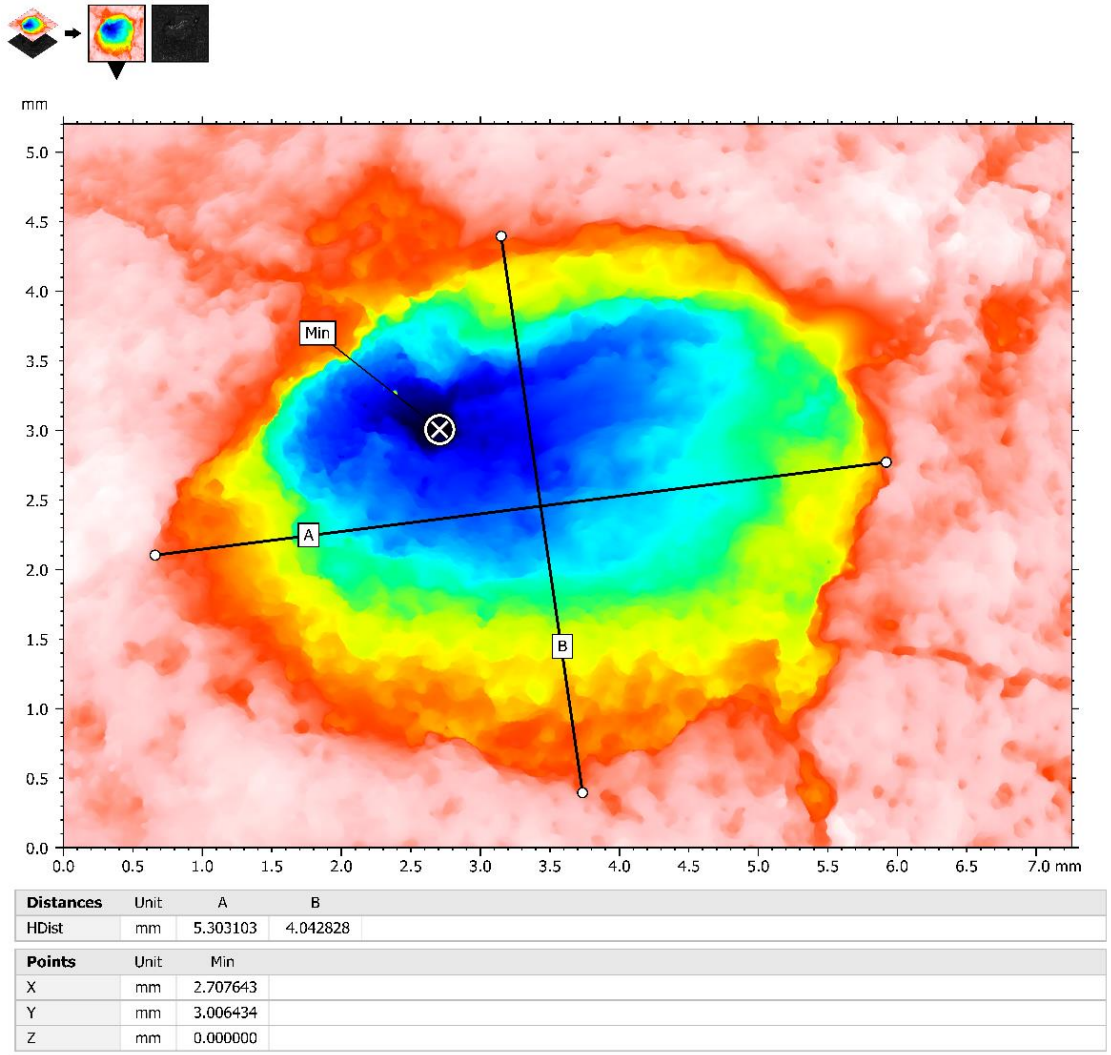

Distances	Unit	A	B
HDist	mm	5.303103	4.042828

Points	Unit	Min
X	mm	2.707643
Y	mm	3.006434
Z	mm	0.000000

Figure 2.7: Distance measurement using the “Distance” tool.

The other measurements were acquired using the “Volume of a hole” function, with the least squares plane method. The area of the mark is manually selected by creating an outline of the exact borders of each mark, identified by the first colour change in the image (Fig. 2.8). The measurements provided by this function are the projected area (surface area of the tooth mark), volume (volume of bone missing), maximum and mean depth of the mark.

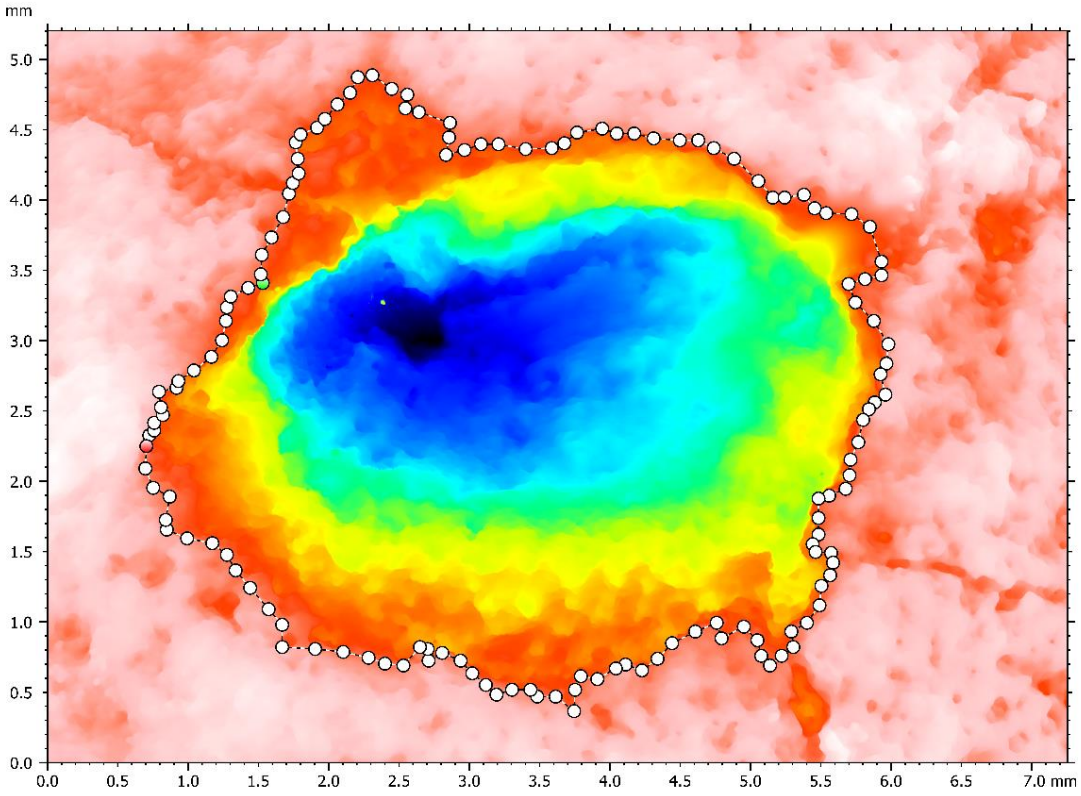

Parameters	Unit	Hole
Projected area	mm²	16.315648
Volume	mm³	8.839547
Max. depth/height	mm	1.167045
Mean depth/height	mm	0.541783

Figure 2.8: Tooth mark area measurements using the “Volume of a hole” function.

The rest of the measurements taken relate to the central and deepest profiles of each tooth mark (Fig. 2.9). Firstly, the studiable of the tooth mark is

rotated on its major axis and cropped to its top and bottom margins. Then the "Extract profile" operator is employed to create a profile that represents the middle of the mark (longitudinally), and one that passes through the deepest point of the mark, both perpendicular to its major axis.

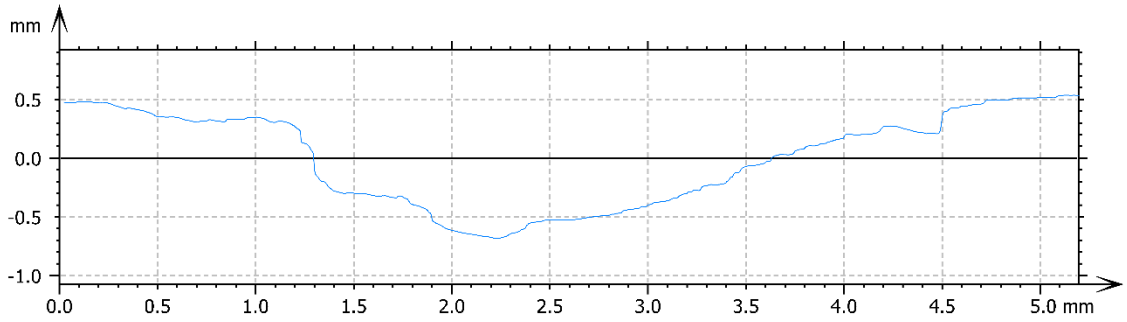

Parameters	Value	Unit
Length	5.197765	mm

Figure 2.9: Image of the initial profile.

The values measured for both profiles are depth, area, width, opening angle, floor radius and roughness (Ra). Maximum depth and area were calculated using the "Area of a hole" function, with the "Under the waterline" option (Fig. 2.10.).

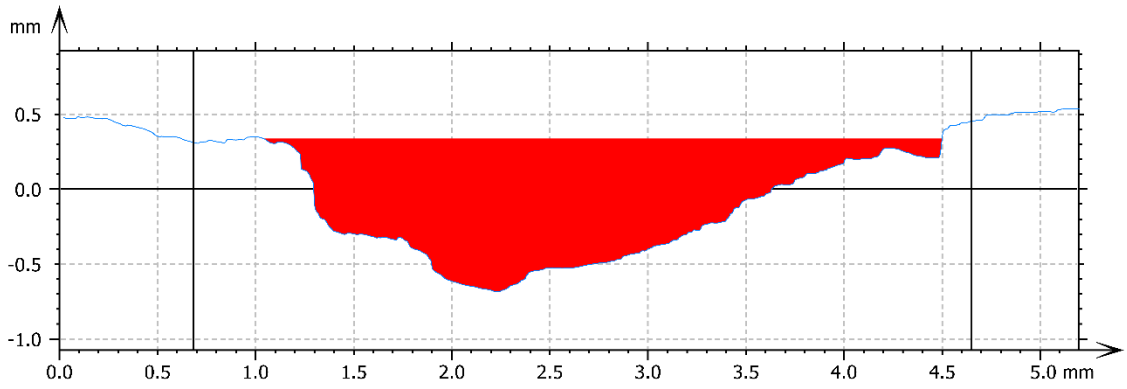

Parameters	Value	Unit
Maximum depth	1.034263	mm
Area of the hole	1.940021	mm²

Figure 2.10: Maximum depth and area measurements using the "Area of a hole" function.

The coordinates of the edges of the mark based on the “waterline” were recorded in order to extract the section of the profile that reflects the actual mark using the “Extract area” function. The remaining measurements concern the extracted profile (Fig. 2.11). The total length of the extracted profile reflects the width of the mark. Roughness (Ra) refers to the arithmetic mean deviation from the roughness profile, which is the mean line recorded in the evaluation length. It is provided in the “Parameters table”.

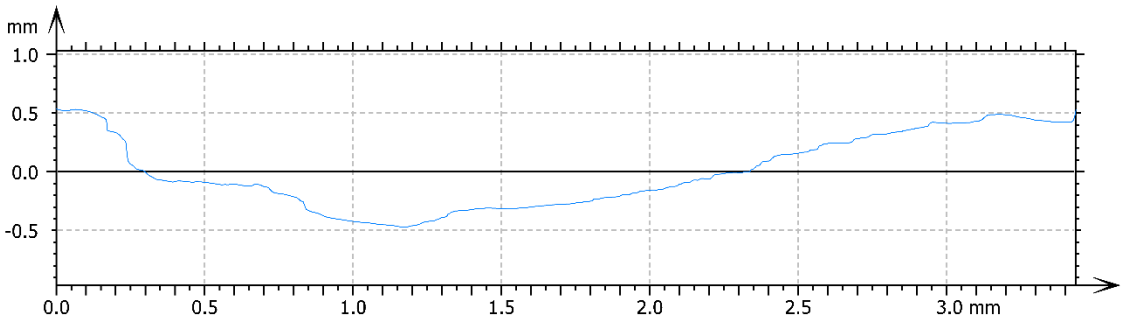

Parameters	Value	Unit
Length	3.436402	mm

Figure 2.11: Image of the extracted profile, representing the actual tooth mark.

Lastly, contour analysis was performed to measure the opening angle and floor radius of both profiles (Fig. 2.12). The opening angle is measured by calculating the angle between two segments, one of which spans from the first measured point to the deepest point of the extracted profile, and the second from the deepest to the last measured point. The flour radius is calculated from an arc that starts at the first measured point and terminates at the last point of the extracted profile. It represents the best fit of all the profile points.

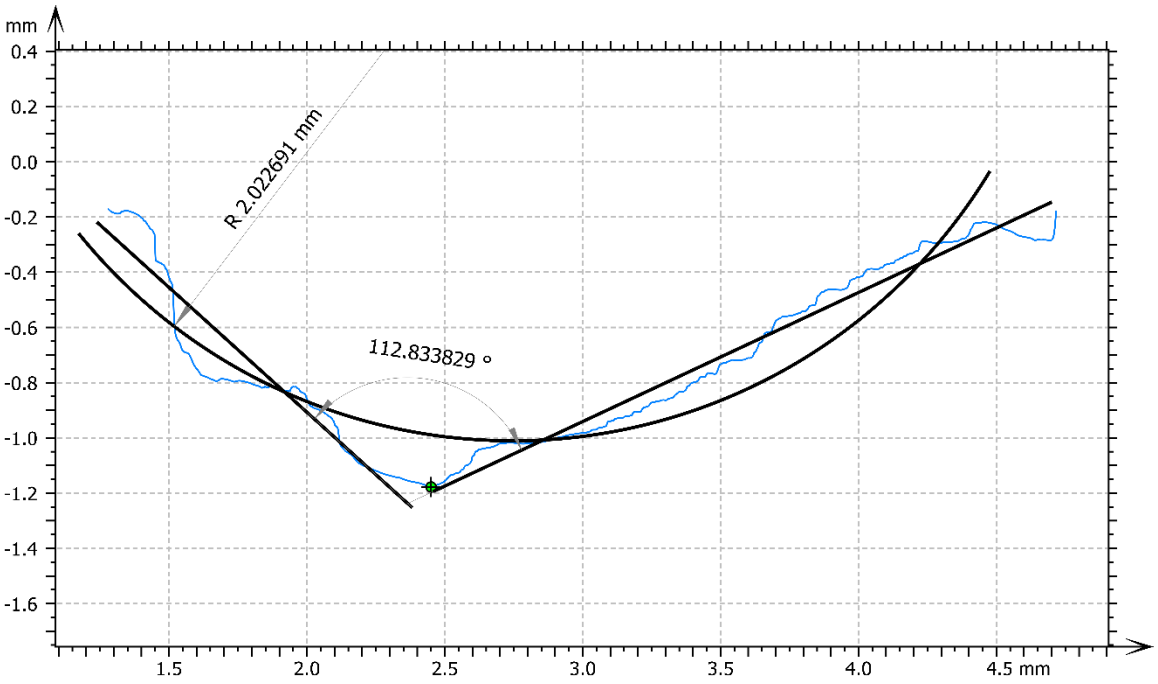

Figure 2.12: Contour analysis where the opening angle and floor radius of the profile are measured.

Statistical analysis was performed for the pit measurements, to investigate variation between the *Equus* (size group 4) and Bovini (size group 5) samples. The normal distribution of all samples was investigated through the Shapiro-Wilk normality test. The possible statistical differences between the two samples were tested using either the Mann - Whitney test, for pairs that did not display normal distribution, or the *t*-test, for pairs where both variables displayed normal distribution.

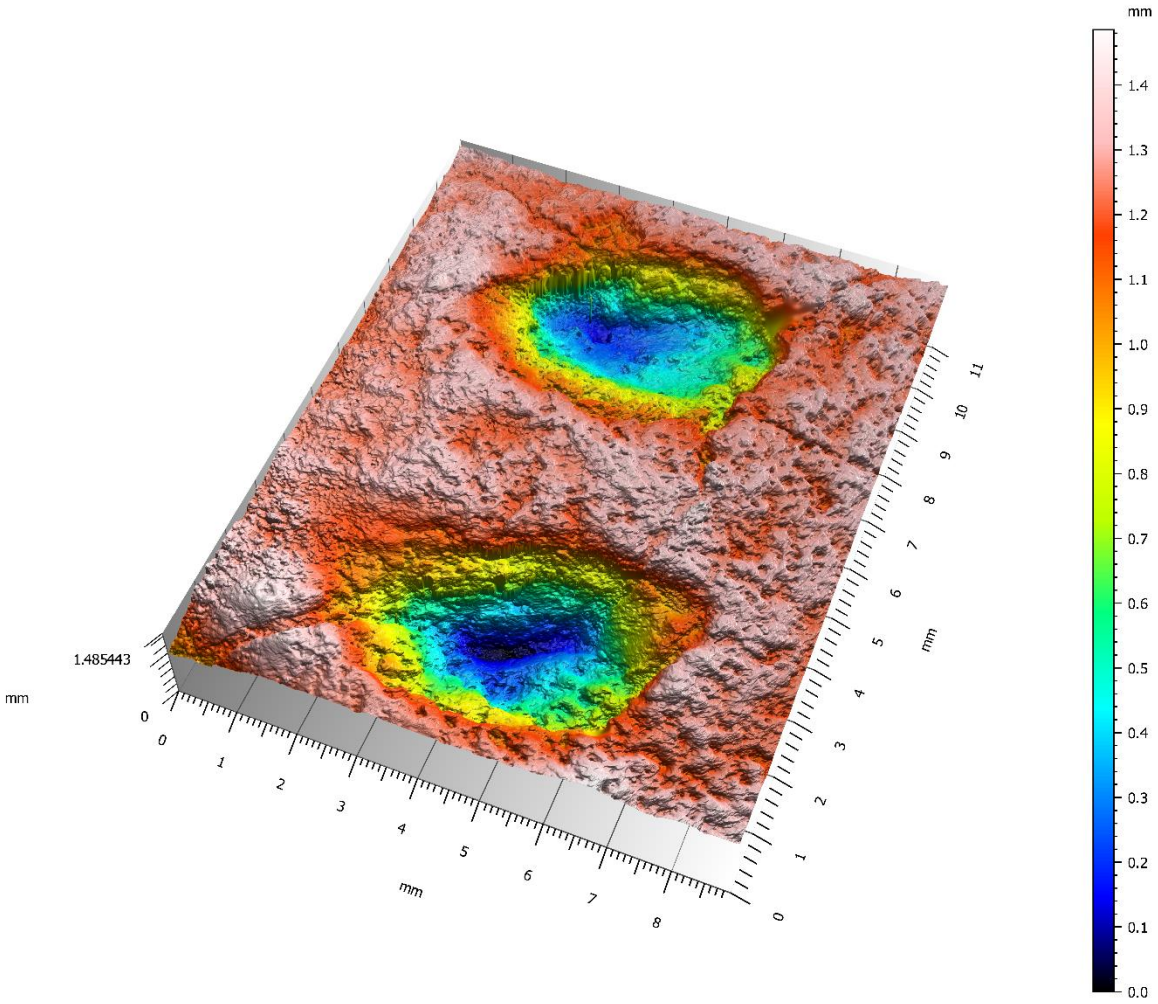

Figure 2.13: 3D depiction of patched studiable after the removal of the bone form.

3. Results

3.1. Body mass estimations

The mean body mass (subadult juvenile and adult individuals, i.e., excluding young juveniles) of the medium-sized *Equus* species is estimated at 257 kg, and for the large-sized one at 343 kg. They both fall in Palombo (2010)'s size group 4 (150–349 kg). For *Praemegaceros*, the mean body mass, estimated from both cranial and postcranial variables is 478 kg, classifying it in Palombo (2010)'s size group 5 (350–1000 kg). For *Palaeotragus*, the estimate for the mean body mass is 896 kg, classifying it in size group 5, as well. Considering also a mean body mass of 426 kg and 600 kg for *Leptobos* and *Bison*, respectively (Kostopoulos et al., 2018; Maniakas, 2019), all the Bovini sample is included in size group 5.

3.2. Skeletal part representation

NISP - MNE - MNI - MAU - articulated/isolated elements

In order to understand the processes involved in the accumulation and modification of the assemblage and assess whether any specific pattern of bone survivorship exists, the frequency of skeletal parts was analysed. The representation of skeletal parts is provided in terms of number of identified specimens (NISP; Table 3.1), minimum number of elements (MNE; Table 3.2) and minimum animal units (MAU; Table 3.3; Figure 3.1). NISP values are given for all elements while MNE values are focused on long limb bones and MAU on axial and long limb bone elements. All values are provided separately for *Equus,* Bovini, *Palaeotragus* and *Praemegaceros*. MNE values show that metapodials are abundant in both *Equus* and Bovini. *Equus* tibiae are very abundant as well. The femur is the least represented element in both. *Palaeotragus* and *Praemegaceros* are represented only by few specimens. MAU values clearly suggest a preferential accumulation / preservation of tibiae and metapodials.

NISP						
	EQUUS	**BOVINI**	***PALAEOTRAGUS***	***PRAEMEGACEROS***	**INDET.**	**TOTAL**
atlas	4	1	0	0	0	5
axis	3	1	0	0	0	4
3rd-6th cervical vertebrae	12	0	0	0	3	15
7th cervical vertebrae	2	0	0	0	0	2
other vertebrae	0	0	0	0	6	6
sacrum	1	0	0	0	0	1
scapula	11	2	0	0	2	15
pelvis	2	2	1	0	5	10
humerus	11	7	0	0	2	20
radius	11	7	1	0	1	20
ulna	3	6	0	0	3	12
metacarpal	25	12	1	0	0	38
femur	7	3	0	0	0	10
tibia	26	8	0	1	4	39
metatarsal	22	13	1	0	0	36
lateral metapode	53	3	0	0	0	56
carpals	61	31	0	0	0	92
astragalus	14	8	2	1	1	26
calcaneus	13	7	1	0	3	24
other tarsals	39	21	0	0	1	61
phalanx I	23	15	1	2	0	41
phalanx II	17	19	0	1	0	37
phalanx III	23	12	1	2	0	38
patella	0	1	0	0	0	1
other sesamoids	47	41	0	0	1	89
metapode indet.	6	0	0	0	0	6
Total	436	220	9	7	0	672

Table 3.1: NISP values for *Equus,* Bovini, *Palaeotragus, Praemegaceros*, indeterminate size group 4/5 fragments (indet.) and total.

MNE						
	Equus			**Bovini**		
	dex	**sin**	**total**	**dex**	**sin**	**total**
humerus	5	6	11	2	3	5
radio-ulna	5	5	10	3	4	7
metacarpal	13	12	25	7	5	12
femur	3	4	7	2	1	3
tibia	15	10	25	5	3	8
metatarsal	13	8	21	6	7	13
	Palaeotragus			***Praemegaceros***		
	dex	**sin**	**total**	**dex**	**sin**	**total**
humerus	0	0	0	0	0	0
radio-ulna	0	1	1	0	0	0
metacarpal	1	0	1	0	0	0
femur	0	0	0	0	0	0
tibia	0	0	0	1	0	1
metatarsal	1	0	1	0	0	0

Table 3.2: MNE values for *Equus,* Bovini, *Palaeotragus* and *Praemegaceros* long limb bones.

MAU per taxon						
	Equus	**Bovini**	***Palaeotragus***	***Praemegaceros***	**Indet.**	**Total**
atlas	4	1	0	0	0	5
axis	3	1	0	0	0	4
3rd- 7th cervical vertebrae	2.8	0	0	0	0.6	3.4
sacrum	1	0	0	0	0	1
scapula	5.5	1	0	0	1	7.5
humerus	5.5	3.5	0	0	1	10
radius	5	3.5	0.5	0	0.5	9.5
ulna	1.5	3	0	0	1.5	6
metacarpal	12.5	6	0.5	0	0	19

pelvis	2	2	1	0	4	9
femur	3.5	1.5	0	0	0	5
tibia	12.5	4	0	0.5	2	19
astragalus	7	4	1	0.5	0.5	13
calcaneus	6.5	3.5	0.5	0	1.5	12
metatarsal	10.5	6.5	0.5	0	0	17.5

Table 3.3: MAU values for *Equus,* Bovini, *Palaeotragus, Praemegaceros,* indeterminate size group 4/5 fragments (indet.) and total.

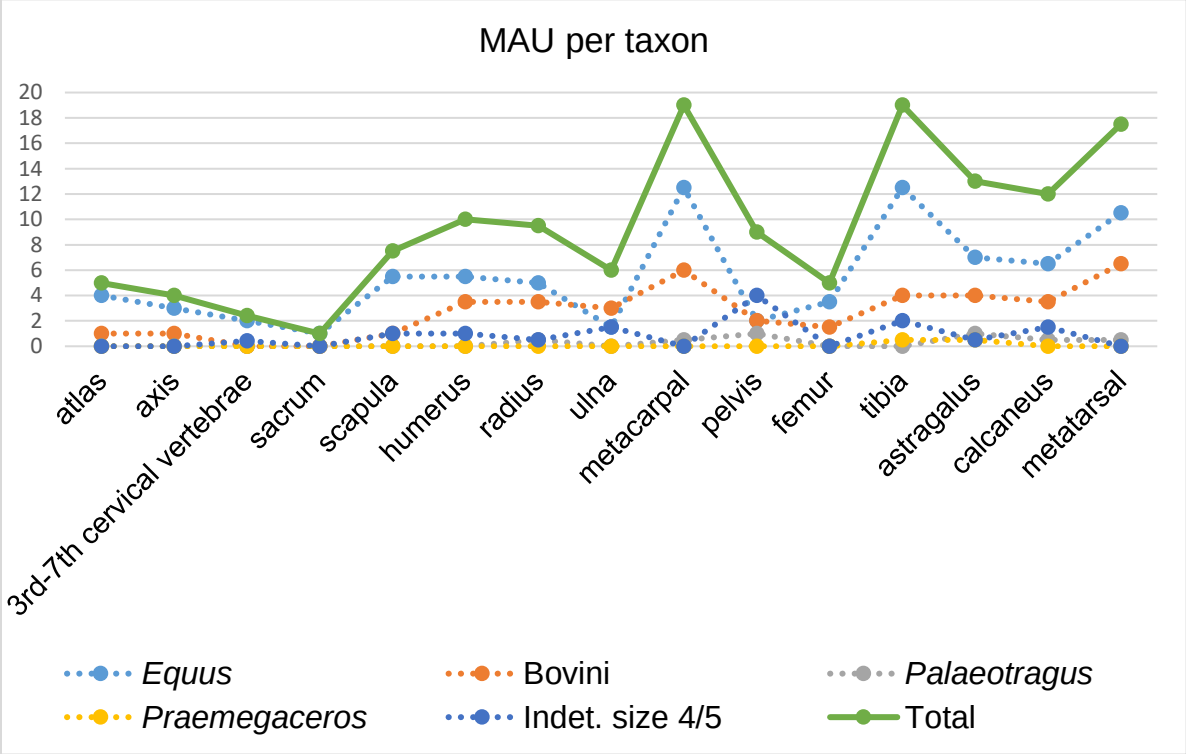

Figure 3.1: MAU values for *Equus,* Bovini, *Palaeotragus, Praemegaceros,* indeterminate size group 4/5 fragments (indet.) and total.

The minimum number of individuals (MNI) was calculated from the MNE values of tibiae in *Equus* and metapodials in Bovini. *Equus* (medium- and large-sized species together) is represented by a minimum of 15 individuals (13 of whom are classified as subadult juveniles – adults) and Bovini (*Leptobos* and *Bison* together) by 7.

The percentage of articulated elements has been correlated, among other things, with prey availability (e.g., Fourvel and Mwebi, 2011) and predator species (e.g., Haynes, 1982). Figures 3.2 and 3.3 display the proportions of articulated and isolated elements for *Equus* and Bovini. In *Equus* isolated elements are prevalent (66%; yet articulated ones are relatively abundant and represented by 44%), with the exception of radio-ulnae and metatarsals (articulation with the lateral metatarsals is included), where articulated elements surpass 50%. The percentage of articulated metapodials in *Equus* is actually slightly lower, due to the presence of isolated metapodials (*n* = 6) that cannot be classified as belonging either to the front or hind limb due to their low-grade/incomplete preservation and were therefore excluded from this analysis. In contrast most elements in Bovini appear articulated more often (59%), with metapodials being the only exception.

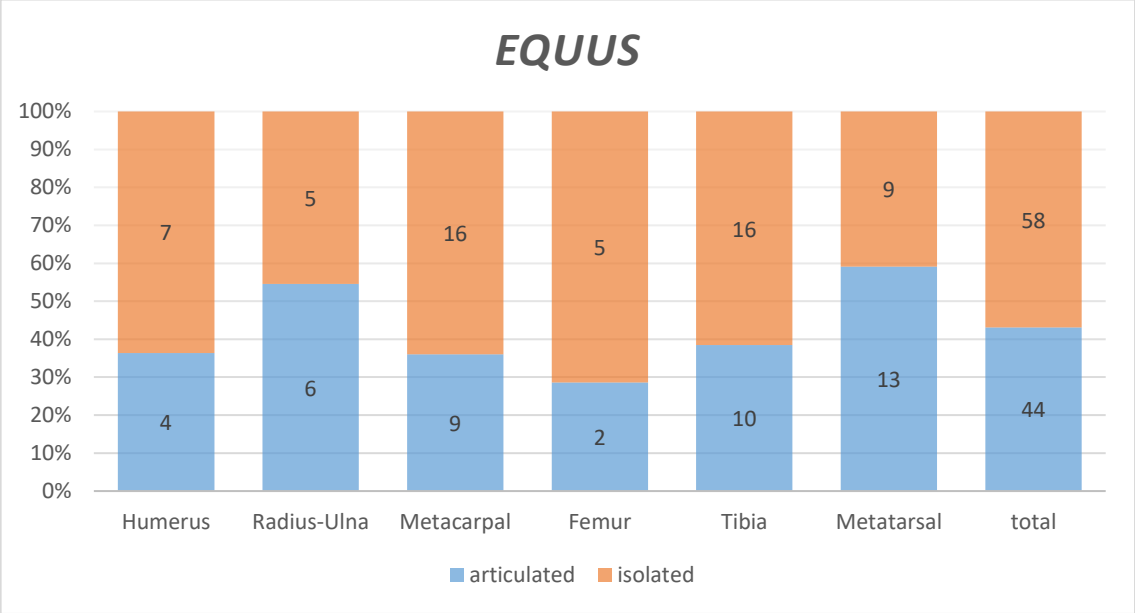

Figure 3.2: Percentages and raw values of articulated vs. isolated long limb bones in the *Equus* sample.

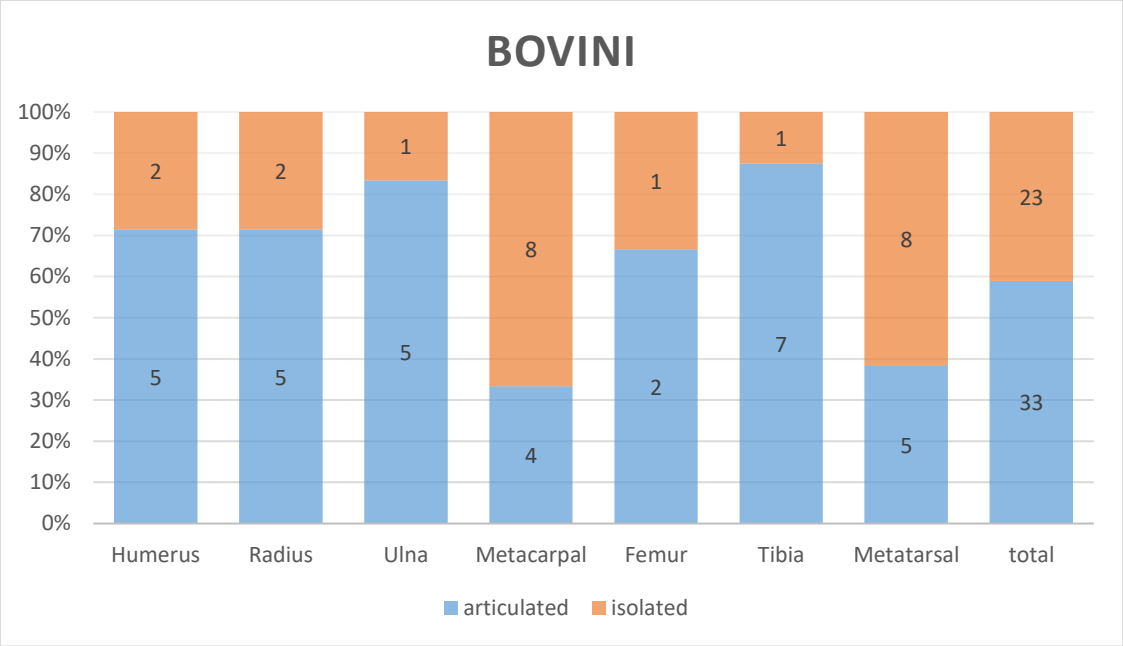

Figure 3.3: Percentages and raw values of articulated vs. isolated long limb bones in the Bovini sample.

The correlation between limb completeness and anatomical placement is also examined. Table 3.4 presents the abundance of complete or almost complete limbs in relation to their location on the body. In the *Equus* sample hind limbs are more abundant, whereas no clear pattern is observed in Bovini.

	Number of complete / almost complete limbs			
	front dex	**front sin**	**hind dex**	**hind sin**
Equus	1	2	4	4
Bovini	2	3	3	1

Table 3.4 : Number of complete or almost complete front and hind limbs for *Equus* and Bovini.

Bone damage patterns

In order to quantify bone destruction in the TSR long bone sample and identify whether any specific pattern exists, bones were classified according to the analytical method of Domínguez-Rodrigo et al. (2015). The taphotypes (T) for *Equus* and Bovini are shown in Figures 3.4 and 3.5 and expanded upon below. The most common taphotypes for the humerus, femur, and tibia are shown in Figure 3.6 for *Equus* and Figure 3.7 for Bovini.

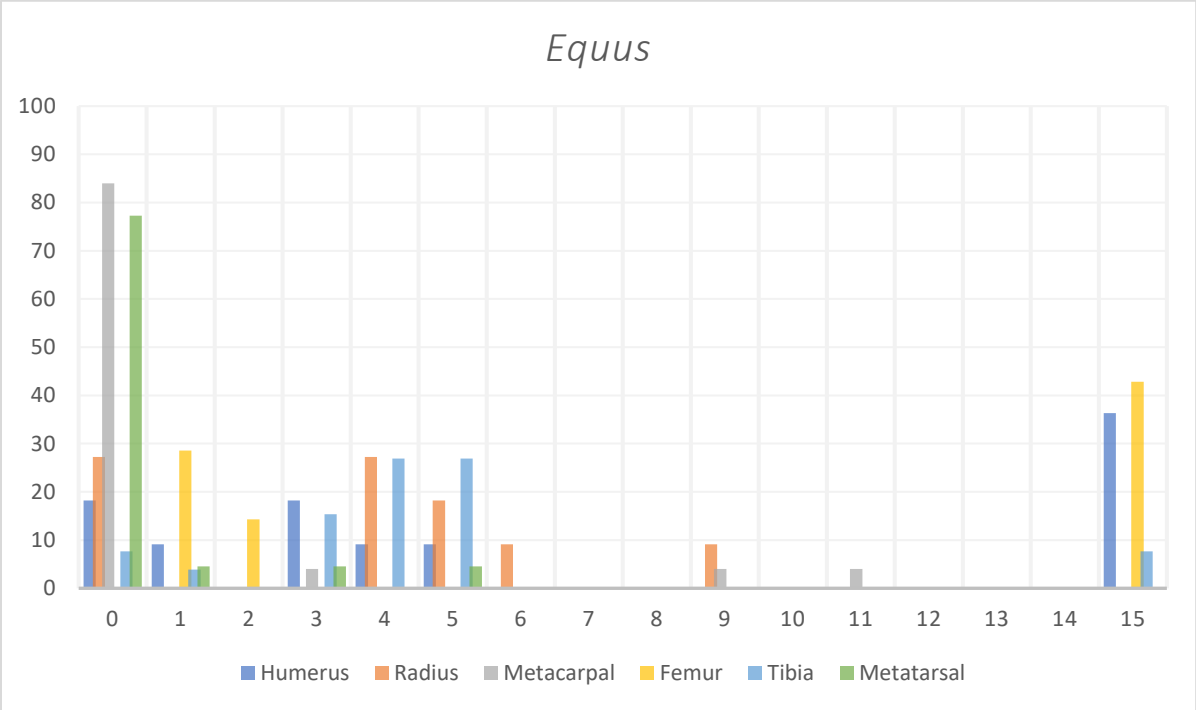

Figure 3.4: Percentages of taphotypes observed for each element in the *Equus* sample.

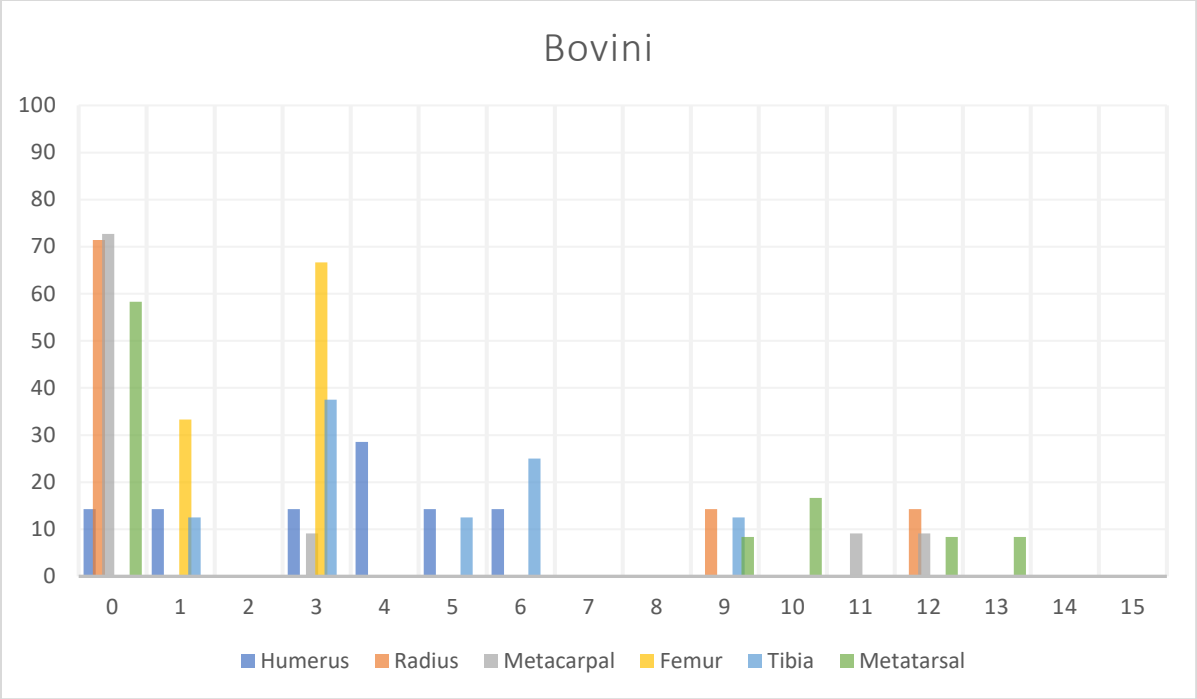

Figure 3.5: Percentages of taphotypes observed for each element in the Bovini sample.

Humerus: In equids humeri display intense deletion of both ends, with a high percentage of shafts (T15: 36.4%), and a significant percentage of complete elements (T0: 18.2%). The proximal epiphysis is always absent in partially deleted bones, while the majority preserve the distal end (T1, T3, T4, T5). In bovids, there is a similar percentage of complete bones (14.3%). The deletion is limited to the proximal half (T1, T3, T4, T5, T6).

Radius: In equids a significant number of radii appear complete (T0: 27.3%). A considerable number retain only the distal half (T4 and T5: 27.3% and 18.2%, respectively). 9.1% of the elements retain only the distal epiphyses (T6), while another 9.1% appear almost complete, lacking the distal end. The percentage of complete radii in the bovid sample is substantially higher (T0: 71.4%). The remaining radii present deletion of the distal end, with 14.3% belonging to T9, while another 14.3% presents more intense deletion (T12).

Metacarpal: The majority of metacarpals appear complete (T0; 84.0% in equids and 72.7% in bovids).

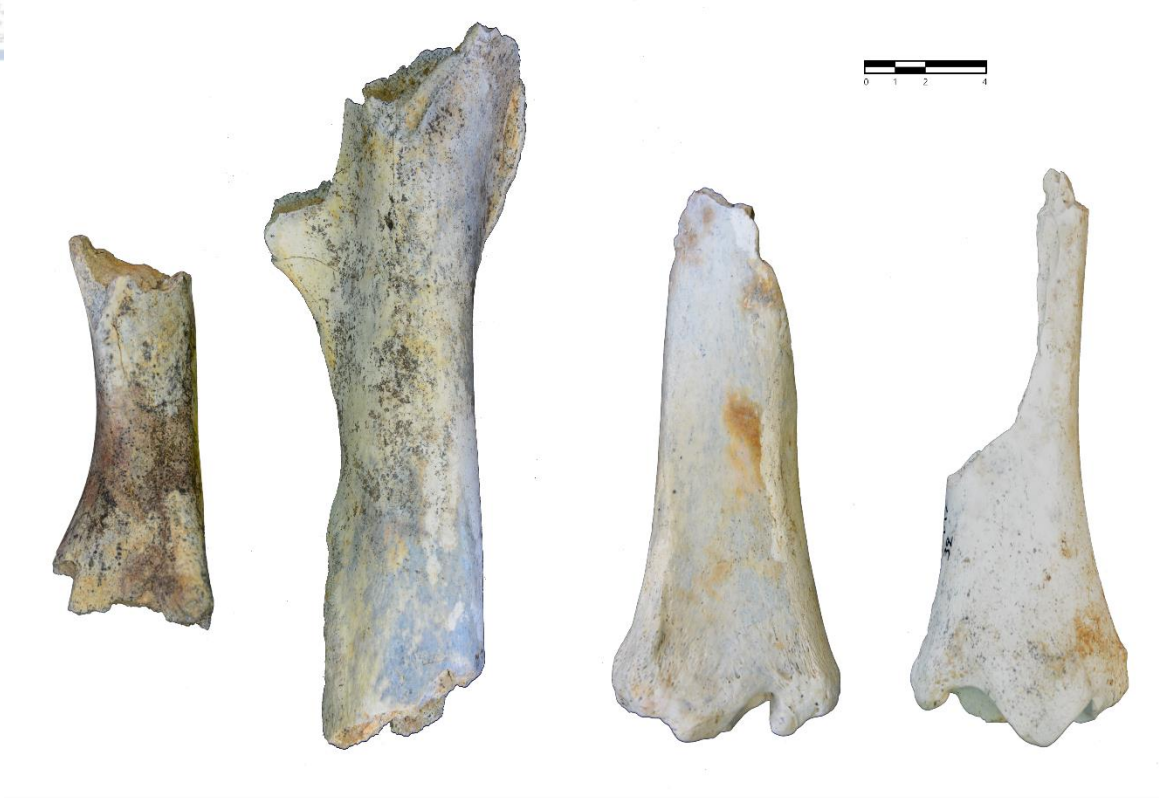

Figure 3.6: Most common taphotypes for humerus (T15), femur (T15) and tibia (T4 and T5) in *Equus*. From left to right: TSR-142, G20-15, G20-4 and F17-32. Scale in cm.

Femur: In equids T15 predominates (42.9%). The remaining femora appear almost complete, with partial or complete deletion of the proximal epiphysis (T1: 28.6%; T2: 14.3%). In contrast, in bovids the deletion is limited to the proximal shaft (T3: 66.7%; T3: 33.4%).

Tibia: In equids complete or almost complete tibiae are scarce (T0: 7.7%; T1: 3.8%). The majority retain only the distal half (T4 and T5: 26.9% each), while a significant percentage also retains part of the proximal shaft (T3: 15.4 %). 7.7% lack both epiphyses (T15). In bovids no complete tibiae are present. The majority lack the proximal epiphysis (T3: 37.5%; T6: 25.0%; T5: 12.5%), while 12.5% retain part of it (T1). Another 12.5% lacks the distal epiphysis (T9).

Metatarsal: Most metatarsals appear complete (T0: 77.3% in equids; 58.3% in bovids). In the remaining metatarsals, the deletion is limited to the proximal end in equids (T1, T3, T5) and the distal end in bovids (T9, T10, T12, T13).

Figure 3.7: Most common taphotypes for humerus (T4), femur (T3) and tibia (T3) in Bovini. From left to right: specimens F18-63, E22-5 and F19-32. Scale in cm.

An alternative way to portray surviving bone sections (proximal/distal epiphysis, proximal/middle/distal shaft) is depicted in Figure 3.8, where the raw abundances of bone sections are given for each element, for the total of long limb bones included in this study. Metapodials comprise a very large part of the sample and are usually preserved complete. Tibiae are also very abundant, although the proximal epiphysis and shaft are rarely preserved. Radii display a considerable preservation of all bone portions, with a preferential deletion of both ends in relation to the diaphysis. Stylopodials (upper limb bones) are the least preserved elements,

with humeri usually lacking the distal epiphysis and shaft, and femora appearing frequently only as diaphyseal cylinders.

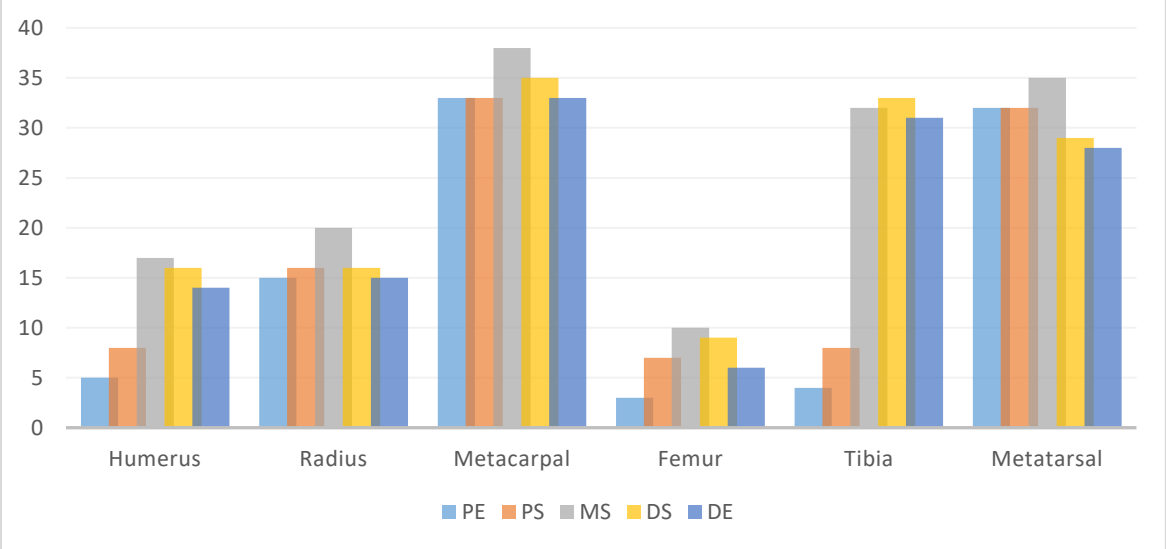

Figure 3.8: Raw abundances of bone sections per element, for all long limb bones included in the study (PE = proximal epiphysis, PS = proximal shaft, MS = middle shaft, DS = distal shaft, DE = distal epiphysis).

Since the abundance of elements and bone portion appears to be non-random, further analysis is performed in order to determine the variables that can explain the selection of specific parts. For this purpose, the possible correlation of mineral density, marrow cavity volume, fat weight and abundance of epiphyses was examined. The abundance of *Equus* long limb bone epiphyses in relation to their mineral density and marrow cavity volume is given in Figures 3.9 and 3.10, respectively.

Figure 3.9 shows a statistically significant positive relationship between epiphysis abundance and bone mineral density, described by the following equation:

$$\text{Abundance} = 58.654\ (\text{Density}) - 16.058,\ R^2 = 0.779$$

Epiphyses of high mineral density (metapodials, distal tibia) are prevalent in the *Equus* sample. On the other hand, epiphyses with lower mineral density (humerus, femur, radius, and proximal tibia) are present in significantly lesser amounts.

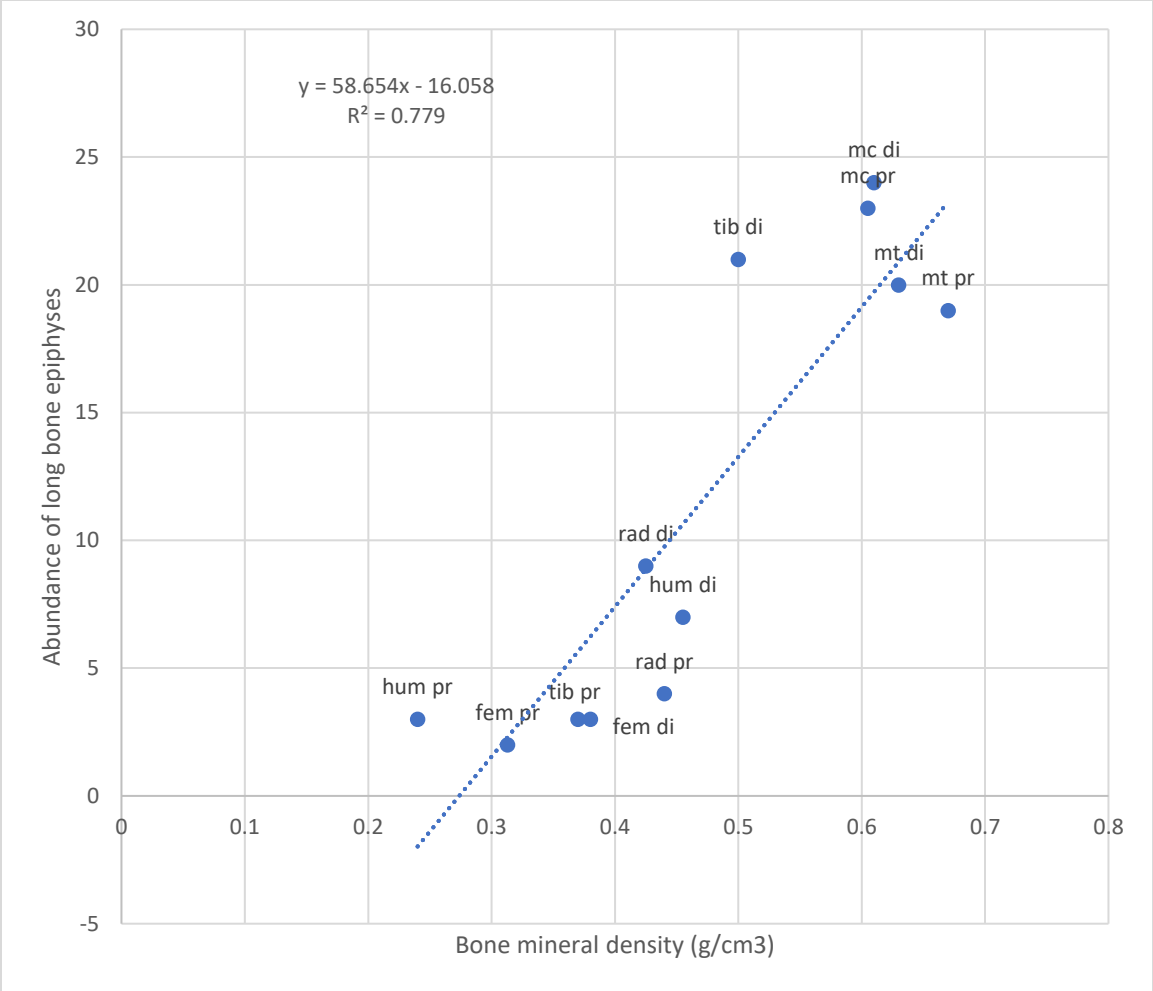

Figure 3.9: Least square regression analysis of raw abundance of bone epiphyses, in relation to their mineral density, in the *Equus* sample. Data for bone mineral density by Lam et al. (1999), (hum = humerus, rad = radius, mc = metacarpal, mt = metatarsal, pr = proximal, di = distal).

Figure 3.10 shows that there is an inverse relationship between the abundance of epiphyses in *Equus* and their bone marrow content, described by the following equation:

Log (abundance of epiphyses) = - 0.8615 [Log (bone marrow content)] + 1.8092, $R^2 = 0.6202$

Epiphyses of reduced marrow content appear more frequently in the assemblage that those with higher marrow yield.

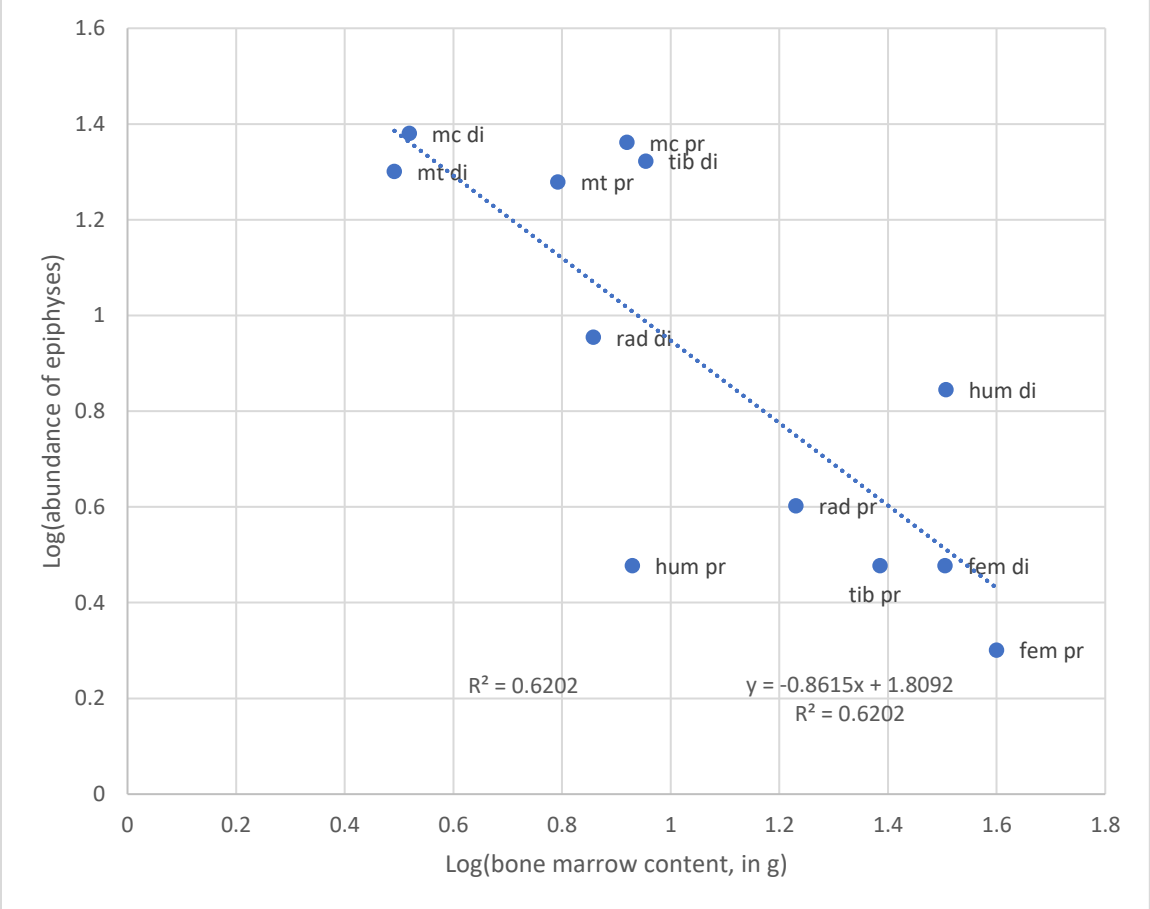

Figure 3.10: Least square regression analysis of raw abundance of bone epiphyses, in relation to their marrow content, in the *Equus* sample. Data for bone marrow content by Outram and Rowley-Conwy (1998), (hum = humerus, rad = radius, mc = metacarpal, mt = metatarsal, pr = proximal, di = distal).

For the Bovini sample the relationship between the abundance of long limb bone epiphyses relative to fat weight was examined (Fig. 3.11).

There is some correlation between the abundance of epiphyses in the Bovini sample and their fat weight. They demonstrate an inverse relationship described by the following equation:

$$\text{Abundance} = -0.0257\ (\text{fat weight}) + 8.5843,\ R^2 = 0.537$$

Epiphyses with low fat content appear in higher numbers (e.g., metapodials, distal tibia).

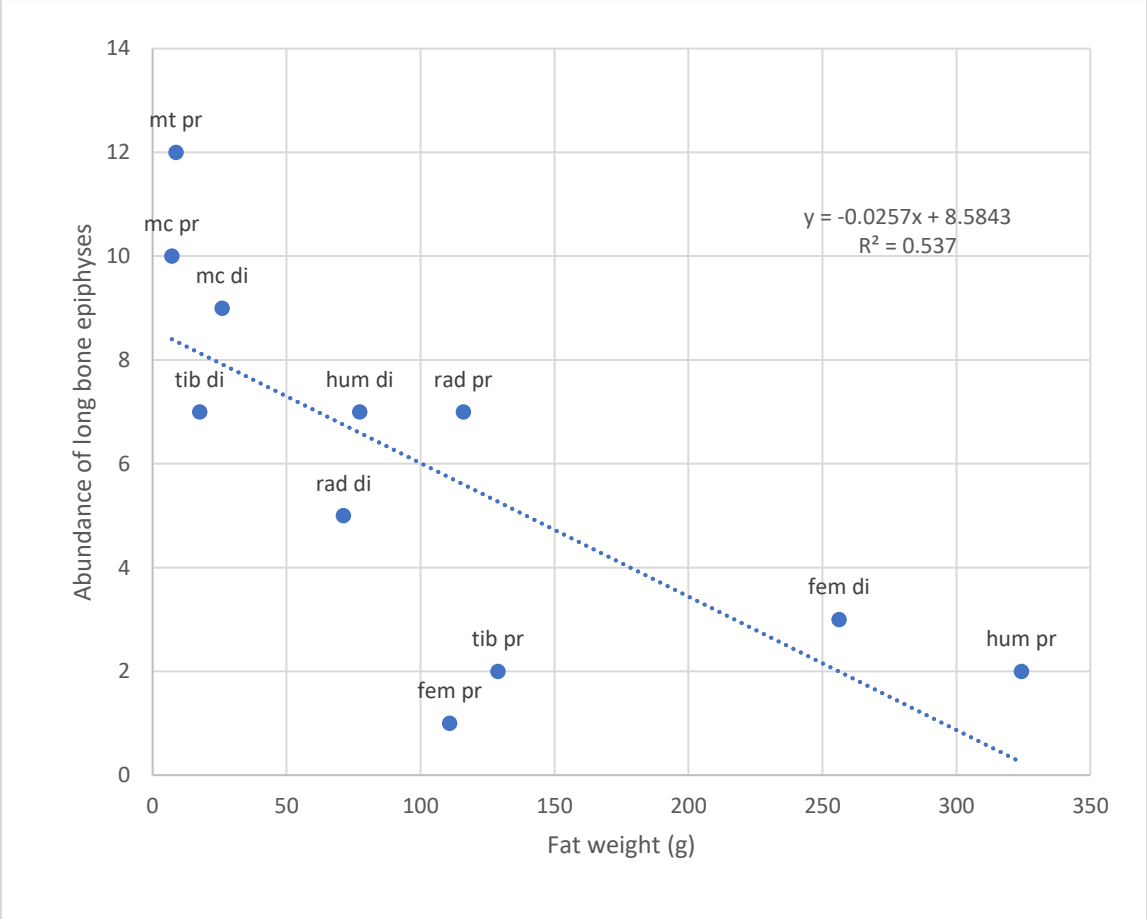

Figure 3.11: Least square regression analysis of raw abundance of bone epiphyses, in relation to their fat weight, in the Bovini sample. Data for fat weight by Brink (1997), (hum = humerus, rad = radius, mc = metacarpal, mt = metatarsal, pr = proximal, di = distal).

The regression analysis results show a clear corelation between nutrient content of bones and their deletion. Bone portions high in nutrients (high fat and marrow yields) are present in lower frequencies, whereas those with low nutritive value (high mineral density) are more abundant. This correlation suggests selective bone portion survivorship.

3.3. Carnivore tooth mark analysis

Frequencies

Tooth marks appear frequently in the assemblage. The most abundant types are pits (*n* = 475), followed by scores (*n* = 201), whereas punctures are rare (*n* = 11). Furrowing is present in stylopodials (upper limb bones), ulnae, vertebrae, and notably in a few calcanei that exhibit intense deletion (Fig. 3.16). The percentages of tooth-marked elements for the *Equus* and Bovini samples are presented in Figures 3.12 and 3.13, respectively. In the case of vertebrae only the cervical ones are considered. Tooth marking is more prevalent in stylopodials with a percentage of 33.3% of proximal and 14.3% of distal humeri, and 66.7% of distal femora. Stylopodials appear more frequently gnawed in general, in both *Equus* and Bovini. The femur is the most tooth-marked element in both categories (85.7% and 100%, respectively), while the percentage of modified humeri is considerably higher in *Equus* (81.8% as opposed to 57.1% in Bovini). Zygopodials (intermediate limb bones) show significant percentages of gnawing (68.0% in *Equus* tibiae and 50.0% in Bovini tibiae as well as radio-ulnae in both). Lower limb bones exhibit considerably lower percentages. Metapodials, in general, appear gnawed in moderate percentages, that do not surpass 35.0%. *Equus* scapulae are considerably gnawed (45.5%), in contrast to Bovini, where none shows gnaw marks. This could be attributed to the low number of scapulae in the latter (2 specimens). In the Bovini sample the pelvis appears 100% gnawed, although it is represented by just one specimen. Some examples of carnivore modification are shown in Figures. 3.16–3.18 and Appendix Figures 11– 14.

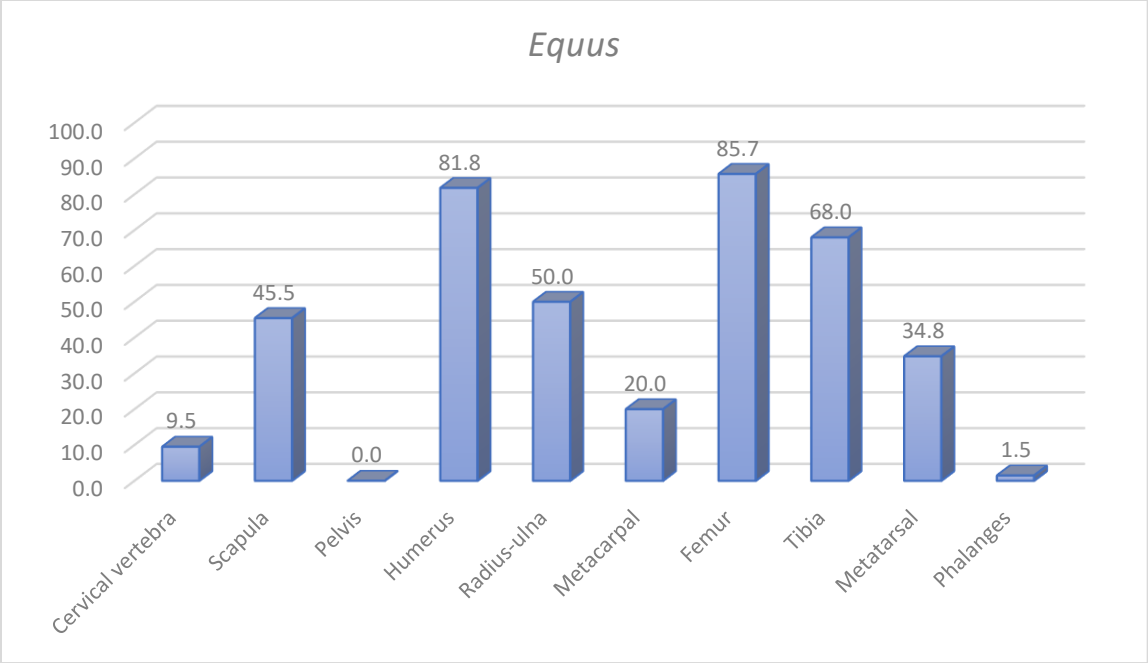

Figure 3.12: Percentages of tooth-marked bones in the *Equus* sample. The raw abundance and percentage of tooth-marked specimens is given for each element.

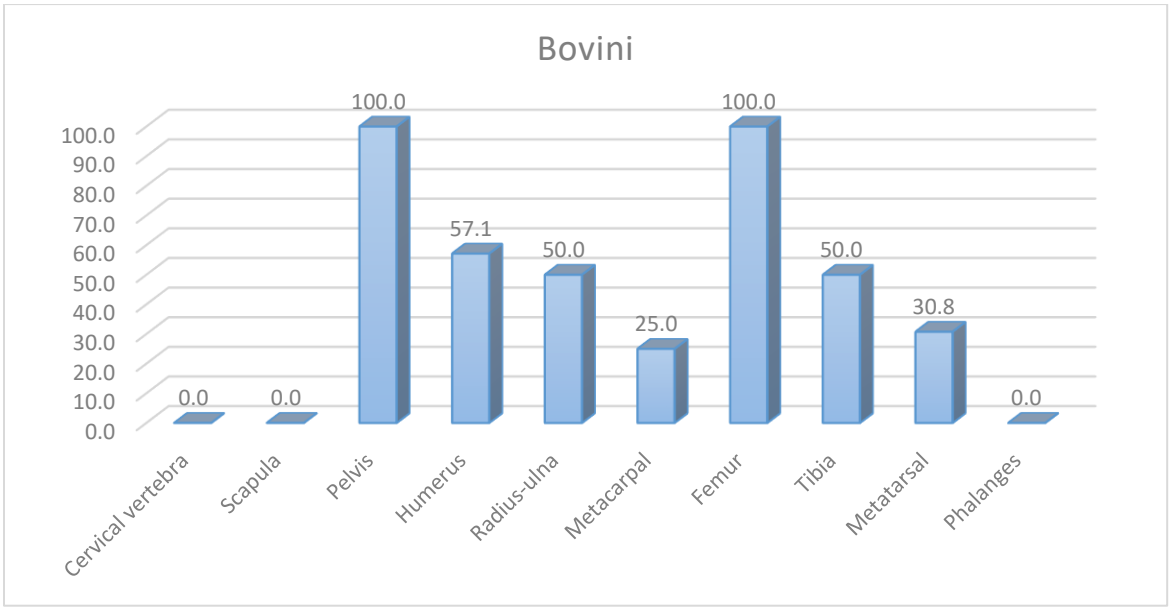

Figure 3.13: Percentages of tooth-marked bones in the Bovini sample. The raw abundance and percentage of tooth-marked specimens is given for each element.

Among the tooth-marked bones, in equids the most frequent one is tibia (28.8%), followed by humeri (15.3%) and metatarsals (13.6%), while radio-ulnae and femora appear modified in equal amounts (10.2%); other elements that present modifications are metacarpals and scapulae (8.5%), cervical vertebrae (3.4%) and phalanges (1.7%). In Bovini, tibia, humeri, radio-ulnae and metatarsals show the same frequency (17.4%) among the tooth-marked bones, followed by femora and metacarpals (13.0%); the only other element displaying tooth marks in Bovini is the pelvis, represented by only one specimen (4.3%). Overall, it is evident that long limb bone elements bear vast majority of damage induced by carnivores (Figs. 3.14 and 3.15).

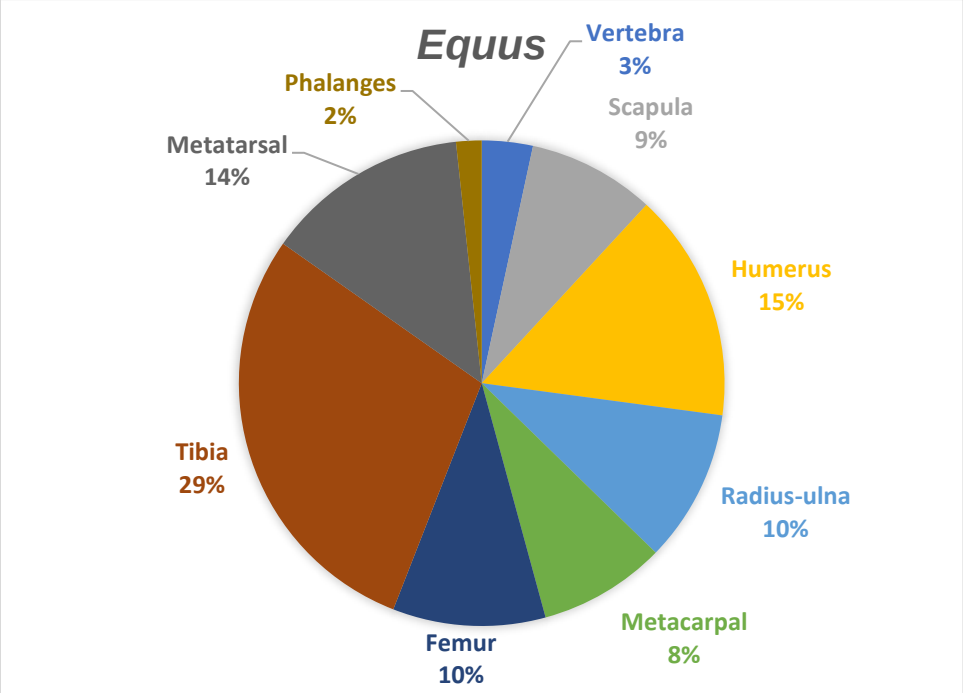

Figure 3.14: Frequencies of elements among tooth-marked bones for the *Equus* sample.

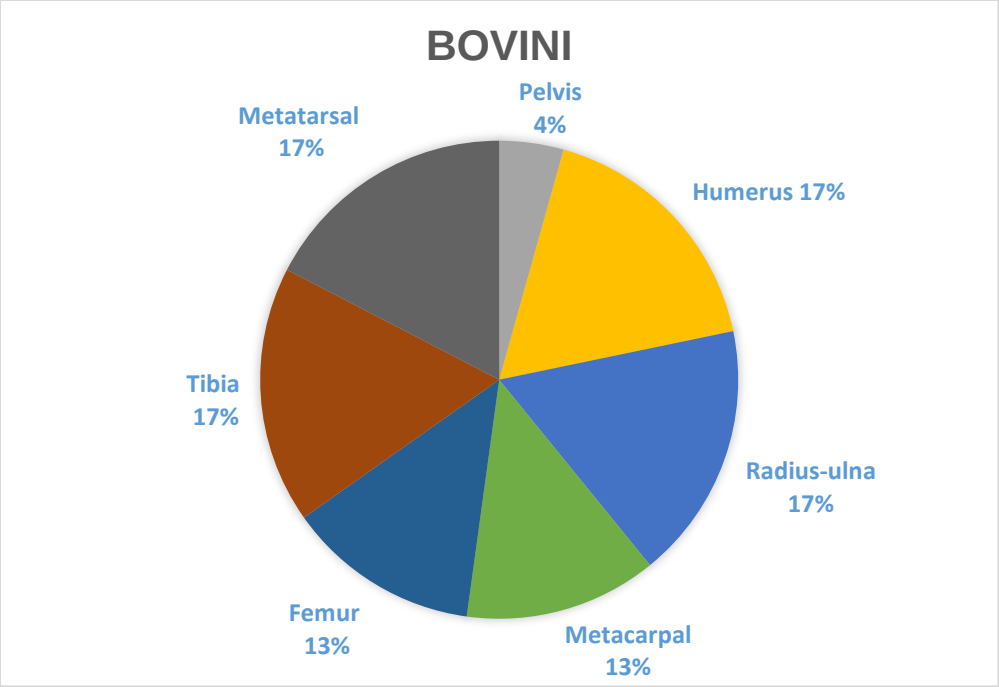

Figure 3.15: Frequencies of elements among tooth-marked bones for the Bovini sample.

Figure 3.16: *Equus* calcanei exhibiting intense deletion (left: medial view of F19-22; right: lateral view of F14-4). Scale in cm.

Figure 3.17: *Equus* humerus shaft fragment (G20-7) with pits and broad scores on lateral view (left), and pits and intense scoring on medial view (right). Scale in cm.

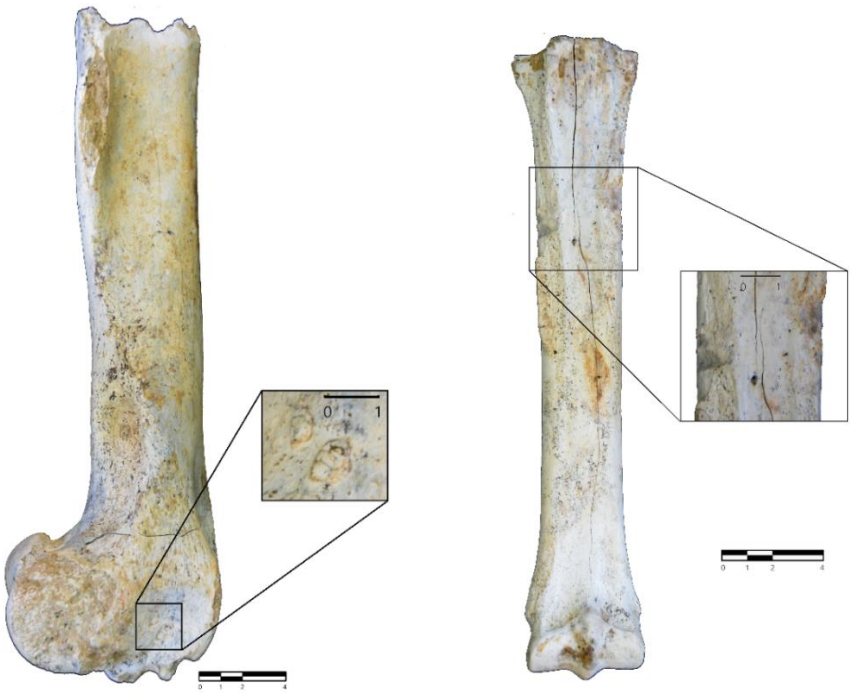

Figure 3.18: *Equus* femur (H21-11; medial view) with punctures (left) and *Equus* metacarpal (G19-20; posterior view) with scoring (right). Scale in cm.

Anatomical distribution

The anatomical distribution of tooth marks can indicate the predator taxon, since different carnivores modify bone portions in diverse frequencies (Haynes, 1983; Parkinson et al., 2015). Table 3.5 presents the frequency of tooth-marked bone sections per long bone element, in *Equus* and Bovini. It is important to note that even some areas that are represented by a very low number of specimens, such as femora and humeri epiphyses in both taxa, and tibiae proximal shafts in *Equus*, exhibit substantial clustering of tooth marks.

	Equus											
portion/element	**Humerus**		**Radius**		**Metacarpal**		**Femur**		**Tibia**		**Metatarsal**	
	TM	**%**	**TM**	**%**	**TM**	**%**	**TM**	**%**	**TM**	**%**	**TM**	**%**
Proximal end	1/3	33.3	1/7	14.3	0/23	0.0	0/2	0.0	0/2	0.0	0/19	0.0
Proximal shaft	1/6	16.7	1/8	12.5	1/23	4.4	3/6	50.0	4/5	80.0	0/19	0.0
Middle shaft	7/11	63.6	3/12	25.0	3/24	12.5	4/7	57.1	13/25	52.0	4/22	18.2
Distal shaft	5/9	55.6	0/10	0.0	0/24	0.0	4/6	66.7	9/24	37.5	2/20	10.0
Distal end	3/7	42.9	0/10	0.0	0/22	0.0	1/3	33.3	2/23	8.7	5/20	25.0
Total	17/36	47.2	5/47	10.6	4/116	3.5	12/24	50.0	28/79	35.4	11/100	11.0
	Bovini											
portion/element	**Humerus**		**Radius**		**Metacarpal**		**Femur**		**Tibia**		**Metatarsal**	
	TM	**%**	**TM**	**%**	**TM**	**%**	**TM**	**%**	**TM**	**%**	**TM**	**%**
Proximal end	0/2	0.0	1/7	14.3	0/10	0.0	1/1	100.0	0/2	0.0	0/12	0.0
Proximal shaft	0/2	0.0	0/7	0.0	1/10	10.0	0/1	0.0	0/3	0.0	2/12	16.7
Middle shaft	2/6	33.3	5/7	71.4	3/13	23.1	3/3	100.0	4/6	66.7	4/12	33.3
Distal shaft	0/7	0.0	0/6	0.0	1/11	9.1	0/3	0.0	1/8	12.5	0/8	0.0
Distal end	1/7	14.3	0/5	0.0	0/11	0.0	2/3	66.7	0/7	0.0	1/7	14.3
Total	3/24	12.5	6/32	18.8	5/55	9.1	6/11	54.6	5/26	19.2	7/51	13.7

Table 3.5: Frequency of tooth-marked bone portions, per element, for *Equus* and Bovini, presented both in raw abundances (TM) and percentages (%).

For the purpose of acquiring a more comprehensive view of the spatial distribution of tooth marks on each bone type, a GIS approach was employed. Figure 3.19 presents the results of the GIS spatial analysis for upper, and Figure 3.20 for lower limb long bones of *Equus* and Bovini specimens. Plots of individual tooth marks per type are given in Appendix Figures 5 and 6. The tooth marks considered in the spatial analysis are pits, scores, and punctures. The number of elements, as well as the number of tooth marks is lower in the Bovini sample (tooth mark n = 345 for *Equus* and n = 102 for Bovini). Tooth mark clusters are visible in both groups, for all elements. However, their distribution varies among different elements, while differences are also evident between the *Equus* and Bovini samples. *Equus* elements are tooth-marked on all aspects, while Bovini on all except posterior and lateral aspects of humeri, posterior tibiae and lateral metatarsals.

Humeri show clusters that are limited in the distal half in Bovini, while in *Equus* significant clustering is visible across the entire diaphysis and distal epiphysis. Radii appear predominately tooth-marked on middle shafts, in both categories. Metacarpals exhibit substantially lighter tooth marking, with the presence of small clusters.

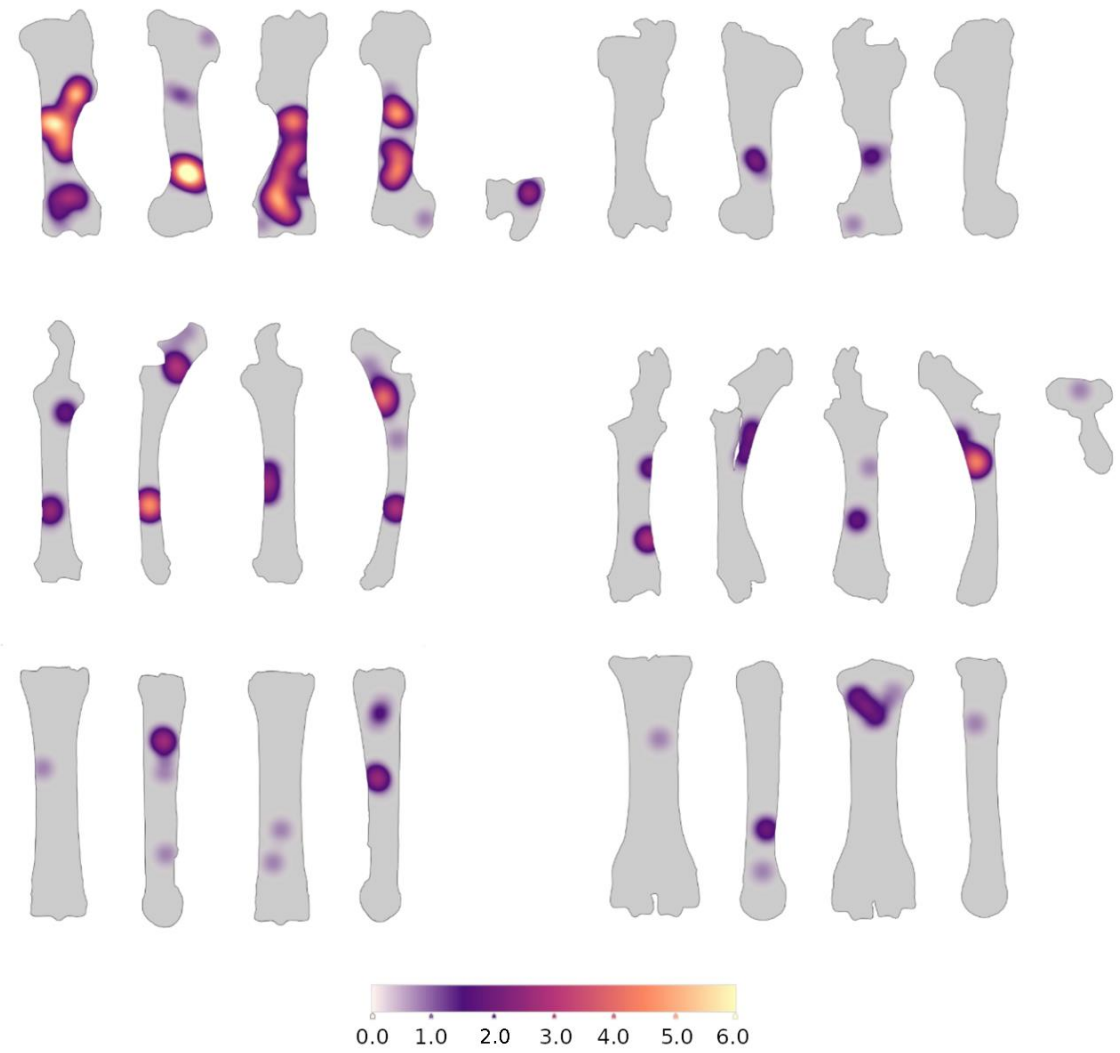

Figure 3.19: Heatmap of tooth marks (pits, scores, punctures) in posterior, medial, anterior, and lateral views of humerus, radio-ulna and metacarpal of *Equus* (left) and Bovini (right). Distal and proximal views are depicted only when tooth marks are present. Numbers on scale refer to number of tooth marks.

Equus femora exhibit clusters across all bone portions, with a greater concentration of tooth marks in the distal shaft. In contrast, Bovini femora show clusters in the middle shaft and on both epiphyses. Tibiae appear mostly tooth marked on the diaphysis, with a noteworthy concentration of tooth marks extending on the whole medial aspect of the diaphysis, in the *Equus* sample. Metatarsals

appear more tooth marked than metacarpals, with considerable clusters in the distal epiphyses in *Equus*, and the proximal shaft in Bovini. Lower limb elements appear more tooth-marked in general.

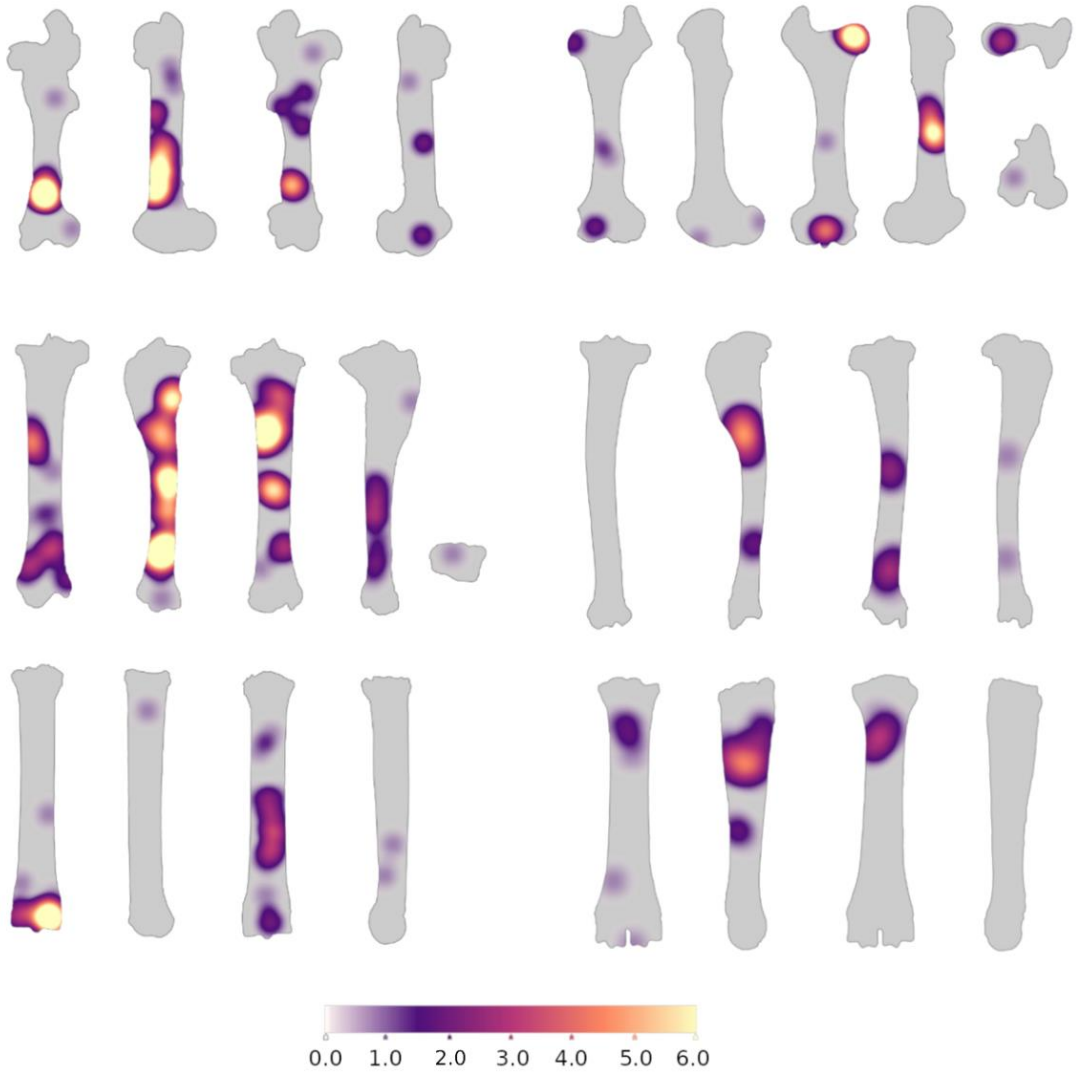

Figure 3.20: Heatmap of tooth marks (pits, scores, punctures) in posterior, medial, anterior, and lateral views of femur, tibia and metatarsal of *Equus* (left) and Bovini (right). Distal and proximal views are depicted only when tooth marks are present. Numbers on scale refer to number of tooth marks.

Macroscopic and microscopic metrical analysis

In order to examine the size and morphology of pits, punctures and scores, several variables were measured employing both standard macroscopic methods and high-resolution 3D techniques with the use of a confocal profilometer. For the macroscopic investigation of tooth marks, length and width measurements were taken with a digital calliper. The mean, median, minimum, maximum, and standard deviation values for length and breadth of scores, pits and punctures are presented in Table 3.6. The results are categorized by bone portion, separately for *Equus*, Bovini and collectively for the size groups 4 and 5 (besides Bovini including also *Praemegaceros* and *Palaeotragus*) specimens. It is notable that dimensions on the epiphysis don't always exceed those on the diaphysis, for pits and scores. It can be hypothesised that once pits and scores reach the higher range of dimensions, they penetrate all layers of cortical bone and are presented as punctures and furrows, respectively. Punctures are substantially larger in cancellous bone, in respect to the thin cortical bone of the near-epiphyses.

scores		***Equus***		**Bovini**		**total size group 4-5**	
		length (mm)	**width (mm)**	**length (mm)**	**width (mm)**	**length (mm)**	**width (mm)**
epiphysis	***n***	6		3		10	
	mean	7.73	1.44	6.31	1.61	7.15	1.50
	median	7.79	1.24	7.47	1.56	7.01	1.52
	SD	4.07	0.84	3.27	1.01	3.53	0.82
	min	2.41	0.52	1.86	0.39	1.86	0.39
	max	14.73	2.96	9.61	2.87	14.73	2.96
near-epiphysis	***n***	40		3		44	
	mean	6.72	1.18	9.81	1.19	7.18	1.22
	median	6.24	0.87	9.19	1.22	6.62	0.88
	SD	2.78	0.72	4.35	0.26	3.39	0.71
	min	2.65	0.50	4.81	0.86	2.65	0.50
	max	14.87	3.26	15.42	1.50	17.66	3.26
middle shaft	***n***	71		14		147	
	mean	6.99	1.27	9.22	1.23	6.88	1.23
	median	6.23	0.99	8.94	1.08	6.25	1.03
	SD	3.47	0.92	4.57	0.44	3.61	0.78

	min	1.06	0.29	2.15	0.65	1.06	0.26
	max	15.49	4.68	20.58	2.01	20.58	4.68
pits		***Equus***		**Bovini**		**total size 4-5**	
		length (mm)	**width (mm)**	**length (mm)**	**width (mm)**	**length (mm)**	**width (mm)**
epiphysis	***n***	27		20		54	
	mean	3.38	1.95	4.04	2.23	3.60	2.05
	median	2.67	1.54	2.60	1.74	2.72	1.64
	SD	2.38	1.16	4.00	1.39	2.99	1.20
	min	1.02	0.61	0.90	0.70	0.90	0.61
	max	9.30	5.03	16.34	5.82	16.34	5.82
near-epiphysis	***n***	49		3		52	
	mean	3.42	2.16	2.37	1.81	3.36	2.14
	median	2.80	1.88	2.10	1.67	2.72	1.88
	SD	1.96	1.07	0.61	0.46	1.93	1.05
	min	0.89	0.59	1.80	1.33	0.89	0.59
	max	10.17	5.40	3.22	2.43	10.17	5.40
middle shaft	***n***	146		58		369	
	mean	3.43	2.15	3.52	2.42	3.49	2.18
	median	2.93	1.97	3.02	2.03	3.00	1.95
	SD	1.92	1.12	1.97	1.31	2.14	1.17
	min	0.64	0.47	0.90	0.64	0.64	0.27
	max	9.03	5.40	12.56	6.38	17.84	6.84
punctures		***Equus***		**Bovini**		**total size 4-5**	
		length (mm)	**width (mm)**	**length (mm)**	**width (mm)**	**length (mm)**	**width (mm)**
epiphysis	***n***	2		2		4	
	mean	10.71	7.14	6.60	5.16	8.66	6.15
	median	10.71	7.14	6.60	5.16	6.78	5.36
	SD	4.27	2.23	0.51	0.65	3.67	1.91
	min	6.44	4.91	6.09	4.51	6.09	4.51
	max	14.98	9.36	7.11	5.81	14.98	9.36
near-epiphysis	***n***	5				5	
	mean	6.06	4.08			6.06	4.08
	median	6.98	4.26			6.98	4.26
	SD	1.52	1.02			1.52	1.02
	min	3.38	2.40				
	max	7.35	5.51				

Table 3 6: Macroscopic analysis: *n*, mean, median, standard deviation (SD), minimum and maximum values for length and width of scores, pits, and punctures. Values are given

separately for the epiphysis, near-epiphysis, and middle shaft of the *Equus*, Bovini, and total size group 4-5 sample (including *Palaeotragus*, *Praemegaceros* and indeterminable bone fragments). Length and width are presented in millimetres.

Aiming to examine any statistical differences, statistical analysis was performed between the *Equus* and Bovini samples, for the bone portions where tooth marks were more abundant (Table 3.7). This comprises epiphyses and middle shafts for pits and middle shafts for scores. Punctures are few across all bone portions. The Shapiro-Wilk test shows that only score dimensions in Bovini present a normal distribution. The Mann-Whitney test for comparing differences between the Bovini and *Equus* samples, shows that the possibility for pit length and width on the epiphysis and middle shafts, as well as for score width in middle shafts, to have the same mean, cannot be excluded. On the contrary, the possibility of same means for score length in middle shafts can be rejected.

		scores MS		**pits EPI**		**pits MS**	
		length	**width**	**length**	**width**	**length**	**width**
Shapiro-Wilk	***Equus***	0.013	0.000	0.001	0.017	0.000	0.000
Shapiro-Wilk	**Bovini**	**0.928**	**0.145**	0.000	0.000	0.000	0.001
Mann-Whitney		0.043	**0.331**	**0.949**	**0.445**	**0.567**	**0.230**

Table 3.7: Results of the statistical analysis of the macroscopic measurements of scores on the middle shaft (MS) and pits on the epiphysis (EPI) and middle shaft (MS). Presented are the results of the Shapiro-Wilk test, for normality, and the Mann-Whitney test for comparing differences between the *Equus* and Bovini samples. Values over 0.05 are in bold.

A comparison of mean length and width values was conducted, in order to gain a perspective on how the TSR sample compares to assemblages modified by extant species. Figures 3.21–3.24 present a comparison between diaphyseal pit

and score dimensions in TSR, and data from actualistic studies (Andrés et al., 2012; Delaney-Rivera et al., 2009; Domínguez-Rodrigo and Piqueras, 2003; Sala et al., 2012, 2014a; Yravedra et al., 2014). The TSR sample in all three groups (*Equus*, Bovini and total size groups 4-5), parallels with data from extant large predators such as *Panthera leo*, *Crocuta crocuta* and *Canis lupus*. Notable, also, is the wider range of dimensions in the TSR sample, especially compared to relatively small predators. Furthermore, the upper range of pits dimensions (on cortical bone) in the TSR sample seems to exceed that of most modern large predators. Additional comparisons regarding tooth marks on the epiphyses are presented in the supplementary material of this study (App. Figs 1–4).

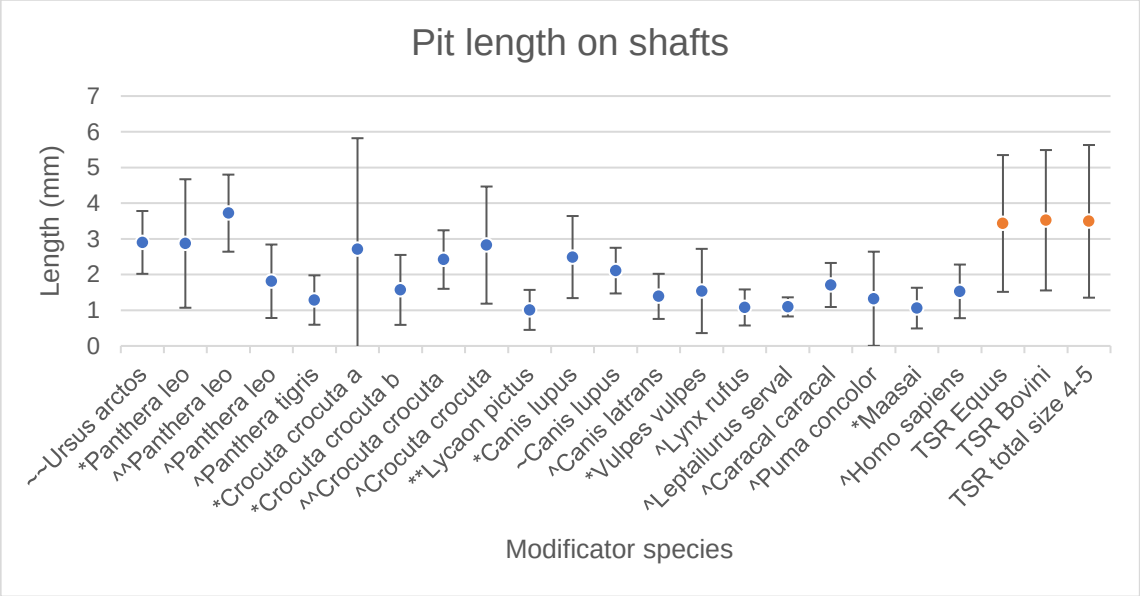

Figure 3.21: Mean values and standard deviation intervals of pit length on the diaphysis. Data from: ~~ Domínguez-Rodrigo and Piqueras (2003), * Andre et al. (2012), ^^ Sala et al. (2012), ^ Delaney-Rivera (2009), ** Yravedra et al. (2014), and ~ Sala et al. (2014) in comparison with *Equus*, Bovini and total of size group 4-5 from TSR.

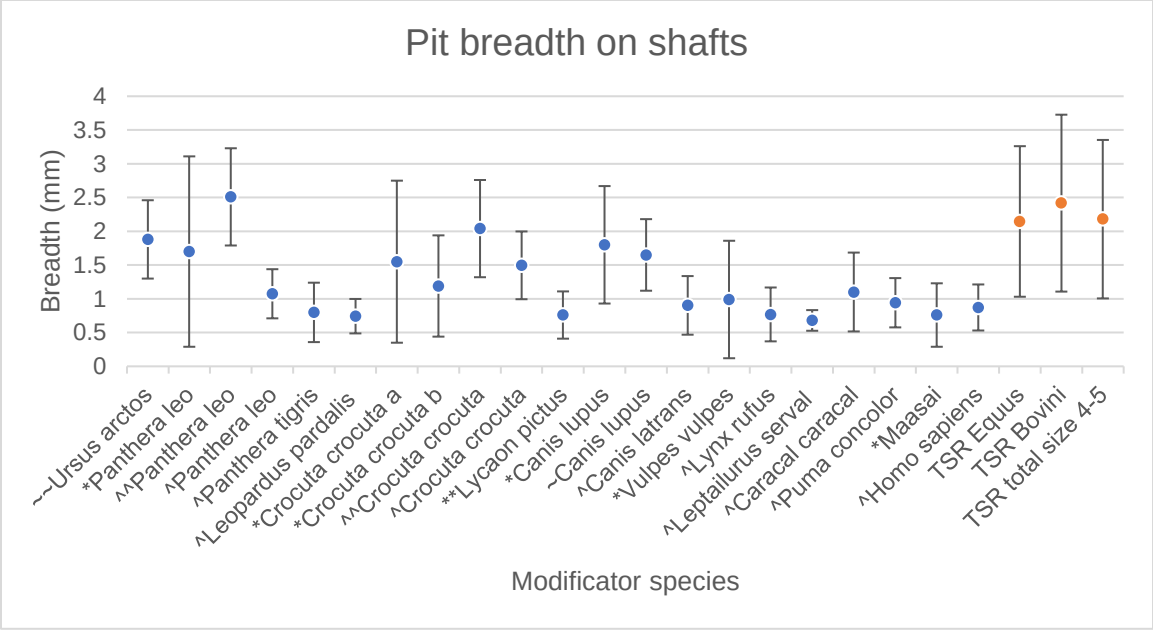

Figure 3.22: Mean values and standard deviation intervals of pit breadth on the diaphysis. Data from: ~~ Domínguez-Rodrigo and Piqueras (2003), * Andre et al. (2012), ^^ Sala et al. (2012), ^ Delaney-Rivera (2009), ** Yravedra et al. (2014), and ~ Sala et al. (2014) in comparison with *Equus*, Bovini and total of size group 4-5 from TSR.

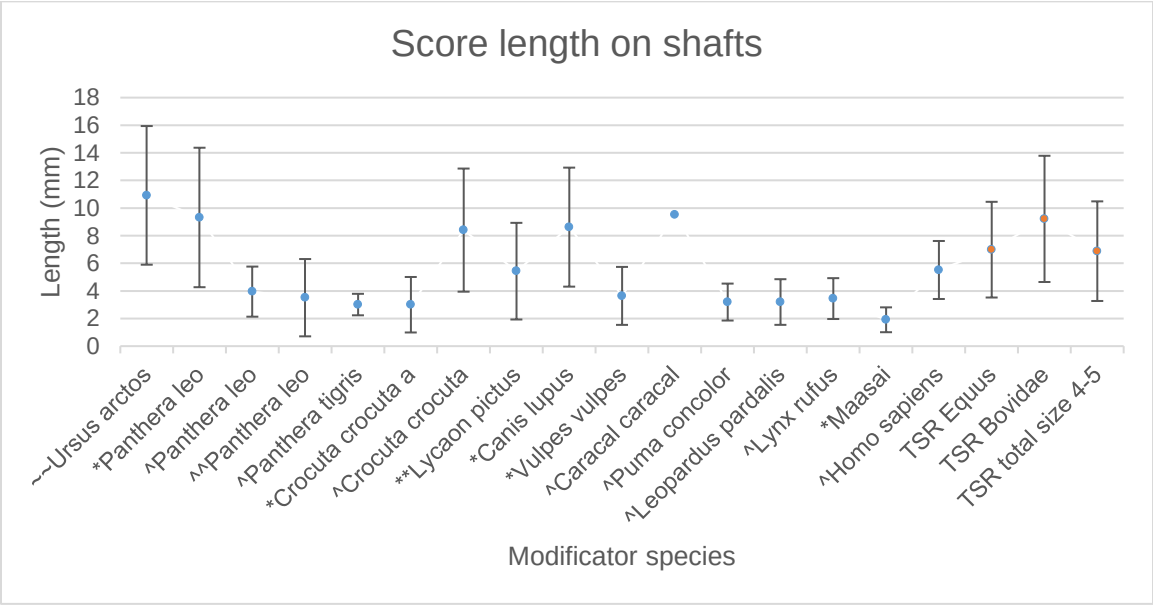

Figure 3.23: Mean values and standard deviation intervals of score length on the diaphysis. Data from: ~~ Domínguez-Rodrigo and Piqueras (2003), * Andre et al. (2012), ^^ Sala et al. (2012), ^ Delaney-Rivera (2009), ** Yravedra et al. (2014) in comparison with *Equus*, Bovini and total of size group 4-5 from TSR.

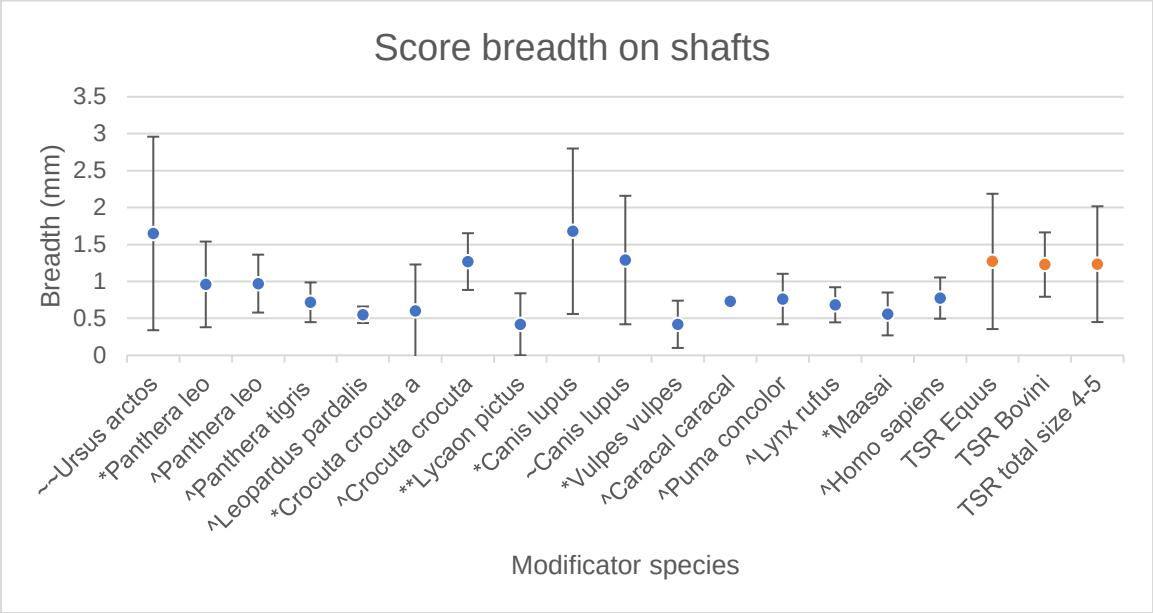

Figure 3.24: Mean values and standard deviation intervals of score breadth on the diaphysis. Data from: ~~ Domínguez-Rodrigo and Piqueras (2003), * Andre et al. (2012), ^^ Sala et al. (2012), ^ Delaney-Rivera (2009), ** Yravedra et al. (2014) in comparison with *Equus*, Bovini and total of size group 4-5 from TSR.

A more comprehensive and detailed metrical examination of the TSR tooth marks was performed by the means of high-resolution 3D analysis. Here, apart from length and width, additional measurements regarding surface area, volume and depth are provided. Moreover, profiles from the central and deepest sections of each tooth mark were examined, providing depth, area, width, roughness (Ra), opening angle and floor radius measurements. The mean, median, standard deviation, minimum and maximum values for 3D, central and deepest profile measurements are given in Tables 3.8, 3.9 and 3.10 respectively. Examples of high-resolution 3D images of tooth marks are presented in Figures 3.25–3.32 and Appendix Figures 15–22.

3D measurements							
		surface area (mm²)	volume (µm³)	maximum depth (µm)	mean depth (µm)	maximum length (mm)	maximum width (mm)
pits	*n*	90					
	mean	9.90	2741977387.11	457.94	210.05	4.48	2.76
	median	7.53	1487986137.50	421.16	197.21	4.11	2.51
	SD	8.34	3286013312.88	256.21	118.39	2.44	1.38
	min	0.29	12113430.00	85.47	34.44	0.84	0.64
	max	32.36	14595205650.00	1363.09	549.91	12.85	6.92
scores	*n*	13					
	mean	12.43	3038260983.00	412.96	191.51	7.77	2.08
	median	8.42	1569000965.00	410.34	208.65	7.57	1.63
	SD	9.89	3697122443.28	201.36	98.99	2.92	1.09
	min	2.38	267272200.00	138.63	62.93	3.93	0.94
	max	39.29	14101312000.00	835.83	358.87	13.93	4.36
punctures	*n*	7					
	mean	34.38	35471448552.29	1732.03	877.42	7.90	5.69
	median	29.38	23150365810.00	1451.99	729.45	7.47	5.40
	SD	16.81	31205287236.80	593.67	347.53	1.90	1.59
	min	16.32	8827138504.00	1167.05	529.27	5.30	3.60
	max	68.11	103331788400.00	2991.16	1517.20	11.52	8.05
total	*n*	110					
	mean	11.76	4859777249.86	533.70	250.33	5.09	2.87
	median	8.45	1919110377.00	437.15	213.36	4.77	2.51
	SD	11.04	11666659272.60	422.76	216.96	2.79	1.57
	min	0.29	12113430.00	85.47	34.44	0.84	0.64
	max	68.11	103331788400.00	2991.16	1517.20	13.93	8.05

Table 3.8: Microscopic 3D measurements of size group 4 and 5 combined, including *Equus*, Bovini, *Palaeotragus*, *Praemegaceros* and indeterminable bone fragments: number of specimens (*n*), mean, median, standard deviation (SD), minimum and maximum values for length and width of pits, scores, and punctures and total (pits, scores, and punctures combined). The values given are surface area (in mm^2), volume (in μm^3), maximum and mean depth (in µm), and maximum length and width (in mm).

Central profile							
		depth (µm)	area (µm²)	width (µm)	Ra (µm)	opening angle (°)	floor radius (µm)
pits	*n*	90					
	mean	391.01	724157.97	2577.71	9.69	151.50	3047.25
	median	367.11	510968.21	2351.22	8.57	146.32	2277.59
	SD	227.68	725926.44	1328.44	5.41	64.56	2744.82
	min	476.44	1.52	110.51	11.79	83.56	23266.47
	max	6689.80	35.95	742.27	15532.00	1387.26	4167368.00
scores	*n*	13					
	mean	284.14	388062.30	1818.50	5.24	144.00	2151.80
	median	298.89	199291.70	1517.27	4.73	145.20	1505.87
	SD	164.11	409433.40	972.58	3.57	18.94	1452.40
	min	77.01	60184.52	966.12	1.52	101.73	678.84
	max	612.90	1508294.59	4331.30	14.54	165.30	5345.08
punctures	*n*	7					
	mean	1497.00	5849579.68	5629.95	20.85	122.53	4044.95
	median	1306.38	4672509.16	5403.49	20.60	117.47	3615.90
	SD	666.34	4086778.93	1807.22	7.46	11.77	2329.34
	min	734.72	2027105.17	3190.71	10.11	109.80	1603.18
	max	2844.28	13025222.92	8687.32	35.53	144.52	9225.82
total	*n*	110					
	mean	452.96	1027751.36	2700.49	9.96	148.81	3020.21
	median	367.11	545816.37	2351.22	8.50	144.90	2288.93
	SD	391.51	1792257.73	1561.69	6.29	59.67	2641.99
	min	64.83	20224.33	476.44	1.52	101.73	11.79
	max	2844.28	13025222.92	8687.32	35.95	742.27	15532.00

Table 3.9: Microscopic central profile measurements of size group 4 and 5 combined, including *Equus*, Bovini, *Palaeotragus*, *Praemegaceros* and indeterminable bone fragments: *n*, mean, median, standard deviation (SD), minimum and maximum values for length and width of pits, scores, and punctures and total (pits, scores, and punctures combined). The values given are depth (in µm), area (in µm^2), width (in µm), Ra (in µm), opening angle (in degrees) and floor radius (in µm).

Deepest profile							
		depth (µm)	area (µm²)	width (µm)	Ra (µm)	opening angle (°)	floor radius (µm)
pits	*n*	90					
	mean	428.39	757652.83	2573.75	10.15	141.46	3050.02
	median	393.26	575156.34	2460.18	9.30	142.51	2244.16
	SD	241.06	762558.34	1347.12	5.50	13.11	3073.45
	min	415.02	1.26	100.80	264.21	264.21	264.21
	max	6261.52	28.45	169.84	16607.50	16607.50	16607.50
scores	*n*	13					
	mean	404.15	593340.55	2105.31	9.93	137.01	2069.72
	median	359.87	357475.35	1642.60	10.08	139.10	1653.79
	SD	221.14	664797.36	1171.60	5.27	17.64	1767.68
	min	120.92	82416.50	1057.42	1.75	105.24	630.12
	max	883.46	2521198.92	4649.92	21.99	161.45	7277.72
punctures	*n*	7					
	mean	1639.13	4127208.41	5273.50	22.08	117.69	2945.61
	median	1258.42	3972549.93	5318.83	19.81	113.60	3091.62
	SD	643.38	3246272.46	1499.55	6.57	8.24	853.13
	min	1034.26	12464.40	3252.13	15.63	107.70	1668.49
	max	2986.91	10929900.00	7855.12	36.51	131.34	4351.88
total	*n*	110					
	mean	503.47	955956.88	2695.56	10.89	139.44	2935.39
	median	415.07	578874.70	2463.55	9.78	140.96	2110.64
	SD	410.51	1377808.98	1507.09	6.28	14.66	2878.13
	min	83.56	12464.40	415.02	1.26	100.80	264.21
	max	2986.91	10929900.00	7855.12	36.51	169.84	16607.50

Table 3.10: Microscopic deepest profile measurements of size group 4 and 5 combined, including *Equus*, Bovini, *Palaeotragus, Praemegaceros* and indeterminable bone fragments: *n*, mean, median, standard deviation (SD), minimum and maximum values for length and width of pits, scores, and punctures and total (pits, scores, and punctures combined). The values given are depth (in µm), area (in µm^2), width (in µm), Ra (in µm), opening angle (in degrees) and floor radius (in µm).

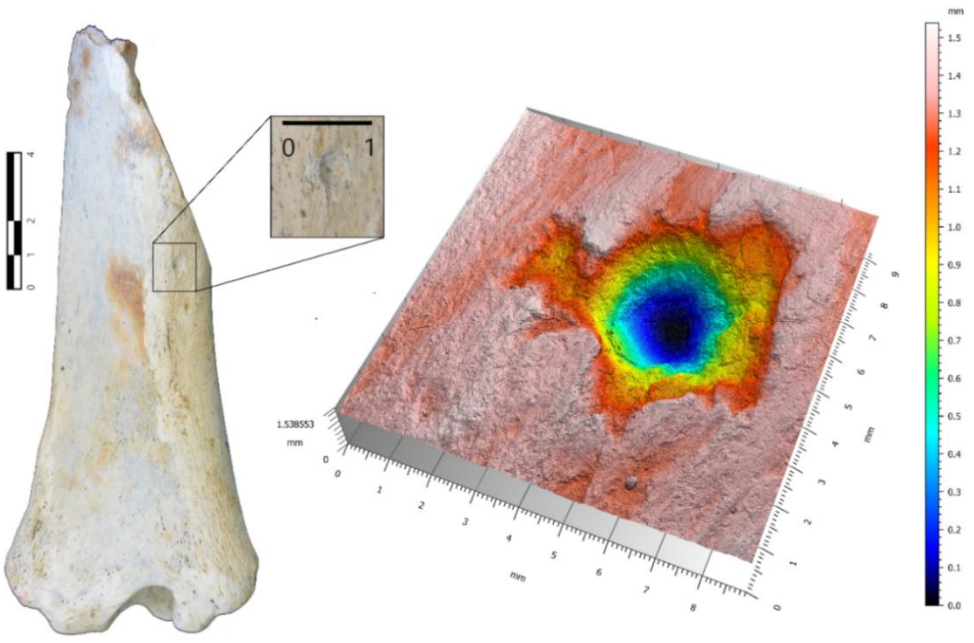

Figure 3.25: Pit on the distal shaft of an *Equuus* tibia (G20-4; anterior view) (left) and its 3D image (right). Scale in cm.

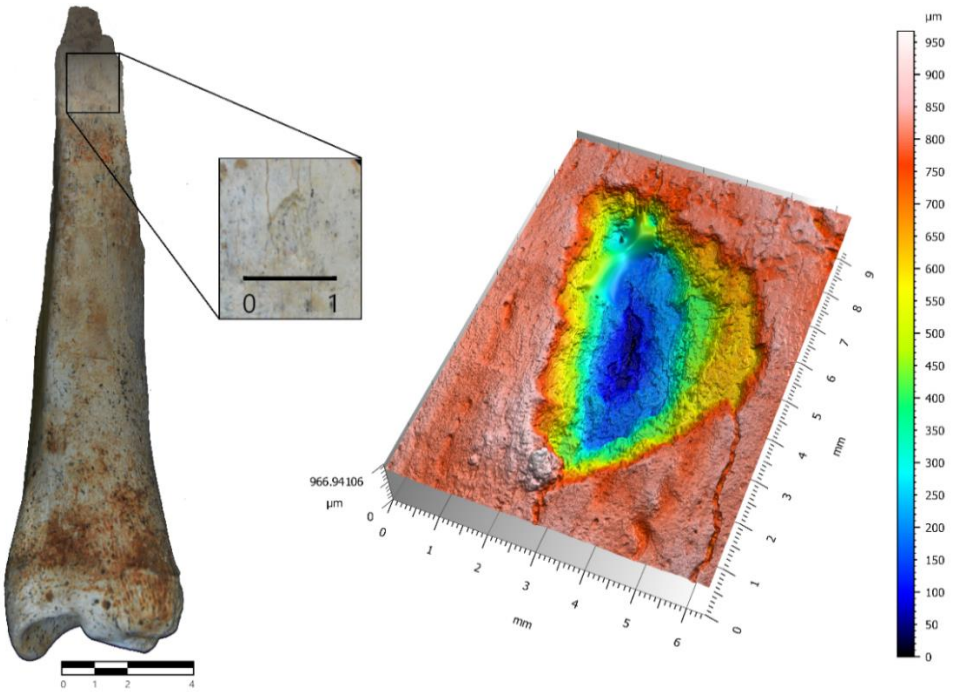

Figure 3.26: Pit on the proximal shaft of an *Equus* tibia (F17-32; lateral view) (left) and its 3D image (right). Scale in cm.

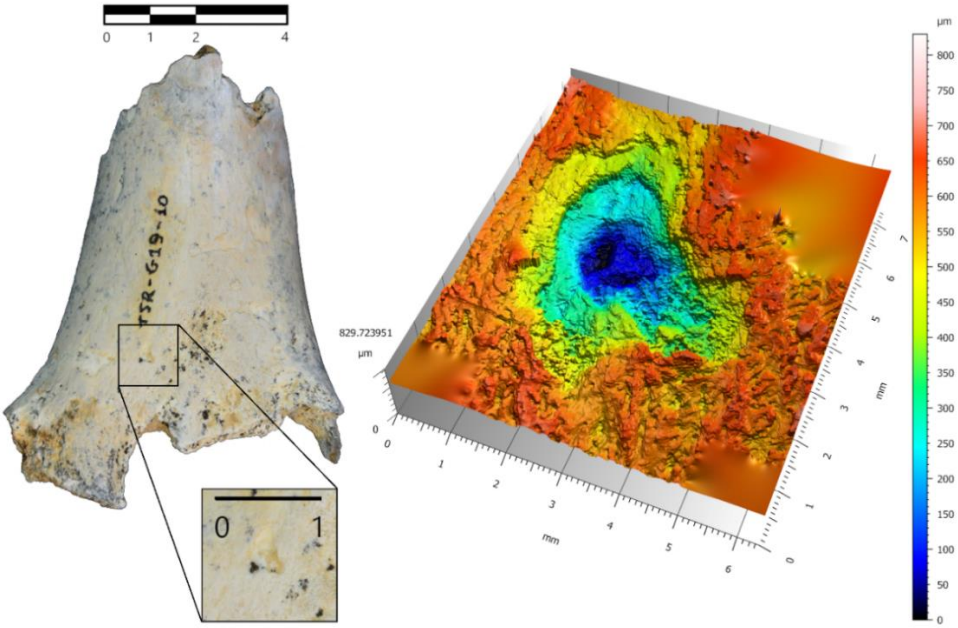

Figure 3.27: Pit on an indeterminate shaft fragment (G19-10) of size class 4/5 (left) and its 3D image (right). Scale in cm.

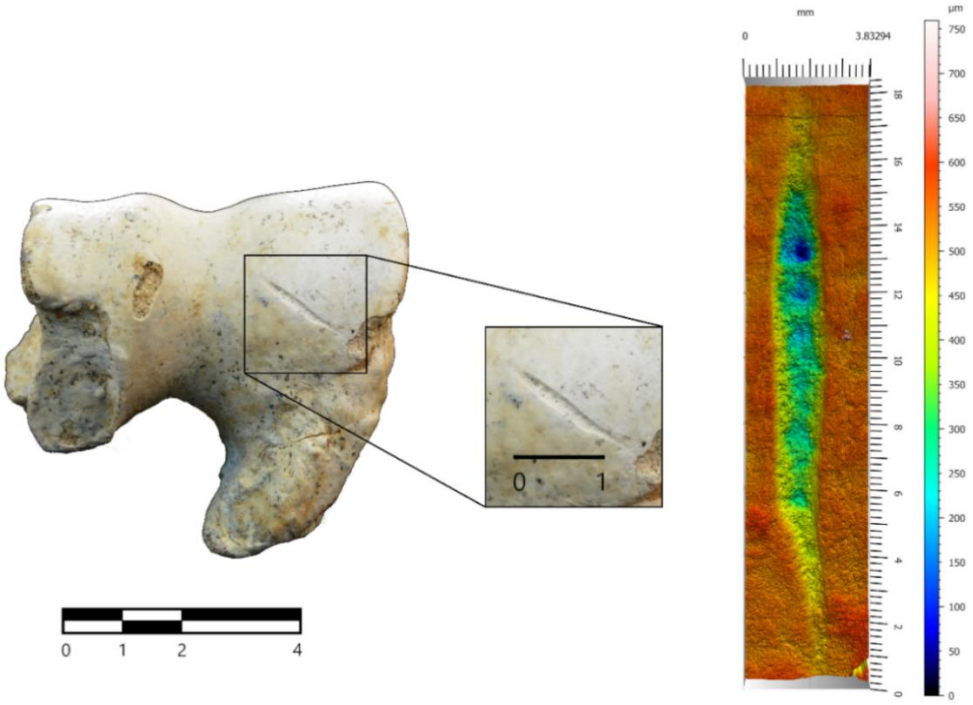

Figure 3.28: Score on the distal epiphysis of an *Equus* humerus (G20-6; distal view) (left) and its 3D image (right). Scale in cm.

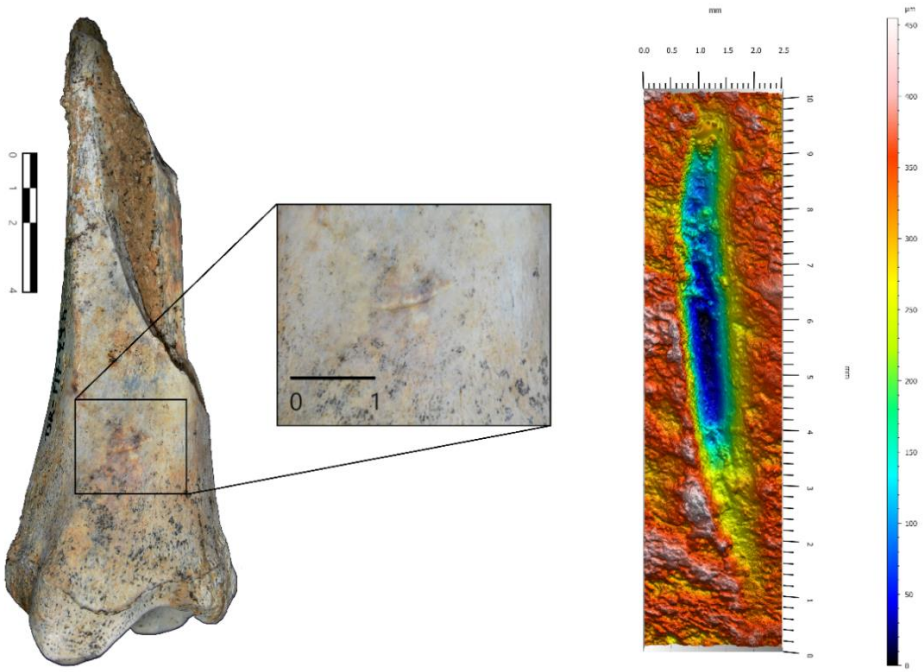

Figure 3.29: Score on the distal shaft of an *Equus* tibia (F17-29; anterior view) (left) and its 3D image (right). Scale in cm.

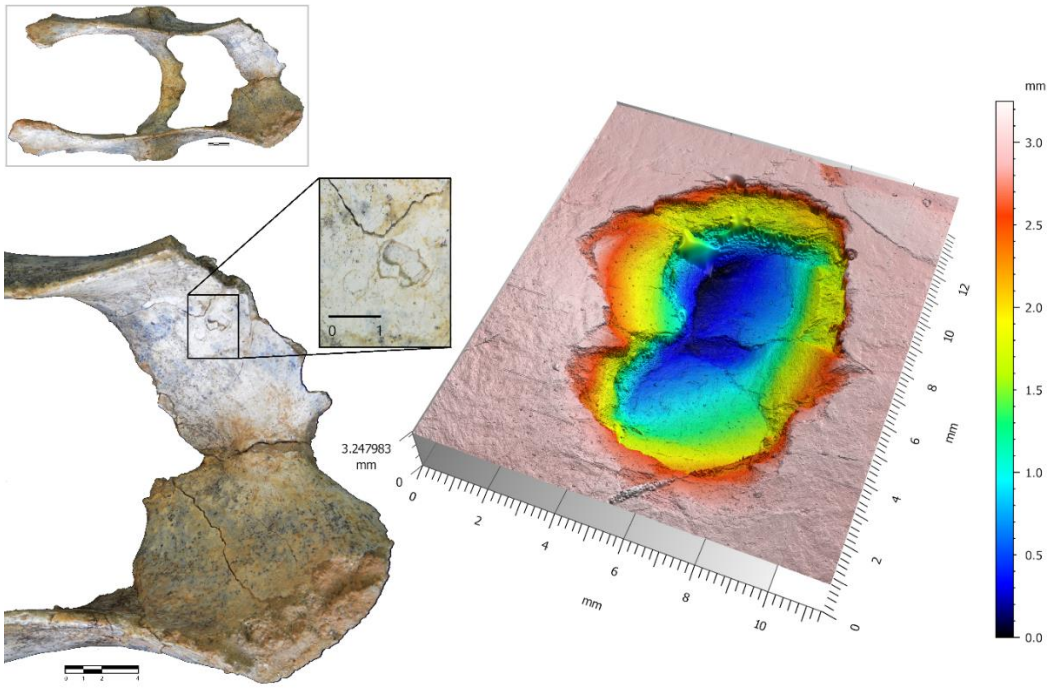

Figure 3.30: Puncture on a Bovini pelvis (G20-40; dorsal view) (left) and its 3D image (right). Scale in cm.

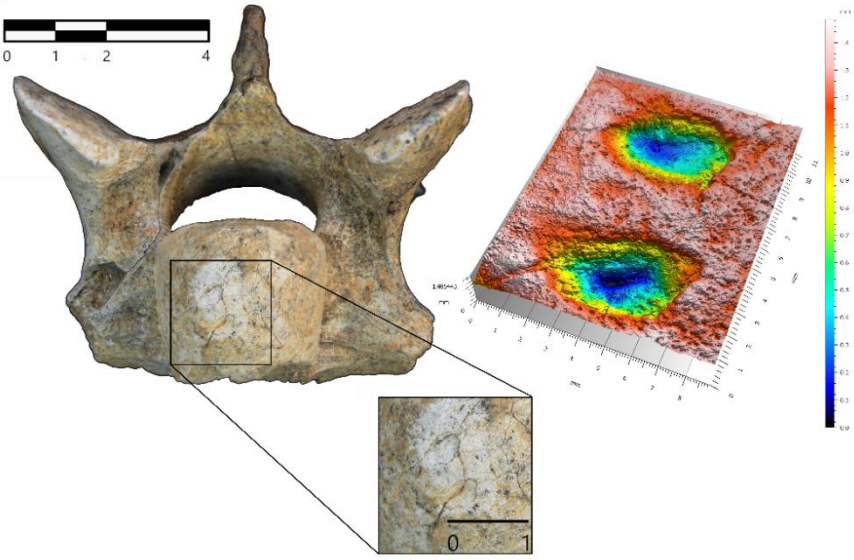

Figure 3.31: Punctures on an *Equus* 7th cervical vertebra (D18-124; rostral view) (left) and its 3D image (right). Scale in cm.

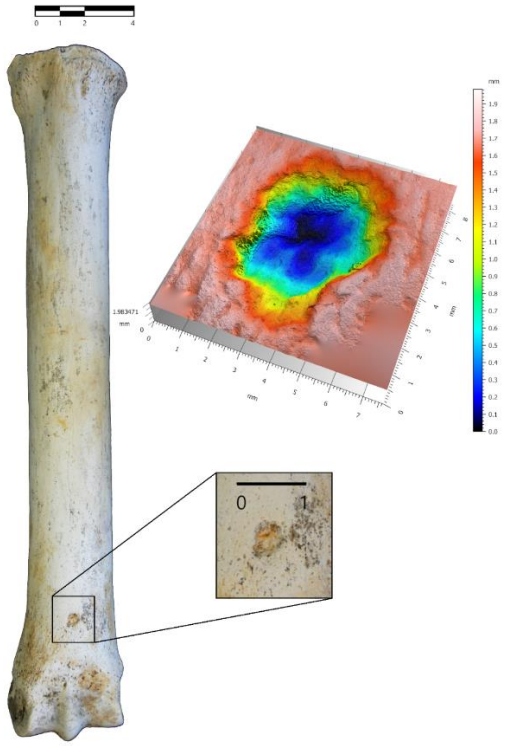

Figure 3.32: Puncture on the distal shaft of an *Equus* metatarsal (G17-23; anterior view) (left) and its 3D image (right). Scale in cm.

Statistical analysis was performed for the pit measurements, to investigate variation between the *Equus* (size group 4) and Bovini (size group 5) sample. The results are given in Table 3.11. The Shapiro-Wilk normality test was conducted for all variables. Then paired tests were performed in order to examine if the two groups can be differentiated according to each variable. Most *Equus* variables showed not normal distributions, so the Mann-Whitney test was used, with the exception of Ra and opening angle measurements in the deepest profile, where the variables exhibited normal distribution in both groups, so the *t*-test was performed instead. The results show that the variables where the two size groups cannot be differentiated are surface area, maximum length, floor radius of the deepest profile and all variables except area in the central profile. It appears that the *Equus* and Bovini samples cannot be differentiated from most measurements of the central profile, while a same mean (or median in case of the *t*-test) can be rejected for most of the 3D and deepest profile measurements.

		Shapiro-Wilk	**Shapiro-Wilk**	**Mann-Whitney / *t*-test**
		Equus	**Bovini**	
3D measurements	**surface area (mm²)**	0.000	**0.160**	**0.070**
	volume (µm³)	0.000	**0.448**	0.045
	maximum depth (µm)	0.000	**0.981**	0.039
	mean depth (µm)	0.000	**0.965**	0.040
	maximum length (mm)	0.001	**0.737**	**0.141**
	maximum width (mm)	0.006	**0.262**	0.016
Central profile	**depth (µm)**	0.000	**0.359**	**0.085**
	area (µm²)	0.000	**0.713**	0.048
	width (µm)	0.004	**0.771**	**0.054**
	Ra (µm)	**0.095**	0.005	**0.068**
	opening angle (°)	0.000	**0.862**	**0.783**
	floor radius (µm)	0.000	**0.085**	**0.082**
Deepest profile	**depth (µm)**	0.000	**0.470**	0.024
	area (µm²)	0.000	**0.754**	0.011
	width (µm)	0.003	**0.784**	0.029
	Ra (µm)	**0.073**	**0.563**	0.004
	opening angle (°)	**0.850**	**0.882**	**0.809**
	floor radius (µm)	0.000	0.009	**0.078**

Table 3.11: Results of the statistical analysis of the microscopic measurements of pits. Presented are the results of the Shapiro-Wilk test, for normality, and the *t* and Mann-

Whitney test for comparing differences between the *Equus* and Bovini samples. Values over 0.05 are in bold.

4. Discussion

Several carnivore taxa have been found at TSR, belonging to the families Canidae, Ursidae, Hyaenidae and Felidae. These include a wolf-like dog *Canis* sp., the bear *Ursus etruscus*, the hyaena *Pachycrocuta brevirostris* and the saber-toothed cat *Megantereon* sp. (Konidaris et al., 2015, 2021; Koufos et al., 2018). In addition to these taxa, the large carnivore fauna from the late Villafranchian of Mygdonia basin also includes the wild dog *Lycaon lycaonoides*, the lynx *Lynx issiodorensis*, the jaguar *Panthera gombaszoegensis* and the saber-toothed cat *Homotherium latidens* (Koufos, 2014, 2018 and references therein), thus most members of the large carnivore guild of the European late Villafranchian (Konidaris and Tourloukis, 2021) are recorded in the basin. Each of these large carnivores was equipped with great hunting, killing, or scavenging capabilities and dental specializations related to their dietary preferences (hypocarnivorous, carnivorous, bone/meat, hypercarnivorous) (Konidaris and Tourloukis, 2021 and references therein), and could modify and consume ungulate bones.

In order to assess the involvement of extinct carnivores in the formation and alteration of fossil assemblages, numerous studies have utilized comparisons with modern analogue species (e.g., Blumenschine, 1988; Arribas and Palmqvist, 1998; Capaldo, 1998; Domínguez-Rodrigo et al., 2007; Sala et al., 2012; Arilla et al., 2014). Several researchers have emphasized the need of a multivariate approach in order to make valid assumptions about bone accumulators/modificators at fossil sites (e.g., Dominguez Rodrigo and Pickering, 2010; Domínguez-Rodrigo et al., 2012; Saladié et al., 2019). This study follows this notion, considering multiple aspects of carnivore alteration of skeletal assemblages, such as skeletal element survivorship, gross limb bone damage, and tooth mark frequency, anatomical distribution and morphometry. The studied TSR sample is comprised of ungulate bones of carcasses belonging to the size groups 4 and 5 of Palombo (2010), thus with a body mass ranging from 150 to 1000 kg.

Gross limb bone damage: Although light gnaw damage is not useful in the identification of the acting carnivore taxa, medium and heavy stages of bone modification can be discriminative (Haynes, 1983). The most representative taphotypes (according to Domínguez-Rodrigo et al., 2015) for each long limb bone are presented in Figures 3.6 and 3.7 (elements that were predominately preserved complete are not depicted). Stylopodial are the most heavily modified elements, in both *Equus* and Bovini, with high percentages of isolated shafts (Figs. 4.1 and 4.2). Radii appear complete frequently, more so in Bovini. Tibiae, on the contrary appear heavily modified with a very low percentage of complete elements. In both groups the majority lack the proximal epiphysis (Fig. 4.3). Metapodials appear mostly complete. The fracturing of midshafts is common in the sample, corresponding to taphotypes 3–5 and 10–12, which are relatively abundant in the studied TSR material. Furthermore, although not quantified in this study, the numerous indeterminate, often tooth-marked, shaft fragments present at the site indicate intense ravaging (Fig. 4.4).

Figure 4.1: Examples of deletion in *Equus* humeri. Posterior view of specimens F19-31, E16-15, G20-6, TSR-142 and G20-7 (from left to right). Scale in cm.

Figure 4.2: Examples of deletion in *Equus* femora. Posterior view of specimens H21-11, G20-15, F16-21 and F18-39 (from left to right). Scale in cm.

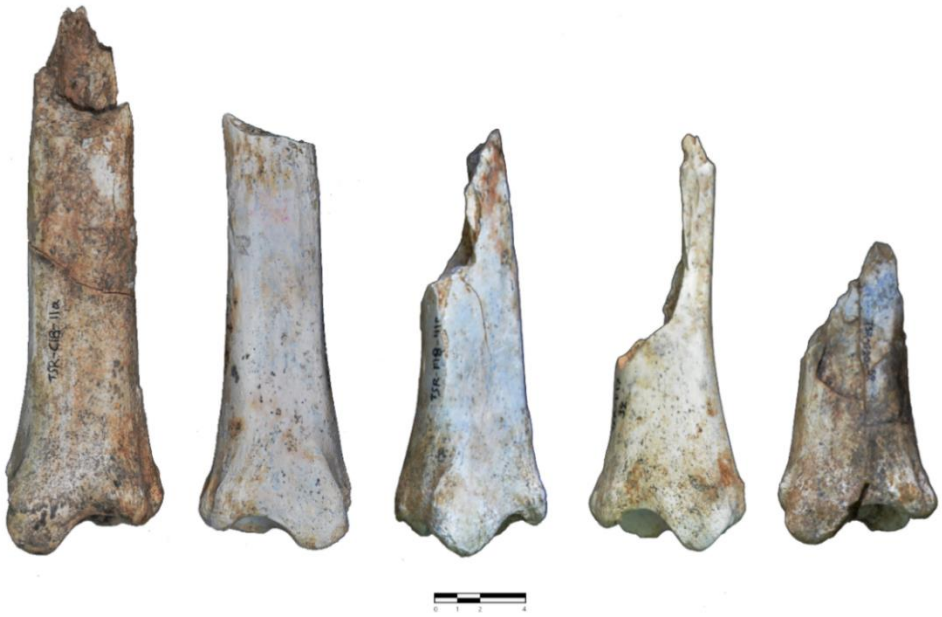

Figure 4.3: Examples of deletion in *Equus* tibiae. Posterior view of specimens C18-11, F18-60, F18-41, F17-32 and G20-52 (from left to right). Scale in cm.

Figure 4.4: Examples of indeterminate size groups 4/5 shaft fragments bearing tooth marks (specimens H16-4, G21-64, F16-12, G22-6, G19-5, G21-84 and G21-85) (from left to right). Scale in cm.

Concerning the bear *Ursus etruscus*, Medin et al. (2017, 2019), performed morphological and dental microwear analyses on *U. etruscus* teeth from Dmanisi (Georgia) and the Orce sites (Guadix-Baza basin, Spain), and concluded that this ursid followed an omnivorous diet, consuming both plant material and vertebrate flesh depending on availability, similar to the extant *Ursus arctos*. Observations of brown bears in the wild showed that they do not fracture ungulate long bones (Haynes, 1983; Sala and Arsuaga, 2013). Saladié et al. (2013) reported fracturing by captive and semi-captive brown bears, although limited to small-sized and juvenile carcasses. Arilla et al. (2014) noted that the intensity of other types of modification (tooth marks, crushing and furrowing) is moderate, and not significantly affected by prey size. Although, modern brown bears have been observed modifying bones, albeit only moderately, the isotopic analyses of Medin et al. (2017) for *Ursus etruscus* teeth from the Orce sites, showed a significant

contribution of fish and plant tissues in its diet. Therefore, the intensity of gross bone damage observed in the TSR sample and the dietary preferences of *U. etruscus*, disqualifies this ursid from being the primary agent of bone modification at the site.

Several studies on large modern felids (in particular *Panthera leo* and *Panthera pardus*) have shown that they do not inflict significant gnaw damage on long bones, noting the absence of considerable epiphyseal deletion and isolated cylinders in felid modified assemblages (e.g., Haynes, 1983; Domínguez-Rodrigo, 1999; Pickering et al., 2011; Gidna et al., 2013). When deletion is present, it is usually limited to specific areas: the caudal side of distal humerus, the proximal ulna and the proximal tibia (Domínguez-Rodrigo et al., 2007); the deletion of limb bone epiphyses has been observed in small-sized carcasses (Parkinson, 2013). In their study concerning zebras preyed upon by wild lions, Pobiner et al. (2020) concluded that significant long limb bone damage was limited to the distal femur - patellar groove, proximal humerus and ulna olecranon process. Like extant felids, sabretooths were also flesh specialists (hypercarnivores, (see e.g., Palombo, 2016, i.e., with >70% meat in their diet (Van Valkenburgh, 1988)), as suggested by the lack of bone crunching dental adaptations (Hartstone-Rose and Wahl, 2008; Hartstone-Rose, 2011). Moreover, some researchers argue that they avoided teeth contact with bone, in order to prevent damage to their remarkably long canines (Emerson and Radinsky, 1980; Valkenburgh and Ruff, 1987; Valkenburgh et al., 1990; Arribas, 1999). The craniodental features of *Megantereon* suggest the exclusive consumption of soft tissues (Palmqvist et al., 2007). Its enlarged canines, in combination with a significant reduction of the premolars and the shortening of the coronoid process, as well as the possession of powerful forelimbs, suggest an increased ability in the killing of larger prey, paired with the consumption of exclusively soft tissues; therefore, leaving considerable amounts of flesh and bones for scavengers, like the hyaena *Pachycrocuta* (Martínez-Navarro and Palmqvist, 1996; Palmqvist et al., 2007; Espigares et al., 2021). Concerning *Homotherium*, although tooth marks have been observed in juvenile mammoth

remains of a *Homotherium* den (Friesenhahn Cave, U.S.A.) with frequencies similar to modern hyaenids and canids, bone cracking was scarce (Marean and Ehrhardt, 1995). Palmqvist et al. (2008) used biogeochemical and ecomorphological data to draw conclusions regarding the most common species preyed upon by the Early Pleistocene carnivores of Venta Micena (Spain). They concluded that *Homotherium latidens* was a cursorial predator that hunted medium- to large-sized open habitat herbivores (*Bison*, *Equus* and *Mammuthus*), while *Megantereon whitei* was an ambushing predator focusing on *Equus*, *Praemegaceros* and *Stephanorhinus*. Besides sabertooths, the other large and hypercarnivorous felid of this period, *Panthera gombaszoegensis*, was a solitary stalking predator that hunted mainly cervids (*Praemegaceros* and medium-sized cervids) (Palmqvist et al., 2008). A smaller-sized felid present in the late Villafranchian carnivore fauna from Mygdonia is *Lynx issiodorensis*. The diet of its putative descendant *Lynx pardinus* (Iberian lynx) consists of mainly rabbits, supplemented with other small mammals and birds and rarely small-sized ungulates (Rodríguez-Hidalgo et al., 2020). *Lynx issiodorensis* was larger than its modern counterpart (Mecozzi et al., 2021) and this was possibly reflected in the size of its prey. However, it is unlikely that it was able to hunt prey as large as the ungulates concerning this study, as well as to produce the intensity of carnivore damage observed in TSR.

Modern wolves (*Canis lupus*) have been observed fracturing ungulate bones to access marrow (Sala et al., 2014a), as well as consuming parts of the bone itself, evident by the presence of bone fragments in their feces (Esteban-Nadal et al., 2010; Fosse et al., 2012). Campmas and Beauval (2008) noted that damage patterns produced by captive wolves and wild hyaenas on large ungulate carcasses, are indistinguishable. Fosse et al. (2012) also mentions that alterations caused by wolves display high variability and cannot be easily distinguished from other large predators. Although both hyaena and wolf modified assemblages can exhibit heavy modification of bones, hyaenas are generally more destructive (Haynes, 1983; Domínguez-Rodrigo et al., 2015). Moreover, carcasses altered by

wild wolves have been shown to reach high degrees of modification only in small-sized animals, or juveniles of medium-sized species (Yravedra, 2011). A similar pattern can perhaps be assumed for the several *Canis* species known from the late Villafranchian–Epivillafranchian of Europe: *C. arnensis*, *C. etruscus*, *C. borjgali*, *C. orcensis*, *C. appolloniensis* and *C. mosbachensis*. Martinez-Navarro et al. (2021) regarded the presence of a comparatively enlarged trigonid blade of the lower carnassial and a robust mandible as indicators of hypercarnivory. Based on this and other morphometric indexes they concluded that *C. orcensis* from Venta Micena and *C. mosbachensis* from Untermassfeld (Germany) were probably hypercarnivorous, *C. apolloniensis* from Apollonia-1 and *C. borjgali* from Dmanisi fall between the range for mesocarnivores and hypercarnivores, whereas *C. arnensis* from Upper Valdarno and *C. etruscus* from Olivola, Upper Valdarno and Pantalla (Italy) are classified as mesocarnivores.

Not all canids modify bones to the same degree. The African wild dog *Lycaon pictus*, which is characterized by hypercarnivory (Hartstone-Rose, 2008) has been shown to modify bones only moderately (Yravedra et al., 2014). The diet of the late Villafranchian–Epivillafranchian *Lycaon lycaonoides* consisted of ungulates with a body mass larger than its own (Palmqvist et al., 1999). Microwear analysis shows that it mainly consumed meat, classifying it as a hypercarnivore (Medin et al., 2017). Its forerunner, *Lycaon falconeri* is also considered to be a hypercarnivore, since its craniodental morphology is similar to that shown in extant hypercarnivorous canids (Palmqvist et al., 1999).

Extant hyaenas vary in body mass and craniodental morphology, and these differences are reflected in their ability to modify carcasses. The larger body size and more specialized premolars of *Crocuta crocuta* (spotted hyaena) suggest a greater capability in bone cracking of large bones, compared to *Hyaena hyaena* (stripped hyaena) and *Parahyaena brunnea* (brown hyaena) (Ewer, 1973; Mills, 1990; Van Valkenburgh and Binder, 2000). This is further supported by dental microwear analysis, that reveals extreme bone cracking abilities for *Crocuta crocuta*, and a meat and bone diet for *Hyaena hyaena* (Bastl et al., 2012). A

characteristic of hyaena modified assemblages is the predominance of limb bones, as they consume axial elements at kill sites (Binford, 1981; Capaldo, 1998). Haynes (1983) observed high destructive behaviour in spotted hyaenas, where in the final stages of utilization the femur was either reduced to short shaft fragments or completely consumed, and the tibia was proximally reduced until less than of third of the shaft survived. Notably the extreme distal end usually appears unmarked. Hill (1989) reported that spotted hyaena modified assemblages display a high percentage of indeterminate fragments, with the majority of bones (especially limb bones) being fractured, and a very high proportion of complete metapodials. The recurring breakage of dense elements through their midshafts is another characteristic that suggest the involvement of hyaenas or possibly canids (Domínguez-Rodrigo et al., 2007). Bones modified by hyaenas display considerably heavier damage than those modified by felids (see Domínguez-Rodrigo et al., 2015, Figure 8).

During the late Villafranchian–Epivillafranchian, the sole hyaenid that appears in the European fossil assemblages is *Pachycrocuta brevirostris* (with the exception of *Chasmaporthetes* which is still present during the earliest late Villafranchian, and the appearance of *Crocuta* at the end of the Epivillafranchian). This hyaenid had an average estimate of body mass of 110 kg (nearly twice that of the spotted hyaena) and unique craniodental adaptations, which indicate great bone fracturing capability (Palmqvist et al., 2011). More specifically, those include robust premolars that along with the carnassials are positioned posteriorly, thus allowing the manipulation of larger bones, a higher, more resistant mandibular corpus, and a well-developed angular process that suggests the possession of large masseter and pterygoid muscles. These adaptations, along with a deeper mandibular corpus and a more developed symphysis compared to extant hyaenas, suggest that the extinct hyaenid possessed drastically higher bone-cracking capabilities than its extant counterparts (Palmqvist et al., 2011). Its postcranial skeleton also shows adaptations for scavenging, with a robust body and shortened distal limb bones less suited for a cursorial lifestyle, but offering strength and

stability for the dismembering and transport of carcass parts to their dens (Turner and Antón, 1996). The faunal and skeletal representation of Venta Micena, a site interpreted as a *Pachycrocuta brevirostris* accumulation, indicates that this carnivore selectively scavenged prey hunted by saber-tooths, as well as the canid *Lycaon lycaonoides* (Palmqvist et al., 1996). Indeed, the preferential deletion of specific long limb bone epiphyses in the TSR sample appears to be correlated to their nutritional value and mineral density. More specifically, epiphyses with low mineral density and high marrow yield appear less frequently in the *Equus* sample. Similarly, in the Bovini sample, the investigation of a possible relationship between fat content and epiphyses survivorship showed that epiphyses richer in fat were deleted more frequently. This pattern of selective deletion according to higher nutritional value has been observed in ungulate carcasses transported by extinct and extant hyaenas to their dens (e.g., Arribas and Palmqvist, 1998; Palmqvist et al., 1996; Leakey et al., 1999).

Skeletal element representation and bone articulations: In addition to the intensity of bone damage in the studied TSR sample, another criterion that excludes felids as the primary modificators of the assemblage is the relative abundance of axial and limb bones. Although ribs cannot be taken into consideration, since their collection was not systematic during the early years of excavation, MAU values of vertebrae and long bones (Table 3.3) show that axial elements are underrepresented in the assemblage, while limb bones are abundant (see also Giusti et al., 2019). These values could suggest hyaena involvement, as it has been observed that spotted hyaenas consume the axial skeleton at kill sites, thus creating assemblages where limb bones are predominant (e.g., Skinner et al., 1986; Capaldo, 1998), whereas felids have been shown to modify axial bones without deleting them (e.g., Domínguez-Rodrigo, 1999).

The ratio of articulated to isolated elements has been correlated with accumulator type, where primary assemblages collected by predators display an abundance of articulated elements, while in secondary assemblages collected by scavengers only metapodials, phalanges and vertebrae appear articulated often

(Palmqvist and Arribas, 2001 and references therein). As an example, in Venta Micena only 20% of elements appear articulated (Palmqvist and Arribas, 2001). In the case of TSR, for the *Equus* sample, the majority of long limb bones appear isolated, with the exception of radii and metatarsals where 54.5 and 56.5% respectively are articulated. On the contrary, most Bovini long limb bones are articulated, but notably 61.5% of metacarpals and 69.2% metatarsals are isolated. The prevalence of isolated elements has also been reported in hyaena den accumulations where prey was scarce, thus the consumption of carcasses reached higher stages (Fourvel and Mwebi, 2011). Taking into account both the *Equus* and Bovini sample, isolated long bone elements predominate slightly, with a percentage of 52.2%. This does not give a clear signal as to the type of accumulator, but it could suggest an abundance in prey. The latter is also supported by the presence of complete and almost complete elements (taphotypes 0 and 1).

Tooth mark frequency and anatomical distribution: The study of the frequency of tooth-marked bone portions and the analysis of spatial distribution of tooth marks revealed relatively intense tooth marking across all long limb bones. The femur is the most frequently tooth-marked element in both examined size groups, followed by the humerus and tibia. Notably, half of radio-ulnae are also tooth-marked. Metapodials exhibit noticeably lower frequencies, in particular metacarpals. Middle shafts are the most tooth-marked bone portions in all elements, except of the femur and metatarsal in *Equus*, where the distal shaft and distal end respectively present higher frequencies. When taking into consideration both *Equus* and Bovini, the only bone portions that appear free of tooth marks are the distal shaft and end of radii, both ends in metacarpals and the proximal end in tibiae. Concerning the spatial distribution of tooth marks, all limb bones display visible clusters. The diaphyses exhibit higher concentrations of tooth marks, nevertheless clusters are visible in both femora epiphyses, as well as in the distal epiphyses of humeri and metatarsals.

The most frequently tooth-marked elements in assemblages modified by modern large felids are the femur, humerus and tibia, with most tooth marks occurring on long limb bone ends, leaving midshaft section with only a few marks (Pobiner, 2007; Parkinson, 2013; Domínguez-Rodrigo et al., 2021). Experiments with captive wolves showed heavy tooth-marking on all long bones, with lower degrees in midshafts, with the exception of radii (Parkinson, 2013). Modern hyaenas show high variability in frequency of tooth marked bone portions, not only among different species, but also between different assemblages created by the same species (see Faith, 2007; Kuhn et al., 2009). In spotted hyaenas, all bone portions across all long bones appear tooth-marked in the experiments of Faith (2007), with higher frequencies for tibiae proximal shafts, humeri distal shafts and ends and radii midshafts. Kuhn et al. (2009) report the presence of tooth marks on all bone portions except proximal epiphyses in tibiae, and middle shafts in humeri and femora; humeri and femora are tooth-marked in higher frequencies. Blumenschine (1988) reported high frequencies (>75%) of tooth marked mid-shaft fragments in assemblages where spotted hyaenas had primary access to bovid limb bones. As is the case with gross bone damage, tooth mark clustering patterns can be interpreted as a spectrum of bone processing intensity, with large felids at the lower, large canids at the middle, and hyaenids at the higher end of the spectrum (Parkinson, 2013).

Tooth mark dimensions: The value of tooth mark dimensions alone as indicator of the species responsible for bone modification has been debated. Domínguez-Rodrigo and Piqueras (2003) argued that dimensions of conspicuous tooth marks can be utilized for determining the size of the carnivore responsible. More specifically, they suggest that pit dimensions on cancellous bone can categorize carnivore taxa into three groups: those with length under 4 mm can be attributed to all carnivores besides lions, those between 4 and 6 mm to middle and large sized carnivores, excluding all felids except lions, and those above 6 mm are produced by large carnivores, mainly lions and hyaenas. Domínguez-Rodrigo et al. (2007) maintained that pit dimensions on cancellous bone are more

discriminative, nevertheless pit measurements on cortical bone can differentiate between small carnivores, that produce pits under 2.2 mm in length and 1.5 mm in breadth, while pits above 4 mm in length and 2 mm in breadth can be confidently attributed to hyaenas and lions. Delaney-Rivera et al. (2009) found almost no correlation between carnivore body mass and tooth mark dimension on the diaphysis, while a weak but consistent positive correlation was observed for epiphyseal tooth marks. At the same time Saladié (2009), Andrés et al. (2012) and Sala et al., (2014b) argued that the best indicator of the responsible carnivore is the pit length on cortical bone. Andrés et al. (2012) argued that the lack of correlation between tooth mark dimensions and carnivore size in Domínguez-Rodrigo and Piqueras (2003)'s and Delaney-Rivera et al. (2009)'s observations can be attributed to small sample size or the use of small-sized carcasses. Overall, researchers agree that tooth mark dimensions can be used as an indicator of carnivore size and should be utilized in a multivariate context in order to lead to more specific conclusions regarding carnivore taxa.

In the TSR sample, pits on cancellous bone have a mean length of 3.38, 4.04 and 3.60 mm in the *Equus*, Bovini and total size 4/5 sample, respectively. For cortical bone mean length/breadth values for the same groups are 3.43/2.15 mm, 3.52/2.42 mm, and 3.49/2.18 mm. Therefore, although the mean length does not reach the threshold of 4 mm (Domínguez-Rodrigo et al., 2007), breadth values above 2 mm suggests hyaenid or lion involvement for TSR. The comparison of TSR pit dimensions on shafts (Figs. 3.21–3.24) with measurements from modern experiments also suggests that the carnivore responsible for the alterations was of large body size, analogue to modern brown bears, lions, spotted hyaenas and wolves. Notably, the upper range of pits dimensions on cortical bone seems to exceed that of most modern large predators. Finally, it is important to note the dimensions of punctures on cancellous bone. Mean lengths of 10.71, 6.60 and 8.66 mm and mean breadths of 7.14, 5.16 and 6.15 mm for *Equus*, Bovini and total size 4/5 sample, respectively, suggest the involvement of carnivores that possessed teeth of proportional size in order to produce such impressions.

3D tooth mark analysis: Regarding the 3D tooth mark analysis, because the employed method is relatively new, comparative data for specific carnivore taxa is not available. For this reason, the comparisons were limited within the TSR sample, between the two studied size groups: size group 4, represented by *Equus* and size group 5, represented by Bovini. The results of statistical analyses showed that the possibility of equal means between the two groups must be rejected for most 3D measurements, as well as for most measurements regarding the deepest profile of the mark. On the contrary, a same mean cannot be rejected for most measurements of the central profile. These preliminary results suggest that measurements of central profiles of tooth marks do not show any significant differences between size groups.

Comparison with Venta Micena: One of the sites, where the taphonomic signature of *Pachycrocuta brevirostris* was investigated, is the late Villafranchian site of Venta Micena. This site is interpreted as an accumulation by *Pachycrocuta brevirostris* of portions of prey of flesh-eating carnivores (e.g., saber-toothed cats and wild dogs) in the surroundings of its maternity den (Palmqvist et al., 1996, 2011; Arribas and Palmqvist, 1998; Palmqvist and Arribas, 2001). The two sites show striking similarities in the pattern of consumption activity. In both Venta Micena and TSR the deletion of humeri and tibiae starts from the proximal epiphyses, followed by the fracturing of the diaphysis and finally the gnawing of the distal epiphysis that usually displays intense tooth marking (App Figs. 7–10), although in the case of TSR the distal tibia shows a relatively low abundance of tooth marks. Another common characteristic in the two samples is the consumption of the femur, where both epiphyses are consumed, leaving high frequencies of isolated shafts. The consumption of the radius also shows similarities, with most modified *Equus* specimens revealing a proximodistal deletion sequence. Finally, both in Venta Micena and TSR metacarpals and metatarsals show signs of modification without any particular direction, but their deletion is limited, and they are usually preserved as complete elements. The selective consumption of bone portions for each element in Venta Micena was associated with within bone

nutrient content, as well as bone density (Palmqvist et al., 1996; Arribas and Palmqvist, 1998). The same is true for the TSR sample, where bone portion survivorship shows a positive correlation with bone density, and a negative correlation with fat and marrow content.

General remarks: All the above comparisons regarding skeletal part representation, gross bone damage, and tooth mark frequency, spatial distribution and morphometry, indicate that a large carnivore was the primary biotic agent of bone modification at TSR, with a hyaenid (i.e., *Pachycrocuta brevirostris*) being the main candidate. The similarities of TSR with Venta Micena further support the notion that *Pachycrocuta* was the main agent of bone modification at the site. It is important to note that although the principal taphonomic signal points towards the short-faced hyaena, other carnivores may have probably also contributed to the alteration of bones, but to a lesser degree. This is perhaps expected, considering that *Pachycrocuta* is believed to have acted as a kleptoparasite that scavenged carcasses abandoned by other carnivores, such as the flesh-eating sabre-tooths *Megantereon* and *Homotherium* (Palmqvist et al., 1996; Arribas and Palmqvist, 1998; Palmqvist and Arribas, 2001). Whether TSR could represent a denning site like Venta Micena needs further analyses (e.g., mortality profiles, study of the other size-groups recorded at the site, comparison with modern dens), but the presence of juvenile remains (Konidaris et al., 2015) and coprolites (Konidaris pers. comm. 2021) at the site, both regarded as some of the criteria for the identification of hyaena dens (Kruuk, 1972; Kuhn et al., 2010), could be indications in support.

5. Conclusions

The present study employed a multitude of different analyses in an attempt to identify the principal taphonomic agent of bone modification in the site of Tsiotra Vryssi. Those include the analysis of skeletal part representation, gross bone damage patterns, as well as tooth mark frequency, spatial distribution, and morphometry. The results are summarized below:

- All generated results point towards an intense taphonomic signal of carnivore ravaging.
- The analysis of skeletal part representation shows a highly preferential preservation of limb bones compared to axial elements. Moreover, among long limb bones, those that predominate are metapodials and tibiae, although the latter display heavy deletion of proximal ends and proximal shafts on most specimens. These patterns suggest preferential deletion of nutrient dense elements and bone sections. This is further supported in the regression analysis of surviving epiphyses, where their raw abundances showed significant positive correlation with bone density, and negative correlation with bone marrow content and fat weight.
- Gross bone damage patterns revealed heavy gnaw damage on nutrient dense elements, even more in the *Equus* sample. The most heavily modified elements are humeri, femora and tibiae. Stylopodials appear more frequently as isolated shafts in *Equus*, while in Bovini the distal half usually survives. Tibiae proximal shafts rarely survive. Radii and metapodials are frequently preserved complete.
- All long limb elements appear tooth marked. Stylopodials display the highest frequencies, with most elements being tooth marked in both *Equus* and Bovini. Zygopodials also appear tooth marked frequently, with percentages of 50% or higher. In metapodials the percentage of tooth mark elements is relatively low (<35%). The anatomical distribution of tooth marks varies among different elements, although all of them display significant concentrations. The most frequently tooth-marked bone portion is the middle shaft.

- The comparative analysis of tooth mark dimensions of the TSR sample with data obtained from actualistic studies reveals the involvement of a large-sized carnivore in the alteration of bones. It was not feasible to compare the high-resolution metric data of our sample, since comparative datasets are not available yet.
- All aforementioned data indicate intense carnivore damage on bones, in accordance with assemblages modified by hyaenids. Therefore, the carnivore damage in the TSR assemblage is attributed to the activity of *Pachycrocuta brevirostris*, identified at the site.
- This conclusion is further supported by the similarities of TSR and Venta Micena, where *P. brevirostris* is considered to be the main taphonomic agent of bone modification. Both sites show similar deletion sequences, where the consumption of humeri and tibiae shows a proximodistal direction, femora appear frequently as isolated shafts, while metapodials are mostly preserved complete. The Venta Micena sample also displays preferential deletion of nutrient dense epiphyses.
- Overall, the principal taphonomic signal at TSR suggests the identification of *Pachycrocuta brevirostris* as the main taphonomic agent of bone modifications. Further analyses are needed to examine the possibility of TSR constituting a denning site.
- The high-resolution 3D tooth mark analysis is the first such study of a Lower Pleistocene assemblage modified by carnivores from Europe and the first one, where *Pachycrocuta* comprises the main bone modification agent. This database will be a useful tool for future comparative analyses and will contribute to the taphonomic interpretation of other fossiliferous sites.

References

Andrés, M., Gidna, A.O., Yravedra, J., Domínguez-Rodrigo, M., 2012. A study of dimensional differences of tooth marks (pits and scores) on bones modified by small and large carnivores. Archaeological and Anthropological Sciences 4, 209–219.

Arilla, M., Rosell, J., Blasco, R., Domínguez-Rodrigo, M., Pickering, T.R., 2014. The “bear” essentials: actualistic research on *Ursus arctos arctos* in the spanish Pyrenees and its implications for paleontology and archaeology. PLoS ONE 9, e102457.

Arribas, A., 1999. On the ecological connection betwenn sabre-tooths and hominids: Faunal dispersal events in the Lower Pleistocene and a review of the evidence for the first human arrival in Europe. Journal of Archaeological Science 26, 571–585.

Arribas, A., Palmqvist, P., 1998. Taphonomy and palaeoecology of an assemblage of large mammals: Hyaenid activity in the Lower Pleistocene site at Venta Micena (Orce, Guadix-Baza Basin, Granada, Spain). Geobios 31, 3–47.

Bastl, K., Semprebon, G., Nagel, D., 2012. Low-magnification microwear in Carnivora and dietary diversity in *Hyaenodon* (Mammalia: Hyaenodontidae) with additional information on its enamel microstructure. Palaeogeography, Palaeoclimatology, Palaeoecology 348–349, 13–20.

Bello, S.M., Verveniotou, E., Cornish, L., Parfitt, S.A., 2011. 3-dimensional microscope analysis of bone and tooth surface modifications: comparisons of fossil specimens and replicas. Scanning 33, 316–324.

Binford, L.R., 1981. Bones: ancient men and modern myths. Academic Press, New York.

Binford, L.R., 1984. Faunal remains from Klasies River Mouth. Academic Press, New York.

Blumenschine, R.J., 1988. An experimental model of the timing of hominid and carnivore influence on archaeological bone assemblages. Journal of Archaeological Science 15, 483–502.

Brink, J.W., 1997. Fat content in leg bones of *Bison bison*, and applications to archaeology. Journal of Archaeological Science 24, 259–274.

Budras, K.-D., Sack, W.O., Röck, S., 2011. Anatomy of the horse. Schlütersche, Hannover.

Campmas, É., Beauval, C., 2008. Consommation osseuse des carnivores : résultats de l'étude de l'exploitation de carcasses de bœufs (*Bos taurus*) par des loups captifs. Annales de Paléontologie 94, 167–186.

Capaldo, S.D., 1998. Simulating the formation of dual-patterned archaeofaunal assemblages with experimental control samples. Journal of Archaeological Science 25, 311–330.

Damuth, J.D., MacFadden, B.J. (Eds.), 1990. Body size in mammalian paleobiology: estimation and biological implications. Cambridge University Press, Cambridge, New York.

De Renzi, M., 1997. Información tafónómica e infórmación paleobiológica ¿un falso dilema? Journal of Iberian Geology 23, 183–210.

Delaney-Rivera, C., Plummer, T.W., Hodgson, J.A., Forrest, F., Hertel, F., Oliver, J.S., 2009. Pits and pitfalls: taxonomic variability and patterning in tooth mark dimensions. Journal of Archaeological Science 36, 2597–2608.

Domínguez-Rodrigo, M., 1999. Flesh availability and bone modifications in carcasses consumed by lions: palaeoecological relevance in hominid foraging patterns. Palaeogeography, Palaeoclimatology, Palaeoecology 149, 373–388.

Domínguez-Rodrigo, M., Piqueras, A., 2003. The use of tooth pits to identify carnivore taxa in tooth-marked archaeofaunas and their relevance to reconstruct hominid carcass processing behaviours. Journal of Archaeological Science 30, 1385–1391.

Dominguez Rodrigo, M., Pickering, T.R., 2010. A multivariate approach for discriminating bone accumulations created by spotted hyenas and leopards: harnessing actualistic data from east and Southern Africa. Journal of Taphonomy 8, 155–179.

Domínguez-Rodrigo, M., Egido, R.B., Egeland, C.P., 2007. Deconstructing Olduvai: A taphonomic study of the Bed I sites, Vertebrate Paleobiology and Paleoanthropology. Springer Netherlands, Dordrecht.

Domínguez-Rodrigo, M., Gidna, A.O., Yravedra, J., Musiba, C., 2012. A Comparative neo-taphonomic study of felids, hyaenids and canids: An analogical framework based on long bone modification patterns. Journal of Taphonomy 10, 147–164.

Domínguez-Rodrigo, M., Yravedra, J., Organista, E., Gidna, A., Fourvel, J.-B., Baquedano, E., 2015. A new methodological approach to the taphonomic study of paleontological and archaeological faunal assemblages: a preliminary case study from Olduvai Gorge (Tanzania). Journal of Archaeological Science 59, 35–53.

Domínguez-Rodrigo, M., Gidna, A., Baquedano, E., Cobo-Sánchez, L., Mora, R., Courtenay, L.A., Gonzalez-Aguilera, D., Mate-Gonzalez, M.A., Prieto-Herráez, D., 2021. A 3D taphonomic model of long bone modification by lions in medium-sized ungulate carcasses. Scientific Reports 11, 4944.

Efremov, I.A., 1940. Taphonomy: a new branch of paleontology. Pan-American Geologist 74, 81–93.

Eickhoff, S., Herrmann, B., 1985. Surface marks on bones from a neolithic collective grave (Odagsen, Lower Saxony). A study on differential diagnosis. Journal of Human Evolution 14, 263–274.

Eisenmann, V., Sondaar, P., 1998. Pliocene vertebrate locality of Çalta, Ankara, Turkey. 7. Hipparion. Geodiversitas 20, 409–439.

Eisenmann, V., Alberdi, M.T., De Giuli, C., Staesche, U., 1988. Studying fossil horses: collected papers after the “New York International Hipparion

Conference, 1981." Presented at the New York International Hipparion Conference, E.J. Brill, Leiden, New York.

Emerson, S.B., Radinsky, L., 1980. Functional analysis of sabertooth cranial morphology. Paleobiology 6, 295–312.

Espigares, M.P., Martínez-Navarro, B., Ros-Montoya, S., José Manuel, G.-A., Guerra-Merchán, A., RodrÍguez-Gómez, G., Palmqvist, P., 2021. Hominins, mammoths, saber-tooths and giant hyenas in the Early Pleistocene of the Baza Basin (SE Spain), in: Konidaris, G.E., Barkai, R., Tourloukis, V, Harvati, K. (Eds.), Human-Elephant Interactions: From Past to Present. Tübingen University Press, Tübingen, pp. 47–66.

Esteban-Nadal, M., Cáceres, I., Fosse, P., 2010. Characterization of a current coprogenic sample originated by *Canis lupus* as a tool for identifying a taphonomic agent. Journal of Archaeological Science 37, 2959–2970.

Ewer, R.F., 1973. The carnivores. Cornell University Press, Ithaca, N.Y.

Faith, J.T., 2007. Sources of variation in carnivore tooth-mark frequencies in a modern spotted hyena (*Crocuta crocuta*) den assemblage, Amboseli Park, Kenya. Journal of Archaeological Science 34, 1601–1609.

Fernández-López, S.R., 1991. Taphonomic concepts for a theoretical biochronology. Revista española de paleontología, 6, 37–49.

Fisher, J.W., 1995. Bone surface modifications in zooarchaeology. Journal of Archaeological Method and Theory 2, 7–68.

Fosse, P., Wajrak, A., Fourvel, J.B., Madelaine, S., Esteban-Nadal, M., Cáceres, I., Yravedra, J., Brugal, J.P., Prucca, A., Haynes, G., 2012. Bone modification by modern wolf (*Canis lupus*): A taphonomic study from their natural feeding places. Journal of Taphonomy 10, 197–217.

Fourvel, J.-B., Mwebi, O., 2011. Hyenas' level of dependence on livestock in pastoralist areas in the Republic of Djibouti and Kenya : relation between prey availability and bone consumption sequence. Presented at the XXXI e rencontres internationales d'archéologie et d'histoire d'Antibes - Prédateurs

dans tous leurs états. Évolution, Biodiversité, Interactions, Mythes, Symboles.

Gidna, A., Yravedra, J., Domínguez-Rodrigo, M., 2013. A cautionary note on the use of captive carnivores to model wild predator behavior: a comparison of bone modification patterns on long bones by captive and wild lions. Journal of Archaeological Science 40, 1903–1910.

Gifford-Gonzalez, D., 1991. Bones are not enough: Analogues, knowledge, and interpretive strategies in zooarchaeology. Journal of Anthropological Archaeology 10, 215–254.

Gifford-Gonzalez, D., 2018. An introduction to zooarchaeology. Springer International Publishing, Cham.

Giusti, D., Konidaris, G.E., Tourloukis, V., Marini, M., Maron, M., Zerboni, A., Thompson, N., Koufos, G.D., Kostopoulos, D.S., Harvati, K., 2019. Recursive anisotropy: a spatial taphonomic study of the Early Pleistocene vertebrate assemblage of Tsiotra Vryssi, Mygdonia Basin, Greece. Boreas 48, 713–730.

Hartstone-Rose, A., 2008. Evaluating the hominin scavengingniche through analysis of the carcass-processing abilities of the carnivore guild. Biological Anthropology and Anatomy (PhD Thesis), Duke University, Durham, USA.

Hartstone-Rose, A., 2011. Reconstructing the diets of extinct South African carnivorans from premolar ‘intercuspid notch’ morphology: Reconstructing carnivoran diet from intercuspid notches. Journal of Zoology 285, 119–127.

Hartstone-Rose, A., Wahl, S., 2008. Using radii-of-curvature for the reconstruction of extinct South African carnivoran masticatory behavior. Comptes Rendus Palevol 7, 629–643.

Haynes, G., 1980. Evidence of carnivore gnawing on Pleistocene and recent mammalian bones. Paleobiology 6, 341–351.

Haynes, G., 1982. Utilization and skeletal disturbances of North American prey carcasses. ARCTIC 35, 266–281.

Haynes, G., 1983. A guide for differentiating mammalian carnivore taxa responsible for gnaw damage to herbivore limb bones. Paleobiology 9, 164–172.

Hill, A., 1989. Bone modification by modem spotted hyenas, in: Bonnichsen, R., Sorg, M. (Eds.), Bone modification. University of Maine: Center for the Study of the First Americans, Maine, pp. 169–178.

Howard, H., 1930. A census of the Pleistocene birds of Rancho La Brea from the collections of the Los Angeles Museum. The Condor 32, 81–88.

Konidaris, G.E., Tourloukis, V., 2021. Proboscidea-*Homo* interactions in open-air localities during the Early and Middle Pleistocene of western Eurasia: a palaeontological and archaeolocigal perspective, in: Konidaris, G.E., Barkai, R., Tourloukis, V, Harvati, K. (Eds.), Human-Elephant Interactions: From Past to Present. Tübingen University Press, Tübingen, pp. 67–104.

Konidaris, G.E., Tourloukis, V., Kostopoulos, D.S., Thompson, N., Giusti, D., Michailidis, D., Koufos, G.D., Harvati, K., 2015. Two new vertebrate localities from the Early Pleistocene of Mygdonia Basin (Macedonia, Greece): Preliminary results. Comptes Rendus Palevol 14, 353–362.

Konidaris, G.E., Kostopoulos, D.S., Maron, M., Schaller, M., Ehlers, T.A., Aidona, E., Marini, M., Tourloukis, V., Muttoni, G., Koufos, G.D., Harvati, K., 2021. Dating of the Lower Pleistocene vertebrate site of Tsiotra Vryssi (Mygdonia Basin, Greece): Biochronology, magnetostratigraphy, and cosmogenic radionuclides. Quaternary 4, 1–18.

Kostopoulos, D.S., Maniakas, I., Tsoukala, E., 2018. Early bison remains from Mygdonia Basin (Northern Greece). Geodiversitas 40, 283–319.

Koufos, G.D., 2014. The Villafranchian carnivoran guild of Greece: implications for the fauna, biochronology and paleoecology. Integrative Zoology 9, 444–460.

Koufos, G.D., 2018. New material and revision of the Carnivora, Mammalia from the Lower Pleistocene locality Apollonia 1, Greece. Quaternary 1, 6.

Koufos, G.D., Syrides, G.E., Kostopoulos, D.S., Koliadimou, K.K., 1995. Preliminary results about thestratigraphy and the palaeoenvironment of Mygdonia Basin, Macedonia, Greece. Geobios 28, 243–249.

Koufos, G.D., Konidaris, G.E., Harvati, K., 2018. Revisiting *Ursus etruscus* (Carnivora, Mammalia) from the Early Pleistocene of Greece with description of new material. Quaternary International 497, 222–239.

Kruuk, H., 1972. The spotted hyena: a study of predation and social behavior, University of Chicago Press. Chicago.

Kuhn, B.F., Berger, L.R., Skinner, J.D., 2008. Examining criteria for identifying and differentiating fossil faunal assemblages accumulated by hyenas and hominins using extant hyenid accumulations. International Journal of Osteoarchaeology 20, 15–35.

Kuhn, B.F., Berger, L.R., Skinner, J.D., 2009. Variation in tooth mark frequencies on long bones from the assemblages of all three extant bone-collecting hyaenids. Journal of Archaeological Science 36, 297–307.

Lam, Y.M., Chen, X., Pearson, O.M., 1999. Intertaxonomic variability in patterns of bone density and the differential representation of bovid, cervid, and equid elements in the archaeological record. American Antiquity 64, 343–362.

Leakey, L.N., Milledge, S.A.H., Leakey, S.M., Edung, J., Haynes, P., Kiptoo, D.K., McGeorge, A., 1999. Diet of striped hyaena in northern Kenya: Diet of striped hyaena. African Journal of Ecology 37, 314–326.

Lyman, R.L., 1994. Vertebrate taphonomy, Cambridge manuals in Archaeology. Cambridge University Press, Cambridge, New York.

Maniakas, I., 2019. Contribution to the study of chrono-spatial distribution of palaeocological adaptations of European Pleistocene Bovini based on ecomorphological analyses and geometric morphometrics (Ph.D. Thesis). Scientific Annals of School of Geology, 192, Aristotle University of Thessaloniki, Greece.

Marean, C.W., Spencer, L.M., 1991. Impact of carnivore ravaging on zooarchaeological measures of element abundance. American Antiquity 56, 645–658.

Marean, C.W., Ehrhardt, C.L., 1995. Paleoanthropological and paleoecological implications of the taphonomy of a sabertooth's den. Journal of Human Evolution 29, 515–547.

Martínez-Navarro, B., Palmqvist, P., 1996. Presence of the african saber-toothed felid *Megantereon whitei* (Broom, 1937) (Mammalia, Carnivora, Machairodontinae) in Apollonia-1 (Mygdonia Basin, Macedonia, Greece). Journal of Archaeological Science 23, 869–872.

Martinez-Navarro, B., Lucenti, S.B., Palmqvist, P., Ros-Montoya, S., Madurell-Malapeira, J., Espigares, M.P., 2021. A new species of dog from the Early Pleistocene site of Venta Micena (Orce, Baza Basin, Spain). Comptes Rendus Palevol 20, 297–314.

Mecozzi, B., Sardella, R., Boscaini, A., Cherin, M., Costeur, L., Madurell-Malapeira, J., Pavia, M., Profico, A., Iurino, D.A., 2021. The tale of a short-tailed cat: New outstanding Late Pleistocene fossils of *Lynx pardinus* from southern Italy. Quaternary Science Reviews 262, 106840.

Medin, T., Martínez-Navarro, B., Rivals, F., Madurell-Malapeira, J., Ros-Montoya, S., Espigares, M.-P., Figueirido, B., Rook, L., Palmqvist, P., 2017. Late Villafranchian *Ursus etruscus* and other large carnivorans from the Orce sites (Guadix-Baza basin, Andalusia, southern Spain): Taxonomy, biochronology, paleobiology, and ecogeographical context. Quaternary International 431, 20–41.

Medin, T., Martínez-Navarro, B., Madurell-Malapeira, J., Figueirido, B., Kopaliani, G., Rivals, F., Kiladze, G., Palmqvist, P., Lordkipanidze, D., 2019. The bears from Dmanisi and the first dispersal of early *Homo* out of Africa. Scientific Reports 9, 17752.

Mills, M.G.L., 1990. Kalahari hyaenas: comparative behavioural ecology of two species. Unwin Hyman, London; Boston.

Outram, A., Rowley-Conwy, P., 1998. Meat and marrow utility indices for horse (*Equus*). Journal of Archaeological Science 25, 839–849.

Pales, L., Garcia, M.A., 1981. Atlas ostéologique pour servir à l'identification des mammifères du quaternaire. 2 : Carnivores. Homme. Paris, CNRS.

Palmqvist, P., Arribas, A., 2001. Taphonomic decoding of the paleobiological information locked in a lower Pleistocene assemblage of large mammals. Paleobiology 27, 512–530.

Palmqvist, P., Martínez-Navarro, B., Arribas, A., 1996. Prey Selection by terrestrial carnivores in a Lower Pleistocene paleocommunity. Paleobiology 22, 514–534.

Palmqvist, P., Arribas, A., Martínez-Navarro, B., 1999. Ecomorphological study of large canids from the lower Pleistocene of southeastern Spain. Lethaia 32, 75–88.

Palmqvist, P., Torregrosa, V., Pérez-Claros, J.A., Martínez-Navarro, B., Turner, A., 2007. A re-evaluation of the diversity of *Megantereon* (Mammalia, Carnivora, Machairodontinae) and the problem of species identification in extinct carnivores. Journal of Vertebrate Paleontology 27, 160–175.

Palmqvist, P., Pérez-Claros, J.A., Janis, C.M., Figueirido, B., Torregrosa, V., Gröcke, D.R., 2008. Biogeochemical and ecomorphological inferences on prey selection and resource partitioning among mammalian carnivores in an Early Pleistocene community. PALAIOS 23, 724–737.

Palmqvist, P., Martínez-Navarro, B., Pérez-Claros, J.A., Torregrosa, V., Figueirido, B., Jiménez-Arenas, J.M., Patrocinio Espigares, M., Ros-Montoya, S., De Renzi, M., 2011. The giant hyena *Pachycrocuta brevirostris*: Modelling the bone-cracking behavior of an extinct carnivore. Quaternary International 243, 61–79.

Palombo, M.R., 2010. A scenario of human dispersal in the northwestern Mediterranean throughout the Early to Middle Pleistocene. Quaternary International 223–224, 179–194.

Palombo, M.R., 2016. To what extent could functional diversity be a useful tool in inferring ecosystem responses to past climate changes? Quaternary International 413, 15–31.

Pante, M.C., Muttart, M.V., Keevil, T.L., Blumenschine, R.J., Njau, J.K., Merritt, S.R., 2017. A new high-resolution 3-D quantitative method for identifying bone surface modifications with implications for the Early Stone Age archaeological record. Journal of Human Evolution 102, 1–11.

Parkinson, J., 2013. A GIS image analysis approach to documenting Oldowan hominin carcass acquisition: Evidence from Kanjera South, FLK Zinj, and Neotaphonomic Models of Carnivore Bone Destruction (Ph.D. Thesis). City University of New York, New York, USA.

Parkinson, J.A., Plummer, T.W., Bose, R., 2014. A GIS-based approach to documenting large canid damage to bones. Palaeogeography, Palaeoclimatology, Palaeoecology 409, 57–71.

Parkinson, J.A., Plummer, T., Hartstone-Rose, A., 2015. Characterizing felid tooth marking and gross bone damage patterns using GIS image analysis: An experimental feeding study with large felids. Journal of Human Evolution 80, 114–134.

Pickering, T., Heaton, J., Zwodeski, S., Kuman, K., 2011. Taphonomy of bones from baboons killed and eaten by wild leopards in Mapungubwe National Park, South Africa. Journal of Taphonomy 9, 117–159.

Pobiner, B.L., 2007. Hominin-carnivore interactions: Evidence from modern carnivore bone modification and Early Pleistocene archaeofaunas (Koobi Fora, Kenya; Olduvai Gorge, Tanzania) (Ph.D. Thesis). Rutgers University, New Jersey, USA.

Pobiner, B.L., 2008. Paleoecological information in predator tooth marks. Journal of Taphonomy 6, 373–397.

Pobiner, B.L., Dumouchel, L., Parkinson, J., 2020. A new semi-quantitative method for coding carnivore chewing damage with an application to modern African lion-damaged bones. PALAIOS 35, 302–315.

Psilovikos, A.A., 1977. Palaeogeographic development of the basin and lake of Mygdonia (Langada-Volvi area), Greece (Ph.D. Thesis). Aristotle University of Thessaloniki, Thessaloniki, Greece.

Rodríguez-Hidalgo, A., Sanz, M., Daura, J., Sánchez-Marco, A., 2020. Taphonomic criteria for identifying Iberian lynx dens in Quaternary deposits. Scientific Reports 10, 7225.

Sala, N., Arsuaga, J.L., 2013. Taphonomic studies with wild brown bears (*Ursus arctos*) in the mountains of northern Spain. Journal of Archaeological Science 40, 1389–1396.

Sala, N., Algaba, M., Arsuaga, J., Aranburu, A., Pantoja-Pérez, A., 2012. A Taphonomic study of the Búho and Zarzamora caves. Hyenas and humans in the Iberian Plateau (Segovia, Spain) during the Late Pleistocene. Journal of Taphonomy 10, 477–497.

Sala, N., Arsuaga, J.L., Haynes, G., 2014a. Taphonomic comparison of bone modifications caused by wild and captive wolves (*Canis lupus*). Quaternary International 330, 126–135.

Sala, N., Arsuaga, J.L., Martínez, I., Gracia-Téllez, A., 2014b. Carnivore activity in the Sima de los Huesos (Atapuerca, Spain) hominin sample. Quaternary Science Reviews 97, 71–83.

Saladié, P., 2009. Mossegades d'omnívors Aproximació experimental i aplicació zooarqueològica als jaciments de la Sierra de Atapuerca (Ph.D. Thesis). Universitat Rovira i Virgili, Tarragona, Spain.

Saladié, P., Huguet, R., Díez, C., Rodríguez-Hidalgo, A., Carbonell, E., 2013. Taphonomic modifications produced by modern brown bears (*Ursus arctos*): Taphonomic modifications produced by modern brown bears. Int. J. Osteoarchaeol. 23, 13–33.

Saladié, P., Fernández, P., Rodríguez-Hidalgo, A., Huguet, R., Pineda, A., Cáceres, I., Marín, J., Vallverdú, J., Carbonell, E., 2019. The TD6.3 faunal assemblage of the Gran Dolina site (Atapuerca, Spain): a late Early Pleistocene hyena den. Historical Biology 31, 665–683.

Shipman, P., 1981. Life history of a fossil. An introduction to taphonomy and palaeoecology. Harvard University Press, Cambridge, Massachutsetts, and London.

Skinner, J.D., Henschel, J.R., van Jaarsveld, A.S., 1986. Bone-collecting habits of spotted hyaenas *Crocuta crocuta* in the Kruger National Park. South African Journal of Zoology 21, 303–308.

Tsoukala, E., Chatzopoulou, K., 2005. A new Early Pleistocene (Latest Villafranchian) site with mammals in Kalamotó (Mygdonia Basin, Macedonia, Greece). Preliminary Report. Mitteilungen der Kommission für Quartärforschung 14, 213–233.

Turner, A., Antón, M., 1996. The giant hyaena, *Pachycrocuta brevirostris* (Mammalia, Carnivora, Hyaenidae). Geobios 29, 455–468.

Van Valkenburgh, B., 1988. Trophic diversity in past and present guilds of large predatory mammals. Paleobiology 14, 155–173.

Van Valkenburgh, B., Ruff, C.B., 1987. Canine tooth strength and killing behaviour in large carnivores. Journal of Zoology 212, 379–397.

Van Valkenburgh, B., Teaford, M.F., Walker, A., 1990. Molar microwear and diet in large carnivores: inferences concerning diet in the sabretooth cat, *Smilodon fatalis*. Journal of Zoology 222, 319–340.

Van Valkenburgh, Binder, W.J., 2000. Biomechanics and feeding behaviour in carnivores: comparative and ontogenetic studies, in: Blake, R.W., Domenici, P. (Eds.), Biomechanics in Animal Behaviour, Experimental Biology Reviews. BIOS Scientific, Oxford, pp. 223–235.

Wauthoz, B., Dorning, K.J., Le Hérissé, A., 2003. *Crassiangulina variacornuta* sp. nov. from the late Llandovery and its bearing on Silurian and Devonian acritarch taxonomy. Bulletin de la Société Géologique de France 174, 67–81.

Wilson, M.V.H., 1988. Taphonomic processes: information loss and information gain. Geoscience Canada 15, 131–148.

Yravedra, J., 2011. A taphonomic study of wild wolf (*Canis lupus*) modification of horse bones in Northwestern Spain. Journal of Taphonomy 9, 37–65.

Yravedra, J., Andrés, M., Domínguez-Rodrigo, M., 2014. A taphonomic study of the African wild dog (*Lycaon pictus*). Archaeological and Anthropological Sciences 6, 113–124.

Appendix

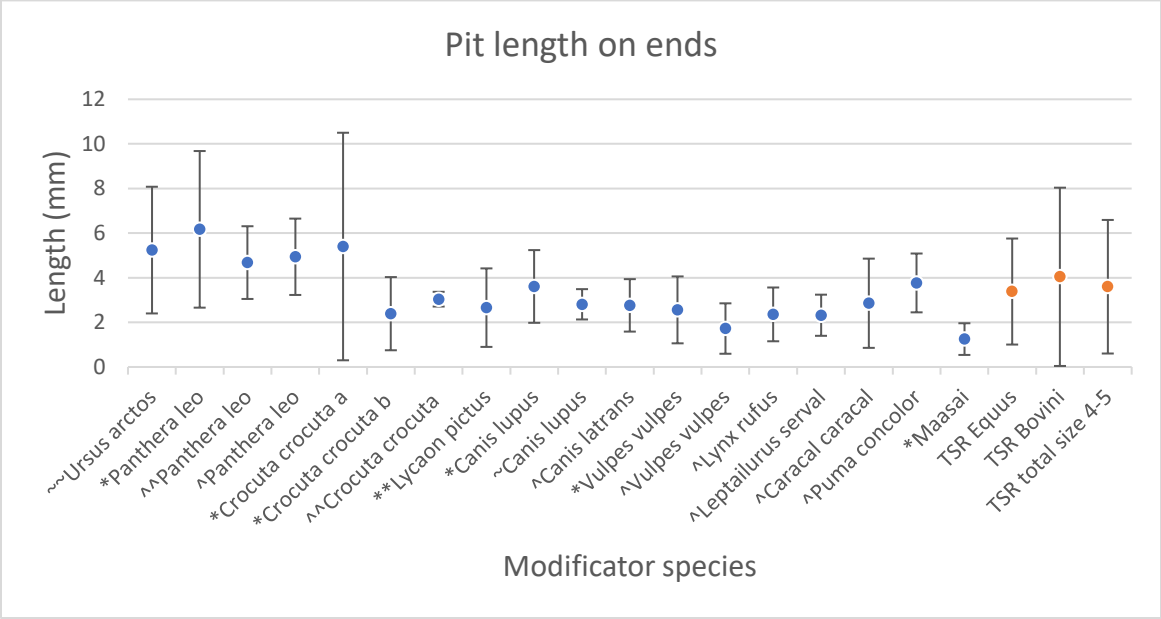

App. Figure 1: Mean values and standard deviation intervals of pit length on the epiphyses. Data from: ~~ Domínguez-Rodrigo and Piqueras (2003), * Andre et al. (2012), ^^ Sala et al. (2012), ^ Delaney-Rivera (2009), ** Yravedra et al. (2014), and ~ Sala et al. (2014) in comparison with *Equus*, Bovini and total of size group 4-5 from TSR.

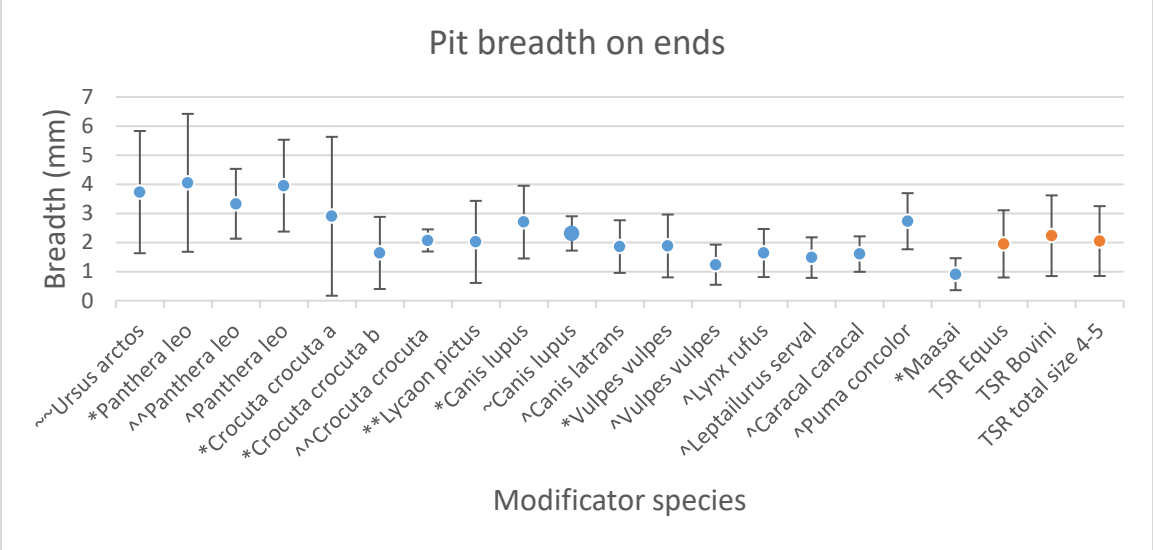

App. Figure 2: Mean values and standard deviation intervals of pit breadth on the epiphyses. Data from: ~~ Domínguez-Rodrigo and Piqueras (2003), * Andre et al. (2012), ^^ Sala et al. (2012), ^ Delaney-Rivera (2009), ** Yravedra et al. (2014), and ~ Sala et al. (2014) in comparison with *Equus*, Bovini and total of size group 4-5 from TSR.

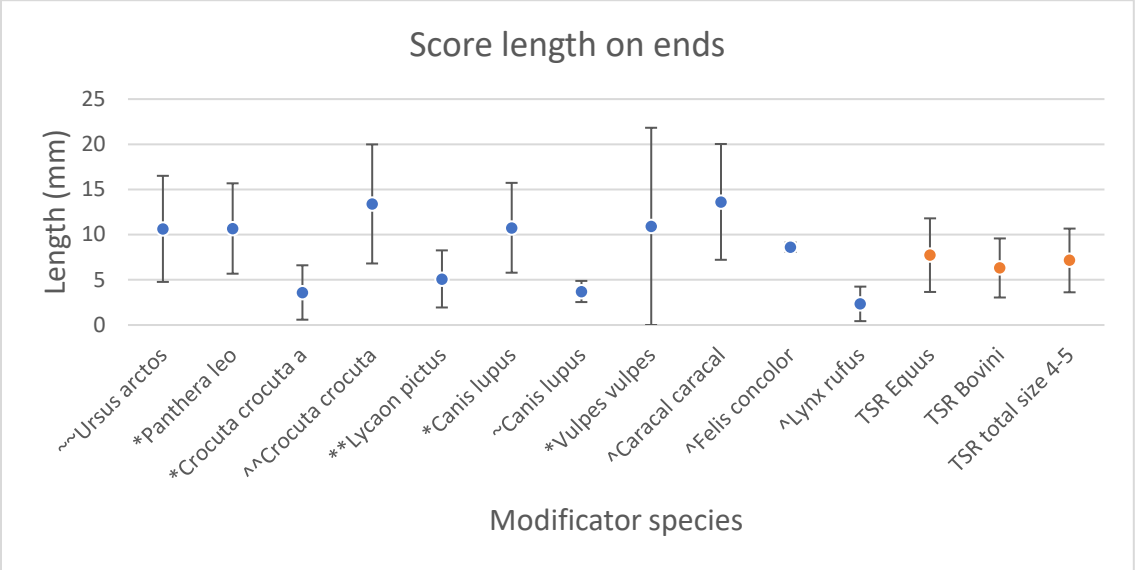

App. Figure 3: Mean values and standard deviation intervals of score length on the epiphyses. Data from: ~~ Domínguez-Rodrigo and Piqueras (2003), * Andre et al. (2012), ^^ Sala et al. (2012), ^ Delaney-Rivera (2009), ** Yravedra et al. (2014), and ~ Sala et al. (2014) in comparison with *Equus*, Bovini and total of size group 4-5 from TSR.

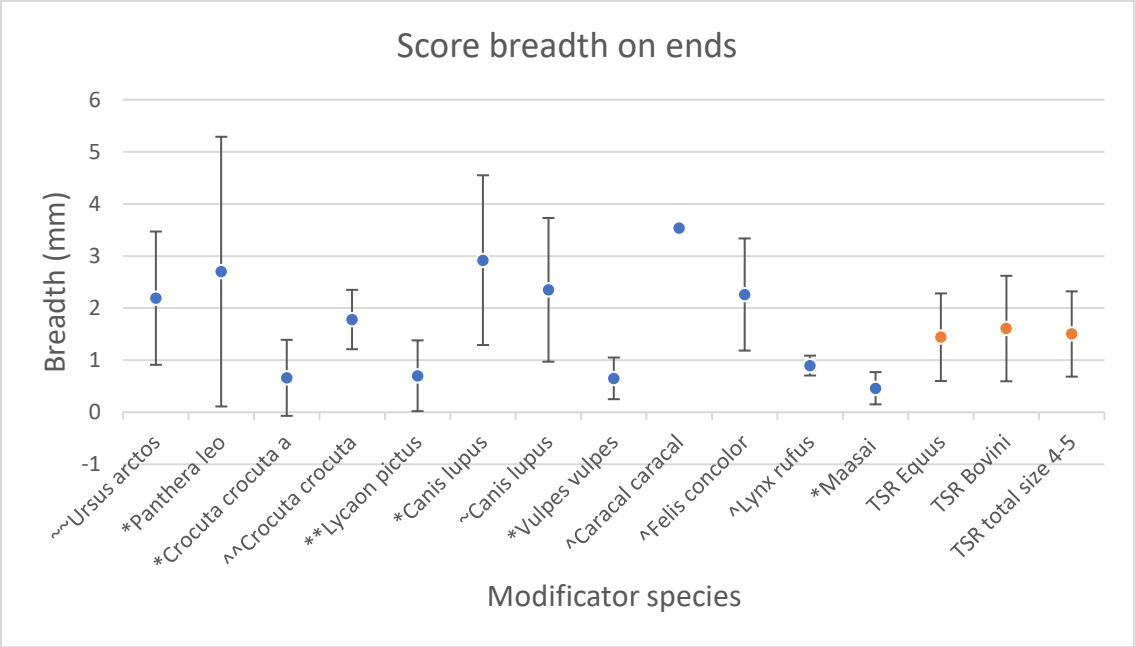

App. Figure 4: Mean values and standard deviation intervals of score breadth on the epiphyses. Data from: ~~ Domínguez-Rodrigo and Piqueras (2003), * Andre et al. (2012), ^^ Sala et al. (2012), ^ Delaney-Rivera (2009), ** Yravedra et al. (2014), and ~ Sala et al. (2014) in comparison with *Equus*, Bovini and total of size group 4-5 from TSR.

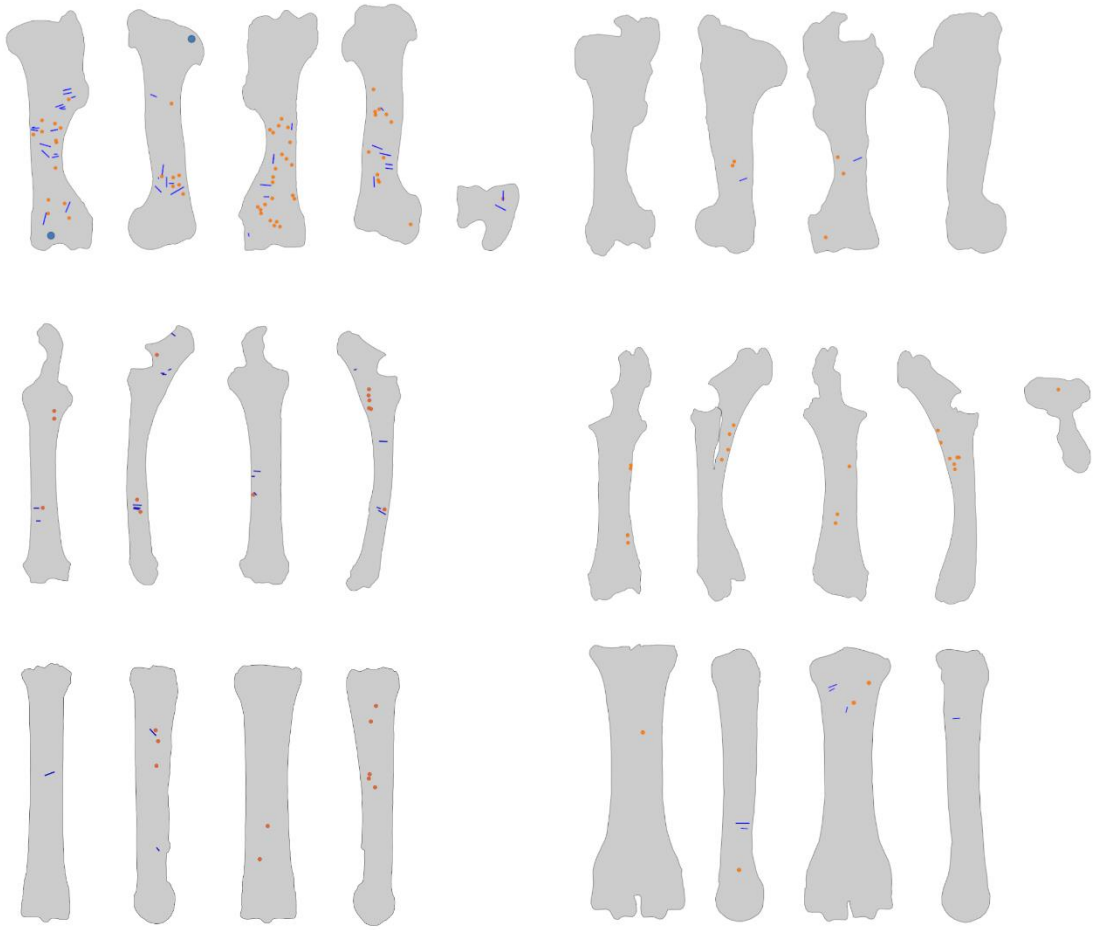

App. Figure 5: Spatial distribution of tooth marks (pits, scores, punctures) of posterior, medial, anterior, and lateral views of humerus, radio-ulna and metacarpal of *Equus* (left) and Bovini (right). Distal and proximal views are depicted only when tooth marks are present. Scores are represented by blue lines, pits by orange points and punctures by light blue points of bigger size.

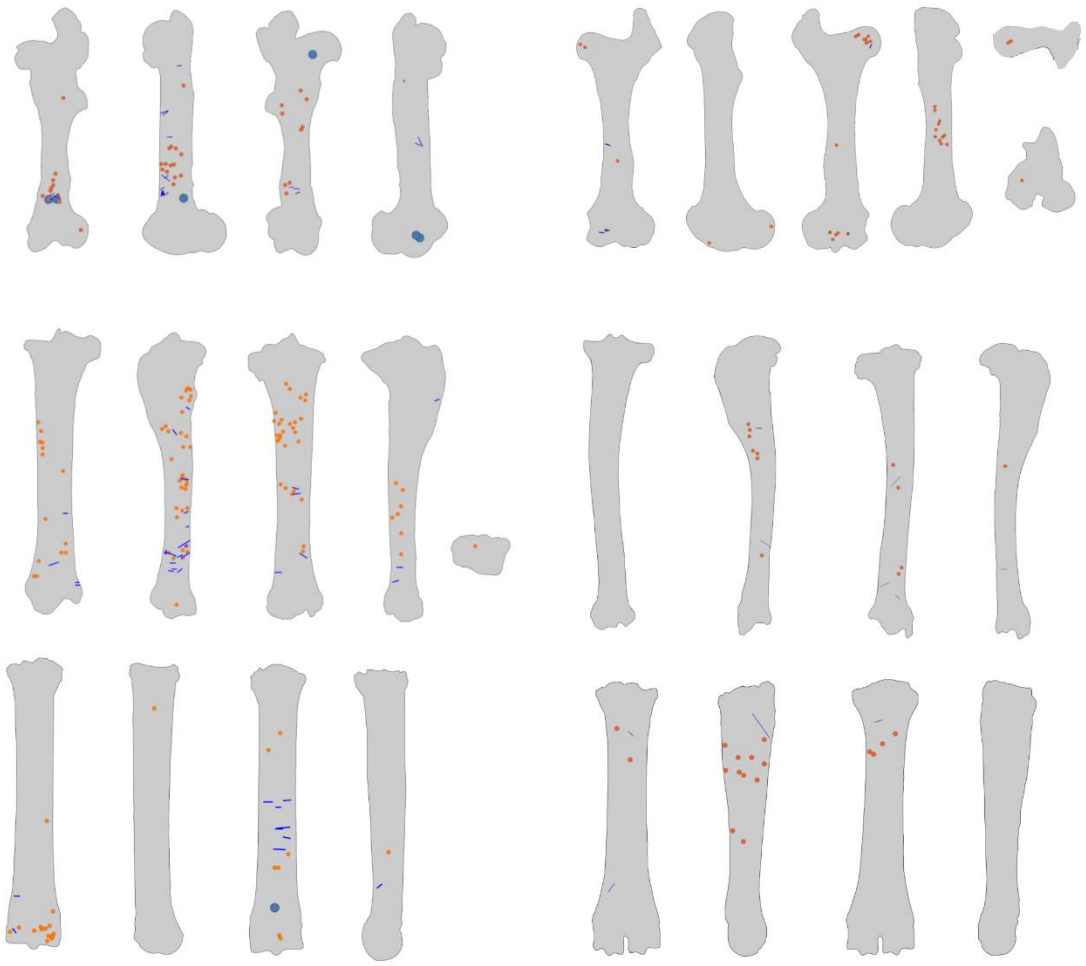

App. Figure 6: Spatial distribution of tooth marks (pits, scores, punctures) of posterior, medial, anterior, and lateral views of femur, tibia and metatarsal of *Equus* (left) and Bovini (right). Distal and proximal views are depicted only when tooth marks are present. Scores are represented by blue lines, pits by orange points and punctures by light blue points of bigger size.

App. Figure 7: *Equus* tibia (C18-14, anterior view) displaying deletion of proximal epiphysis and part of the middle shaft.

App. Figure 8: *Equus* tibiae (from left to right: C18-11, G17-20 and F18-60; posterior view) displaying deletion of proximal half.

App. Figure 9: *Equus* tibiae (from left to right G20-52, G20-4, F17-32 and F18-41; posterior view) displaying deletion of proximal half and part of proximal shaft.

App. Figure 10: *Equus* tibiae (from left to right: D16-22, I19-1 and F15-10) shaft fragments.

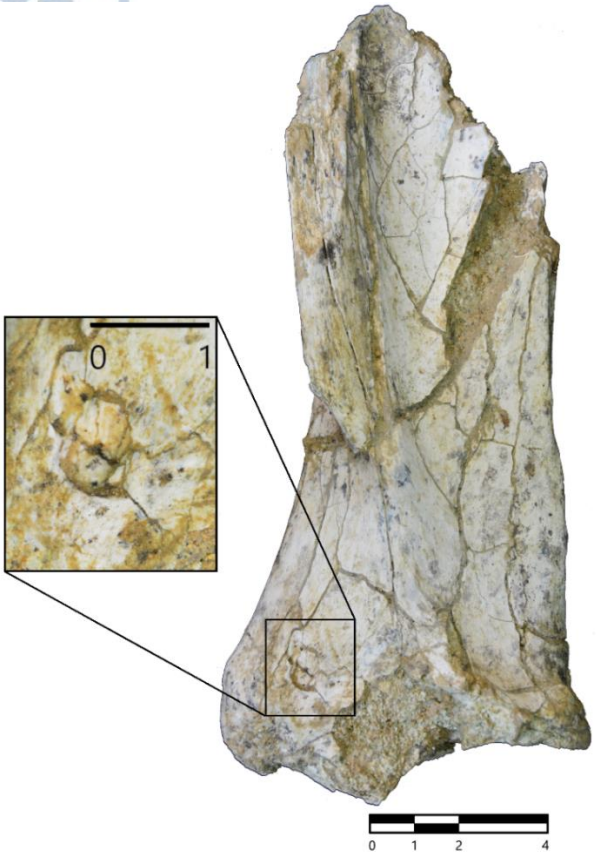

App. Figure 11: *Equus* scapula with puncture (specimen H23-6; lateral view).

App. Figure 12: *Equus* atlas, heavily tooth marked and furrowed (specimen G20-8; dorsal view).

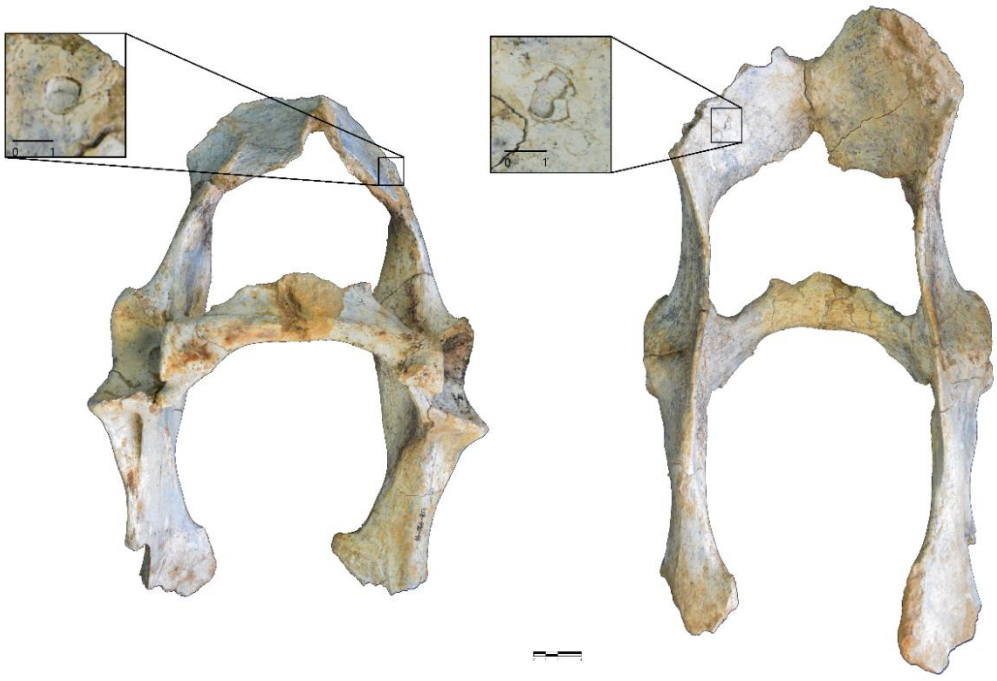

App. Figure 13: Punctures on ventral (left) and dorsal (right) views of Bovini pelvis (specimen G20-40). Scale in cm.

App. Figure 14: Punctures on medial (left) and furrow on lateral (right) views of *Equus* femur (specimen H21-11). Scale in cm.

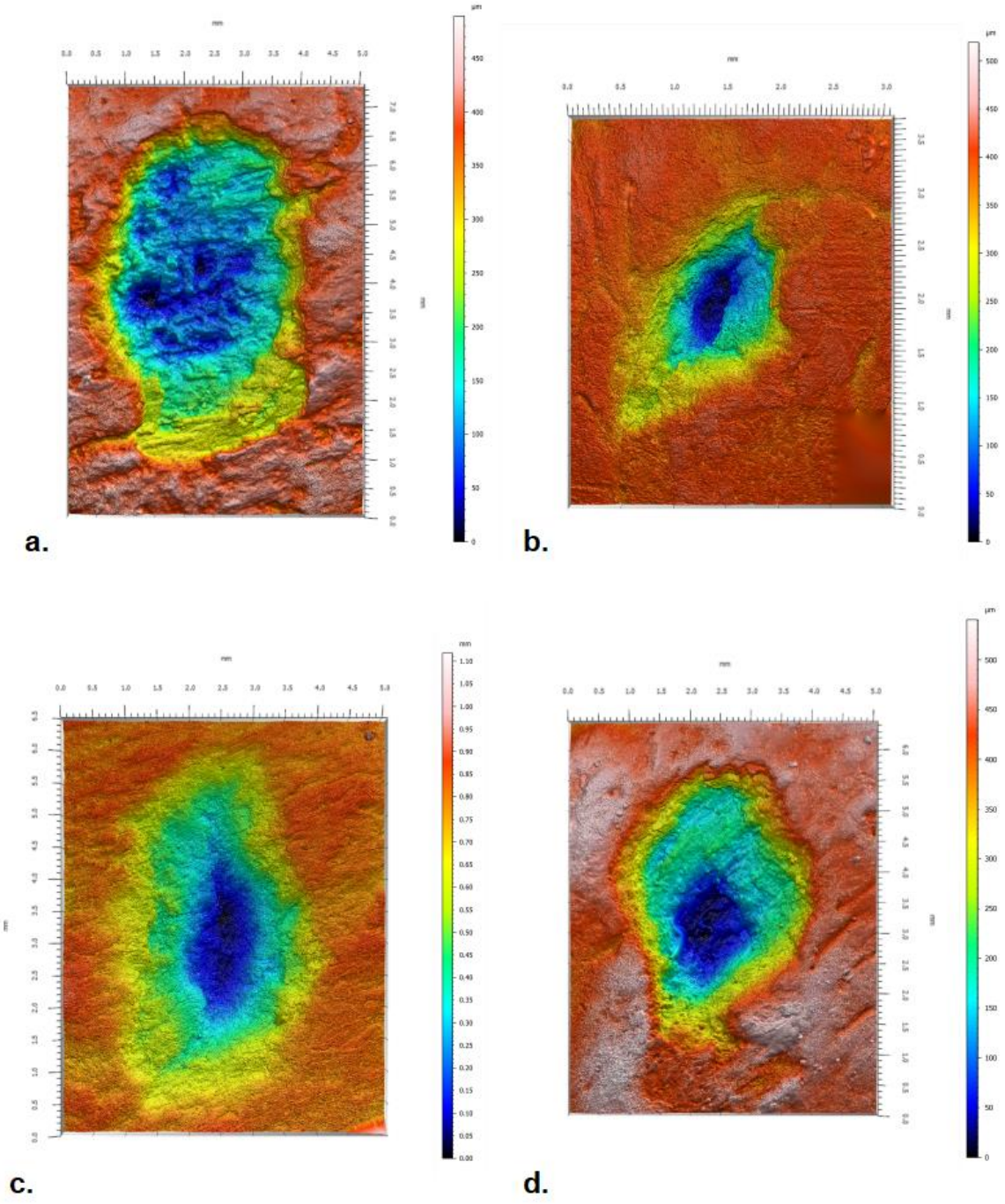

App. Figure 15: Examples of 3D images of pits. (a) F18-60, (b) G20-7, (c) F18-41 and (d) G20-15.

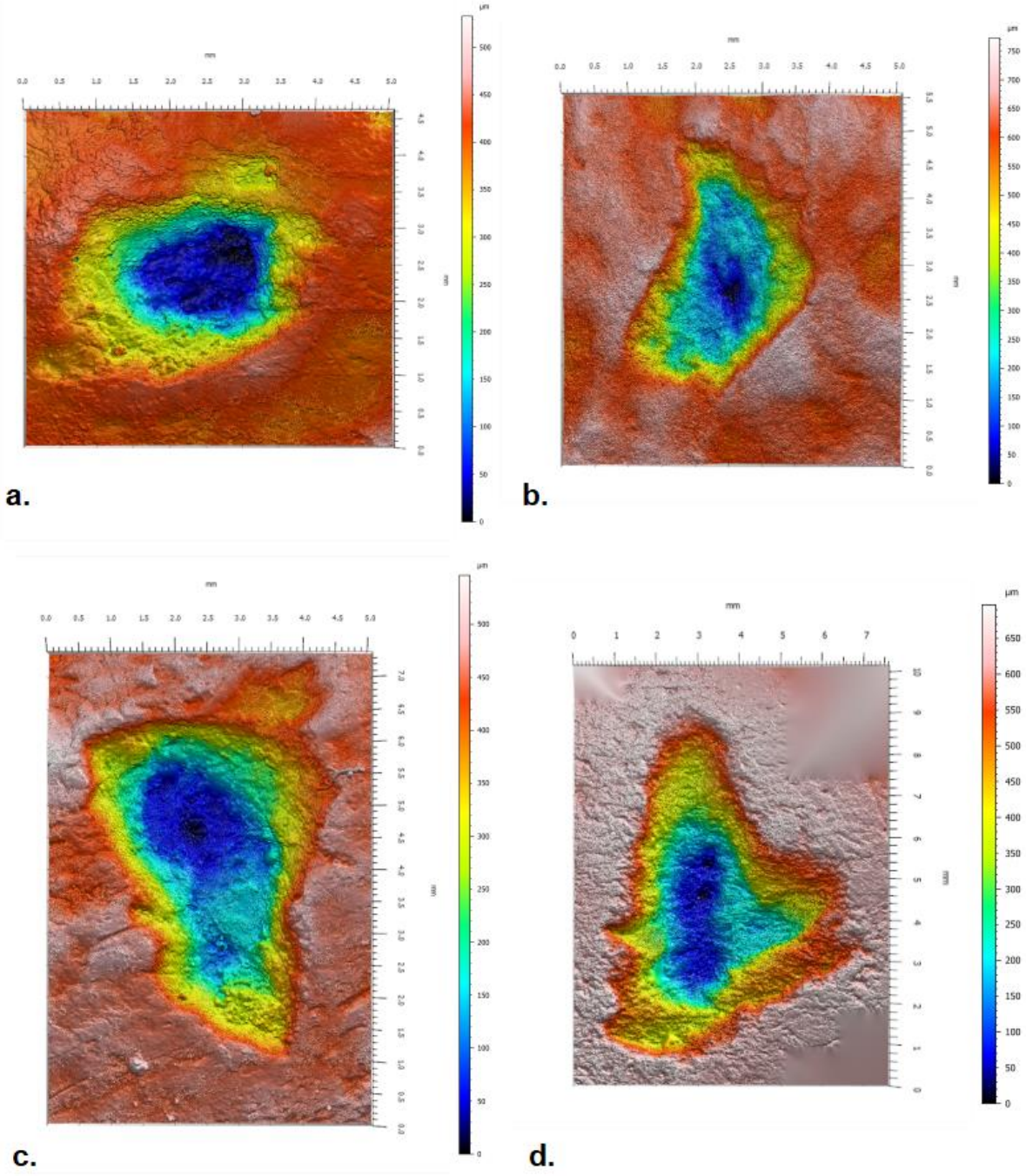

App. Figure 16: Examples of 3D images of pits. (a) I19-1, (b) H18-4, (c) I20-3 and (d) G20-29).

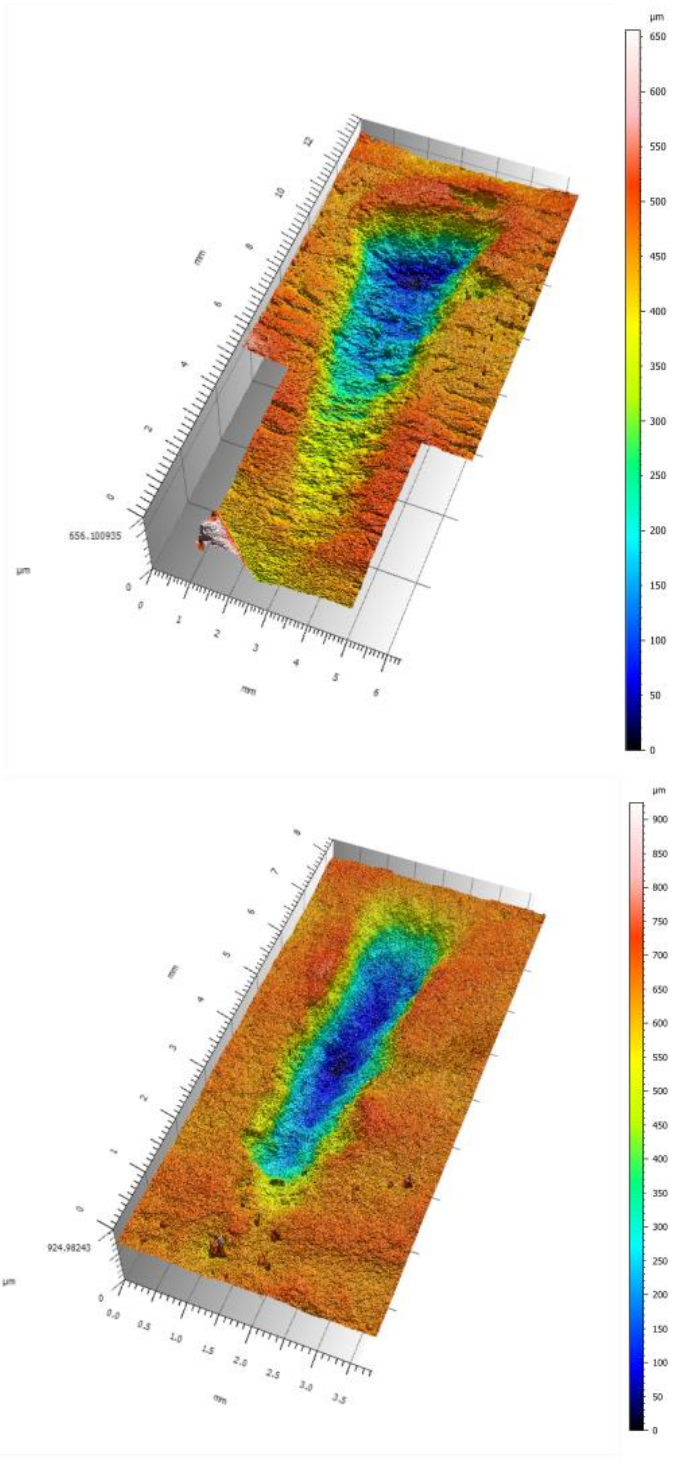

App. Figure 17: Examples of 3D images of scores (specimens G20-15 (top) and H18-4 (bottom)).

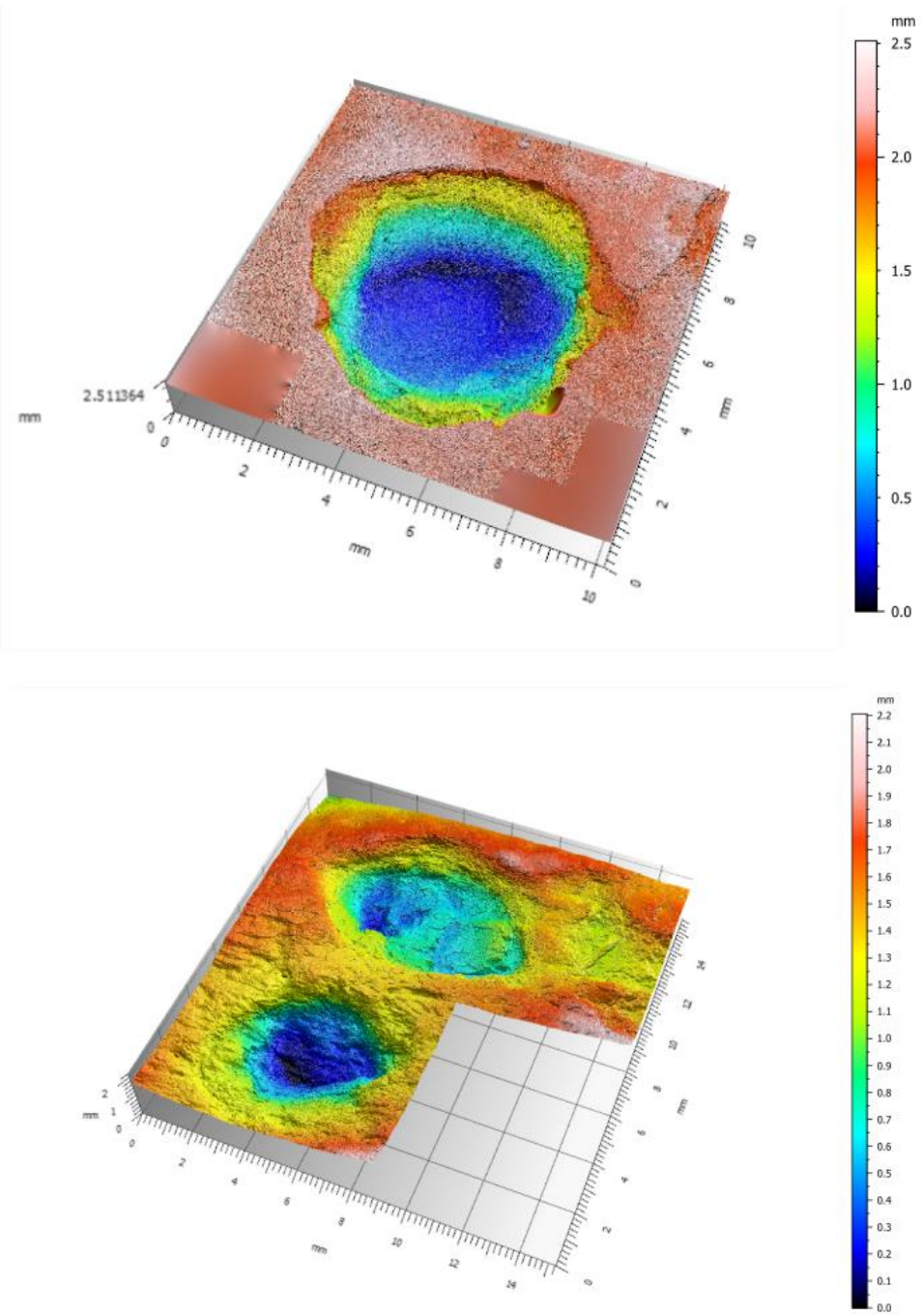

App. Figure 18: Examples of 3D images of punctures (specimens G20-40 (top) and H21-11 (bottom)).

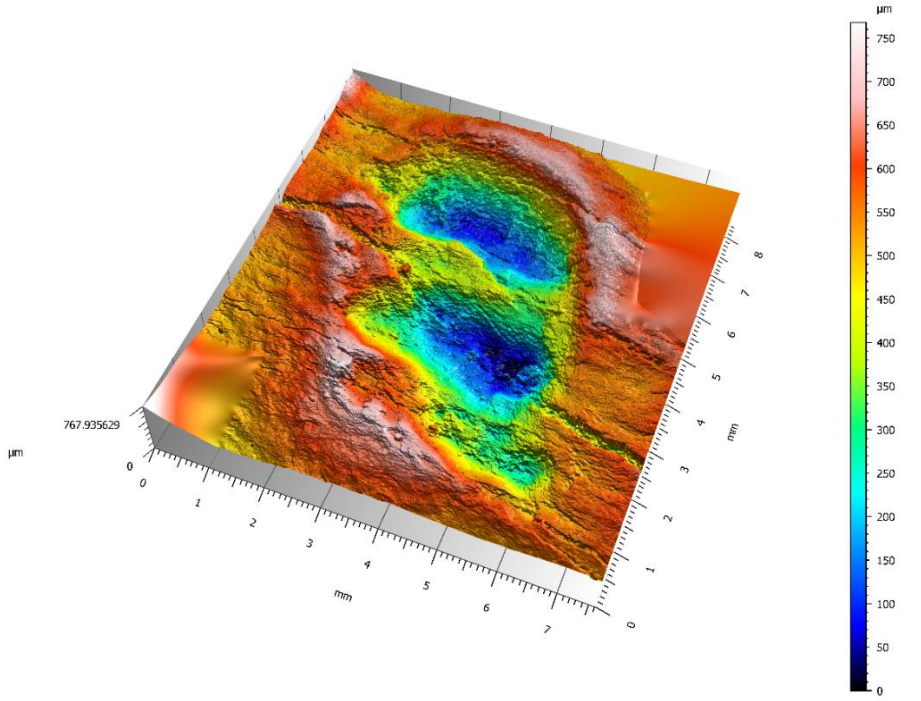

App. Figure 19: 3D image of pits (specimen G22-6).

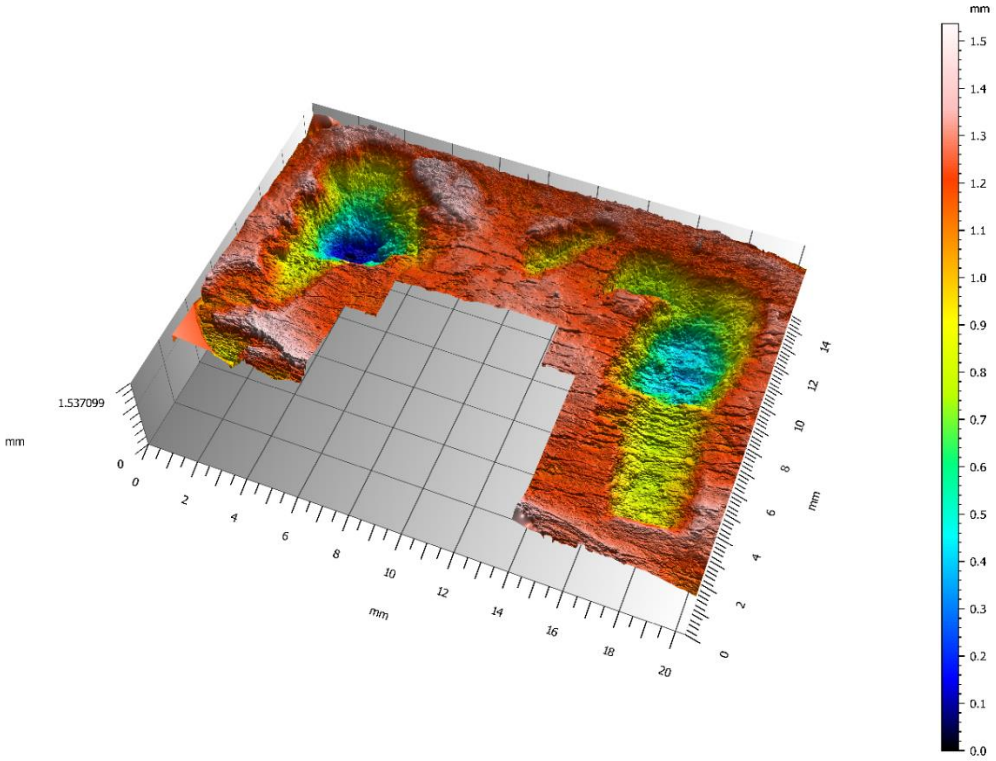

App. Figure 20: 3D image of tooth marks (specimen G21-84).

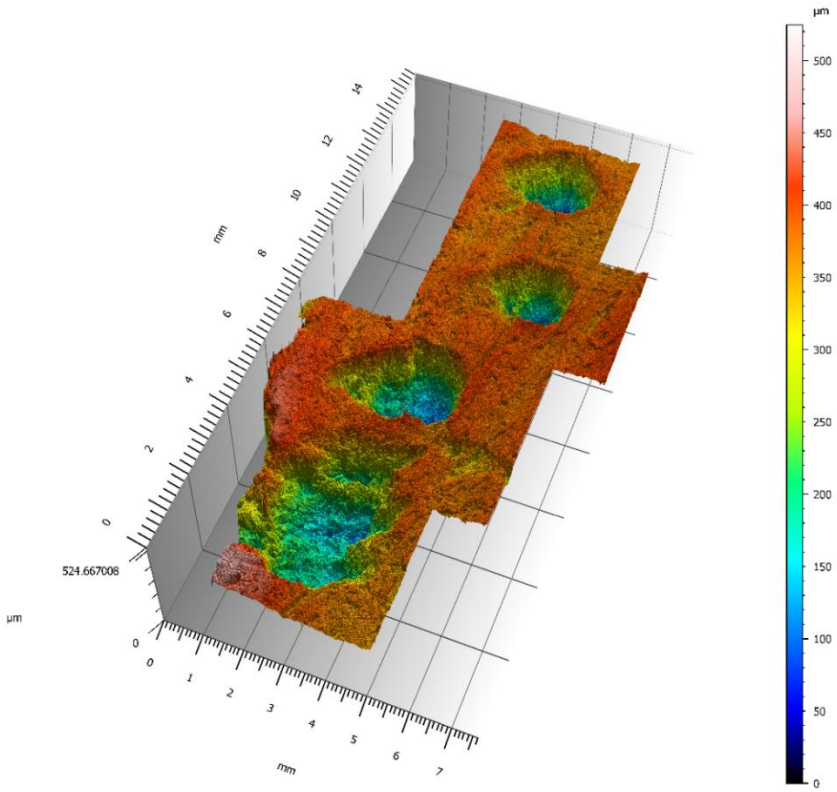

App. Figure 21: 3D image of pits (specimen H16-4B).

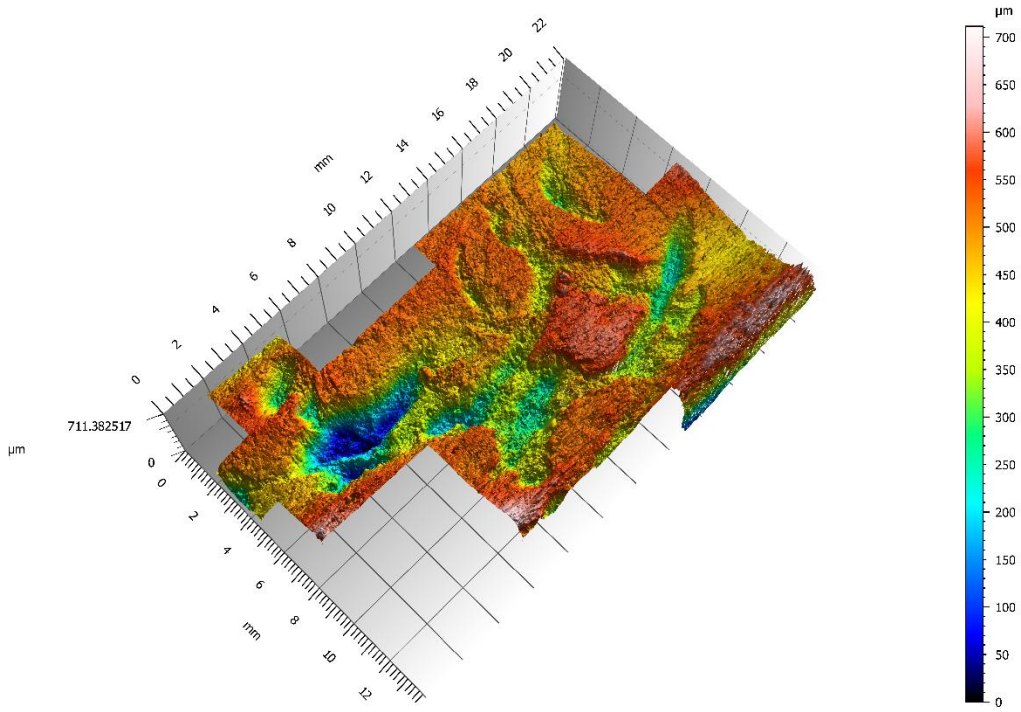

App. Figure 22: 3D image of tooth marks (specimen F20-32).